Detection and Decoding Algorithms of Multi-Antenna Diversity Techniques for Terrestrial DVB Systems

Iker Sobrón Polancos

Supervisors:

Mikel Mendicute Errasti

and

Jon Altuna Iraola

MONDRAGON UNIBERTSITATEA

A thesis submitted for the degree of

Doctor por Mondragon Unibertsitatea

Department of Electronics and Computer Science

Mondragon Goi Eskola Politeknikoa

Mondragon Unibertsitatea

November 2010

Para aita, ama, Josu e Itziar

Y para Irene

When you make the finding yourself
- even if you're the last person on Earth to see the light -
you'll never forget it.

Carl Sagan

Agradecimientos

A lo largo de estos cuatro años de singladura, he tenido la suerte de cruzarme con muchas personas que me han ayudado a que este barco arribe a puerto. Su apoyo, guía y consejo ha permitido que en todo momento tuviera un norte al que dirigirme sin que perdiera el ánimo para continuar hacia adelante. Es por ello que quiero expresar en las siguientes líneas mi más profundo agradecimiento a cada una de ellas, haciéndolas también protagonistas de este momento.

En primer lugar, agradezco a mis directores **Mikel Mendicute** y **Jon Altuna** su apoyo y consejo en los momentos de zozobra, además de la confianza depositada en mí para la realización de esta tesis. Me gustaría dedicar particularmente un especial gracias a **Mikel**, por su infinita paciencia y todo ese valioso tiempo que me ha dedicado desde los comienzos como compañero de despacho hasta hoy, además de por el buen amigo que he tenido la suerte de conocer. También quisiera agradecer a **Vicente Atxa**, **Jose Mari Zabalegui** y **Javier Del Ser** los consejos, recomendaciones y ayuda en los dos primeros años de tesis.

Agradezco a **Mondragon Goi Eskola Politeknikoa** la oportunidad ofrecida gracias a su financiación y medios para el desarrollo de esta investigación. También agradezco a mis compañeros de departamento, **Ane Antía**, **Nestor Arana**, **Eñaut Muxika**, **Alberto Izaguirre** y **Aitzol Iturrospe**, el cordial y acogedor trato que me han dado durante todo este tiempo. Doy las gracias especialmente, a **Javier Oyarzun** por allanarme el camino en los difíciles momentos de la escritura de tesis, a **Unai Garro** por sus eficientes gestiones con Tux y a **Egoitz Arruti**, por la confianza depositada y las facilidades ofrecidas para la consecución de mi trabajo.

Quiero dar las gracias a los miembros del **grupo de televisión digital del Departamento de Tecnología de la Información en la Universidad de Turku**, especialmente a **Jarkko Paavola**, **Jari Tissari** y **Jussi Poikonen**, por darme la oportunidad de realizar una estancia con ellos y ayudarme a desarrollar mi trabajo de investigación.

Por otro lado, debo expresar mi más cálida gratitud a los compañeros de batalla que año tras año han ido entrando en mi vida doctoranda. Ellos han hecho el día a día más ameno y han soportado estoicamente mis delirios y preocupaciones a lo largo de todos estos años. Por

orden ascendente de antigüedad, agradezco a **Joxe Aixpurua**, **Maite Beamurgia**, **Lorea Belategui**, **Iñaki Garitano** y **Aritz Legarda**, los buenos momentos de café que me han ayudado a desconectar en estos últimos meses de escritura; a **Idoia Jiménez**, su agradable compañía, especialmente en esas mañanas cuando Garaia despierta; a **Pello Ochandiano** y **Lorena Martínez**, el compartir tantos quebraderos de cabeza en el diseño del simulador y los interesantes momentos de discusión que hemos vivido. Y por último, a **Maitane Barrenechea**, su inestimable ayuda en la comprensión y el diseño del decodificador esférico, y su agradable compañía todo este tiempo.

Finalmente, me gustaría agradecer a las personas más cercanas a mí, su confianza, paciencia, ánimos y comprensión. A **mis amigos** que han soportado con estoico aguante mis cifrados soliloquios de procesado de señal. Con especial cariño, a mi familia que me ha dado muchos ánimos para alcanzar esta meta, **aita**, **ama**, mi hermano **Josu** y mi hermana **Itziar**, que si no hubiera sido por ellos, nunca podría haber sido lo que soy. Y para acabar, a **Irene**, que ha estado ahí en todo momento para apoyarme, ayudarme o escucharme siempre y cuando lo necesitaba.

Acknowledgments

Throughout this four-year journey, I had the chance of meeting several people who have helped me to the completion of this PhD thesis. Their encouragement, guidance and advise have allowed me to find the correct way and go ahead all the time. For that reason, I would like to express my deepest gratitude to each of them and make them active participants in this moment.

First of all, I am grateful for the assistance and guidance of my supervisors, **Jon Altuna** and **Mikel Mendicute**, as well as for the confidence and faith they showed on me. I particularly wish to thank **Mikel** who helped me with great patience from the beginning of my research until today, as well as being a good friend. Furthermore, I thank **Vicente Atxa**, **Jose Mari Zabalegui** and **Javier Del Ser** for their comments and advises at the two first years of the research.

I would like to thank **University of Mondragón** for funding and providing me all the necessary equipment to carry out this PhD thesis. Also I am grateful to my department colleagues, **Ane Antía**, **Nestor Arana**, **Eñaut Muxika**, **Alberto Izaguirre** and **Aitzol Iturrospe**, for their warm and kind relationship with me along this time. Special thanks to **Javier Oyarzun** who gave me the time I needed to write this work, to **Unai Garro** for his skills in the Tux's world and to **Egoitz Arruti** for his confidence and the facilities provided for the develop of my work.

I also want to thank the **DTV Group from the Department of Information Technology at the University of Turku**, specially **Jarkko Paavola**, **Jari Tissari** and **Jussi Poikonen**, for giving me the chance of visiting them and discussing different matters with them.

On the other hand, I am so grateful to my PhD comrades-in-arms who accompanied me along the last three years. In ascending order of seniority, I wish to express my sincere gratitude to **Joxe Aixpurua**, **Maite Beamurgia**, **Lorea Belategui**, **Iñaki Garitano** and **Aritz Legarda**, for the nice coffee breaks in the last months of writing; to **Idoia Jiménez** for her kind company and encouragement, specially in the quiet and early mornings of Garaia; to **Pello Ochandiano** and **Lorena Martínez**, for sharing so many headaches

building the DVB-T2 framework over which we have performed our researches and for the helpful discussions we had; and finally, to **Maitane Barrenechea** for her help to the sphere decoder understanding and develop, as well as her kind company all this time.

And last, I would like to express my deepest gratitude to the closest-to-me people for their confidence, pacience, encouragement and comprehension. To **my friends** who stoically listened to my coded soliloquies about signal processing. To my dear family who encouraged me to go ahead, **my parents**, my brother **Josu** and my sister **Itziar**. They gave me all the facilities to be what I am. And finally, to **Irene**, who has patiently supported and helped me along this time.

Abstract

This PhD dissertation analyzes the behavior of multi-antenna diversity techniques in broadcasting scenarios of TDT (terrestrial digital television) systems and proposes a low-complexity detection and decoding design for their practical implementation. For that purpose, the transmission-reception chains of the European DVB-T (Digital Video Broadcasting - Terrestrial) and DVB-T2 standards have been implemented over which diversity and MIMO (multiple-input multiple-output) techniques have been assessed through Monte Carlo simulations.

On one hand, the most important multi-antenna diversity techniques such as CDD (cyclic delay diversity), Alamouti code-based SFBC (space-frequency block coding) and MRC (maximum ratio combining), have been evaluated in a DVB-T system over both fixed and mobile Rayleigh and Ricean channels. With the DVB-T2 standard release, multi-antenna processing has actually been introduced in digital television systems. The distributed SFBC configuration proposed in DVB-T2 is analyzed from a performance point of view considering different propagation conditions in an SFN (single frequency network).

On the other hand, error-performance and detection complexity analyses of 2×2 FRFD (full-rate full-diversity) SFBCs are carried out for last-generation DTV (digital television) systems. The use of channel coding based on LDPC (low-density parity check) codes in new standards such as DVB-T2, involves a soft-output MAP (maximum *a posteriori*) detection which results in an increase of the detection complexity. In order to study the FRFD codes behavior in such a BICM (bit-interleaved coded modulation) scheme, the Golden code, which achieves the maximum coding gain, and the Sezginer-Sari code, which has a lower inherent detection complexity as an expense of sacrificing performance gain, have been chosen. Using LSD (list sphere decoder) detection, BER (bit error rate) performance and computational cost results are provided for TDT scenarios.

In order to overcome the variable complexity of the LSD, LFSD (list fixed-complexity sphere decoder) detection is proposed for practical implementations. A redesign of the previously proposed LFSD algorithm for spatial multiplexing MIMO systems has been performed for FRFD SFBCs with close-to-LSD performance. Furthermore, an analysis of the number

of candidates is carried out in order to maximize the efficiency of the algorithm. Due to its fixed complexity, the novel algorithm can be fully pipelined making feasible a realistic implementation in chip.

Resumen

Esta tesis analiza el comportamiento de las técnicas de diversidad multiantena en escenarios de radiodifusión TDT (televisión digital terrestre) y propone un diseño de baja complejidad para la detección de códigos SFBC (*space-frequency block coding*) que facilita una posible implementación práctica. Para ello, se ha implementado la cadena de transmisión-recepción de los estándares europeos DVB-T (*Digital Video Broadcasting - Terrestrial*) y DVB-T2 como entorno de trabajo donde se han incluido y simulado diferentes técnicas de diversidad MIMO (*multiple-input multiple-output*).

Por un lado, se evalúan las técnicas de diversidad multiantena CDD (*cyclic delay diversity*), SFBC con codificación Alamouti y MRC (*maximum ratio combining*) en escenarios fijos y móviles de canales tanto *Rayleigh* como *Ricean* para el sistema DVB-T. En DVB-T2, se analiza la tecnología multiantena propuesta por el estándar para diferentes escenarios de propagación dentro de redes SFN (*single frequency network*).

Por otro lado, se realiza un estudio sobre códigos FRFD (*full-rate full-diversity*) SFBC para su posible inclusión en futuros estándares de televisión digital. El uso de codificaciones de canal más potentes, como los códigos LDPC (*low-density parity check*), implica la utilización de una detección MAP (*maximum a posteriori*) con salida *soft*, incrementando considerablemente la complejidad de la detección. Para realizar el correspondiente análisis de complejidad y rendimiento, se han escogidos dos códigos FRFD. Por un lado, el código *Golden*, que ofrece la máxima ganancia de código y, por otro, el código propuesto por Sezginer y Sari, que consigue reducir la complejidad de detección a costa de perder cierta ganancia de código. Se presentan resultados basados en curvas de BER (*bit error rate*) y número de operaciones sobre un sistema BICM (*bit-interleaved coded modulation*) equivalente a DVB-T2 en escenarios TDT utilizando una detección LSD (*list sphere decoder*).

Para resolver el problema de la complejidad variable del algoritmo LSD, se realiza un rediseño del ya propuesto LFSD (*list fixed-complexity sphere decoder*) para técnicas de multiplexación espacial considerando la estructura de los códigos FRFD SFBC. Asimismo, se evalúa el número de candidatos que ofrece un funcionamiento más eficiente con menor coste computacional. Los resultados de simulación basados en curvas de BER muestran rendimien-

tos cercanos al detector LSD manteniendo el número de operaciones constante. Por lo tanto, este nuevo diseño permite su eficiente y práctica implementación en dispositivos reales.

Laburpena

Doktoretza-tesi honen gai nagusia Lurreko Telebista Digitalerako antena anitzeko dibertsitate tekniken portaera ikertzea da, hartzailerako konplexutasun baxuko algoritmoen diseinua oinarri hartuta. Horretarako, Europako DVB-T eta DVB-T2 telebista digitaleko estandarren igorle-hartzaile kateen simulagailua inplementatzeaz gain, dibertsitate eta MIMO (*multiple-input multiple-output*) algoritmoak garatu eta aztertu dira.

Lehenengo helburu gisa, CDD (*cyclic delay diversity*), Alamouti kodean oinarritutako SFBC (*space-frequency block coding*) eta MRC (*maximum ratio combining*) teknikak ebaluatu dira *Rayleigh* eta *Ricean* ingurunetan, bai komunikazio finko zein mugikorretarako. Argitaratu berri den DVB-T2 estandarrak antena anitzeko prozesaketa telebista sistema digitalean sartu duenez, teknologia honen analisia egin da maiztasun bakarreko telebista sareetarako SFN (*single frequency network*).

Tesiaren helburu nagusia FRFD (*full-rate full-diversity*) SFBC kodigoen ikerketa eta hauek telebista digitalaren estandar berrietan sartzea ahalbidetuko dituzten detekzio sistemen diseinua izan da. Kanalen kodifikazio indartsuagoak erabiltzeak, LDPC (*low-density parity check*) kodeak esaterako, MAP (*maximum a posteriori*) algoritmoan oinarritutako soft irteeradun detektoreen erabilera dakar berekin, detekzioaren konplexutasuna areagotuz. Bi FRFD kode aukeratu dira errendimendu eta konplexutasun analisiak DVB-T2 bezalako BICM (*bit-interleaved coded modulation*) sistemetan egiteko. Alde batetik, irabazi maximoa lortzen duen Golden kodea eta, bestetik, konplexutasun txikiagoa duen Sezginer eta Sarik proposatutako kodea erabili dira. Bit errore edo BER (*bit error rate*) tasan eta konputazio kostuan oinarrituta, emaitzak aurkeztu dira zerrenda dekodeatzaile esferikoa (*list sphere decoder*, LSD) erabiliz.

LSD-aren konplexutasun aldakorraren arazoa konpontzeko, ezpazio-multiplexazioko teknikarako LFSD (*list fixed-complexity sphere decoder*) algoritmoaren berdiseinua garatu da, FRFD SFBC kodeen egitura berezia kontuan hartuta. Algoritmoaren eraginkortasuna maximizatzeko kandidatuen zenbakia ebaluatzen da baita ere. LSD-en antzeko errendimendua duten BER grafiketan oinarritutako simulazio emaitzak aurkezten dira, eragiketa kopurua konstante eta LSD-arenaren baino murritzagoa mantenduz. Beraz, proposatutako diseinu

eraginkorrak, FRFD SFBC antena anitzeko dibertsitatean oinarritutako eskemen inplementazioa ahalbidetu dezakete telebista digitalaren estandar berrietarako.

Declaration of Originality

I hereby declare that the research recorded in this thesis and the thesis itself were developed entirely by myself at the Signal Theory and Communications Area, Department of Electronics and Computer Science, at the University of Mondragon.

The software used to perform the simulations was developed entirely by myself, with the following exceptions:

- The implementation of the basic transmission-reception chain of the DVB-T2 simulator has been jointly designed by Lorena Martínez, Pello Ochandiano and me.
- The implementation of the list fixed sphere decoder has been jointly designed by Maitane Barrenechea and me.

Iker Sobrón Polancos
Department of Electronics and Computer Science
Mondragon Goi Eskola Politeknikoa
Mondragon Unibertsitatea
November, 2010

Contents

List of Figures

List of Tables

Acronyms

AED	accumulated (squared) Euclidean distance
APP	*a posteriori* probability
ASTC	Advanced Television System Comittee
AWGN	additive white Gaussian noise
BCH	Bose-Chaudhuri-Hocquenghem
BER	bit error rate
BICM	bit interleaved coded modulation
BPSK	binary phase shift keying
BSSD	bounded soft sphere detection
CDD	cyclic delay diversity
CDF	cumulative distribution function
CIR	channel impulse response
CN	carrier to noise ratio
COFDM	coded orthogonal frequency-division multiplexing
CSI	channel state information
DAC	digital to analogue conversion
DD	delay diversity
DTMB	Digital Terrestrial Multimedia Broadcast

DTV	digital television
DVB	Digital Video Broadcasting
DVB-H	Digital Video Broadcasting - Handheld
DVB-NGH	Digital Video Broadcasting - Next Generation Handheld
DVB-T2	second generation of Digital Video Broadcasting - Terrestrial
DVB-T	Digital Video Broadcasting - Terrestrial
EGC	equal gain combining
FEC	forward error correction
FDM	frequency-division multiplexing
FFT	fast Fourier transform
FP	Fincke-Pohst
FRFD	full-rate full-diversity
FSD	fixed-complexity sphere decoder
GI	guard interval
GSM	Global System for Mobile Communications
HDTV	high definition television
I	in-phase
IFFT	inverse fast Fourier transform
IID	independent and identically distributed
ISDB-T	Integrated Services Digital Broadcasting - Terrestrial
LDPC	low-density parity check
LFSD	list fixed-complexity sphere decoder
LLR	log-likelihood ratio
LOS	line-of-sight
LSB	least significant bit

LSD	list sphere decoder
MAP	maximum a posteriori
MFN	multiple frequency network
MIMO	multiple-input multiple-output
MISO	multiple-input single-output
ML	maximum likelihood
MMSE	minimum mean squared error
MPEG-2	Moving Picture Experts Group 2
MRC	maximum ratio combining
NLOS	non line-of-sight
NP-hard	non-deterministic polynomial-time hard
OFDM	orthogonal frequency-division multiplexing
OSFBC	orthogonal space-frequency block coding
OSTBC	orthogonal space-time block coding
PAPR	peak-to-average power ratio
PED	partial (squared) Euclidean distance
PD	phase diversity
PEP	pairwise error probability
PI	Pedestrian Indoor channel
PLP	physical layer pipe
PO	Pedestrian Outdoor channel
Q	quadrature
QAM	quadrature amplitude modulation
QEF	quasi-error free
QPSK	quadrature phase shift keying

RA6	Rural Area channel (6 paths)
RQD	rotation and cyclic Q-delay
RS	Reed-Solomon
SC	selective combining
SD	sphere decoder
SDTV	standard-definition television
SE	Schnorr-Euchner
SFBC	space-frequency block coding
SFC	space-frequency coding
SFN	single frequency network
SISO	single-input single-output
SM	spatial multiplexing
SNR	signal to noise ratio
SS	Sezginer-Sari
STBC	space-time block coding
STC	space-time coding
TDT	terrestrial digital television
TPS	transmission parameter signalling
TS	transport stream
TV	television
TU6	Typical Urban channel (6 paths)
TU12	Typical Urban channel (12 paths)
UHF	ultra-high frequency
WiMAX	worldwide interoperability for microwave access
WLAN	wireless local area network

WMAN wireless metropolitan area network

WSSUS wide-sense stationary uncorrelated scattering

ZF zero forcing

List of Symbols

α_k	Attenuation coefficient of the transmitted signal from the SFN transmitter k
$\boldsymbol{b}$	Bit vector
B	OFDM signal bandwidth
B_C	Coherence bandwidth
b	Bit
$\boldsymbol{C}$	Equalization matrix
C_{MIMO}	MIMO channel capacity
C_{SISO}	SISO channel capacity
d	Diversity gain
$\boldsymbol{\Delta}$	Difference matrix between two different codeword matrices
δ	Cyclic delay of the CDD technique
$\mathcal{CN}(0, 2\sigma^2)$	Normal distribution with zero mean and variance $2\sigma^2$
d_{min}	Minimum distance of the QAM constellation
d_{out}	Diversity gain associated to outage error probability
E_b	Average energy per bit
E_s	Average energy per symbol
η	Raw bit rate
f	Frequency

$\boldsymbol{G}$	Code generator complex matrix
$\mathfrak{G}$	List of candidates for the LFSD
$\boldsymbol{G}_R$	Code generator real-value matrix
$\boldsymbol{H}$	Channel matrix
h	SISO channel
$\boldsymbol{H}^{\dagger}$	Pseudoinverse of matrix $\boldsymbol{H}$
$\boldsymbol{H}_{eq}$	Equivalent channel matrix of $\breve{\boldsymbol{H}}\boldsymbol{G}$
$\breve{\boldsymbol{H}}$	Expanded channel matrix
$\boldsymbol{H}^{H}$	Hermitian matrix of $\boldsymbol{H}$
h_{nm}	Channel gain between transmit antenna m and receive antenna n
$\boldsymbol{I}_M$	$M \times M$ identity matrix
$\Im\{s\}$	Imaginary part of the symbol s
L	Number of taps or paths of a multipath channel
$L(b_k)$	LLR of a bit b_k
$L_A(b_k)$	*A priori* information of a bit b_k
L_D	*A posteriori* information
L_E	Extrinsic information
L_{FEC}	Length of a FEC block
$\mathcal{L}$	List of candidates for the LSD
M	Number of transmit antennas
m_c	Number of multiplications for the complex product
$\mathcal{M}$	Set of symbols of the constellation
m_d	Number of multiplications for the Euclidian distance calculation
N	Number of receive antennas
$\boldsymbol{n}$	Tree configuration vector for the LFSD

N_C	Number of payload carrier within a OFDM symbol
N_{cand}	Number of candidates in the list of LSD or LFSD decoders
N_{FFT}	Transmission mode
N_{FEC}	Number of FEC blocks per channel realisation
N_{MC}	Number of channel realisations or Monte Carlos
N_{mult}	Overall number of multiplications
N_{OFDM}	Number of OFDM symbols
n_T	Overall number of visited nodes in the LFSD
ω	Angular frequency
P	Number of points of a constellation
$P_e(\rho)$	Error probability at SNR ρ
$P(\mathbf{X} \rightarrow \hat{\mathbf{X}})$	Pair-wise error probability
Q	Number of coded symbols in the codeword
R	Hypersphere radius of the sphere decoder
r	Multiplexing gain
κ	Rank of a matrix
R_c	Code rate
$\Re\{s\}$	Real part of the symbol s
ρ	Signal to noise ratio
$\boldsymbol{R_{ss}}$	Covariance matrix of the transmitted signal $\boldsymbol{s}$
$\boldsymbol{s}$	Transmitted data symbol column vector
S	Spatial rate
$\hat{s}$	Hard estimate of symbol s
$S_{\mu\mu}$	Doppler power spectral density
s	Transmitted symbol

$\boldsymbol{S}$	$M \times K$ matrix of transmitted symbols
T	Time duration of the codeword
t	Time instant
τ	Tap delay
$\bar{\tau}$	Mean delay of the channel
τ_{rms}	Delay spread of the channel
T_C	Coherence time of channel
T_s	Sampling period
$\boldsymbol{U}$	Cholesky matrix of $\boldsymbol{H}_{eq}^H \boldsymbol{H}_{eq}$
$\boldsymbol{u}$	Vector of uncoded data bits
σ^2	Variance of noise per real component
$\boldsymbol{X}$	Codeword matrix or transmitted signal matrix
$\boldsymbol{x}$	Transmitted signal column vector
$\mathbb{X}$	Set of the mappable bit vectors into the constellation
$\boldsymbol{Y}$	Received signal matrix
$\boldsymbol{y}$	Received signal column vector
y	Received symbol
$\boldsymbol{Z}$	Additive white Gaussian noise matrix
$\boldsymbol{z}$	Additive white Gaussian noise column vector

Capítulo 1

Introducción

Hoy en día convivimos con múltiples sistemas de comunicaciones inalámbricas tales como redes de telefonía móvil, redes de área local WLAN (*Wireless Local Area Network*), redes de área metropolitana WMAN (*Wireless Metropolitan Area Network*) o redes de televisión y radio. Este gran mercado se renueva constantemente con nuevos estándares que optimizan el uso del limitado espectro electromagnético basándose en la tecnología digital. Uno de los sistemas inalámbricos que más tarde se ha incluido al tren de las comunicaciones digitales es la red de televisión terrestre. Europa ha adoptado el primer estándar europeo de televisión digital DVB-T (*Digital Video Broadcasting-Terrestrial*) [ETSI97] como alternativa a la televisión analógica. No obstante, este sistema no está completamente adoptado ya que muchos países europeos están actualmente en la transición analógico-digital debido al lento proceso de adaptación que supone el despliegue de una nueva red de televisión[1].

El sistema DVB-T fue creado en 1997 permitiendo tasas de información en torno a 20 Mbit/s con una buena calidad del servicio. Esto es equivalente a la transmisión de cuatro programas con definición estándar SDTV (*standard-definition television*) por canal. Sin embargo, debido a la continua aparición de nuevas técnicas que mejoran la capacidad y la robustez de los enlaces inalámbricos, el estándar DVB-T se ha quedado atrás en comparación con las tasas de información de cientos de Mbits/s ofrecidas por otros estándares emergentes como IEEE WLAN 802.11n o IEEE WMAN 802.16m. En consecuencia y debido también al desarrollo de la televisión de alta definición HDTV (*high-definition television*), una segunda generación de televisión digital terrestre, llamada DVB-T2, fue lanzada al mercado en 2009 [ETSI09] con el fin de aumentar la capacidad y la robustez de su predecesor hasta alcanzar tasas de bit de unos 40 Mbits/s. Esta tecnología de última generación incluye las técnicas de codificación de canal más potentes, los códigos LDPC (*low-density parity check*), y añade técnicas multiantena como la codificación espacio-frecuencial de bloque ortogonal OSFBC (*orthogonal space-frequency block coding*) [Tarokh99], las cuales permiten acercarse considerablemente al límite teórico de capacidad de Shannon [Shannon48].

[1] España ha realizado el apagón analógico de manera paulatina en las diferentes comunidades autónomas a lo largo del año 2010.

1.1 Motivación y Objetivos

La cada vez mayor demanda y oferta de información en el mercado de las telecomunicaciones, incluida la televisión, y la necesidad creada por el usuario (o por el operador) a la hora de acceder a la información en cualquier momento y/o lugar, genera una continua evolución hacia sistemas que soporten mayores tasas de información con la misma o mayor robustez en su recepción. El límite alcanzado con codificaciones potentes y modulaciones de alto orden en DVB-T2 obliga a la comunidad DVB a buscar otras alternativas para superar estas metas. La tecnología MIMO (*multiple-input multiple-output*) basada en la transmisión-recepción con múltiples antenas ha sido una de las soluciones más eficaces para obtener un incremento de la capacidad con un excelente rendimiento [Foschini96, Telatar99]. Al igual que en otros estándares de comunicación como IEEE WLAN 802.11n o WMAN 802.16e, la inclusión de técnicas MIMO es una propuesta de futuro para el desarrollo de nuevos estándares de televisión digital como DVB-NGH (*Digital Video Broadcasting - Next Generation Handheld*).

La utilización de la tecnología MIMO implica un mayor coste computacional en los algoritmos de detección en el receptor, el cual se traduce asimismo en un mayor coste económico del producto final. Aunque la implementación de estos algoritmos ya ha sido conseguida a nivel de *hardware* [Horseman03, Burg05] para otras tecnologías inalámbricas como WLAN, la alta complejidad de los sistemas de televisión (entrelazadores, codificaciones potentes, grandes tamaños de FFT (*fast Fourier transform*), etc.) hacen que su materialización a nivel de chip conlleve un mayor coste y latencia en los receptores. A esto se puede sumar las limitaciones energéticas y de tamaño que implicaría un producto dirigido a escenarios móviles. Por lo tanto, la búsqueda de un compromiso entre prestaciones y coste computacional resulta clave para la viabilidad de esta tecnología en televisión digital. La principal apuesta en la comunidad DVB son los códigos espacio-frecuenciales de bloque SFBC (*space-frequency block coding*) con los que se puede maximizar el compromiso entre multiplexación espacial y diversidad [Yao03]. La combinación de las técnicas SFBC con la codificación de canal LDPC (*low-density parity check*) de los estándares de última generación implica una detección y decodificación *soft* basada en la detección MAP (*maximum a posteriori*). En el caso de utilizar técnicas MIMO que añadan multiplexación espacial, la detección supone un elevado número de operaciones, especialmente para altos órdenes de modulación. Por lo tanto, el diseño de algoritmos de baja complejidad es crucial para una implementación práctica a nivel de chip.

Así pues, los objetivos principales de esta tesis son:

- Análisis de las técnicas multiantena basadas en codificación espacio-frecuencial sobre escenarios TDT (televisión digital terrestre).

- Desarrollo de algoritmos de detección y decodificación para la inclusión de tecnología

MIMO en futuros estándares de televisión digital.

Para la consecución de los objetivos principales se han propuesto unos objetivos parciales o hitos definidos a continuación:

- Definición de los modelos de propagación dentro de la red TDT.
- Evaluación del rendimiento de los códigos SFBC en diferentes escenarios de televisión estableciendo un compromiso entre eficiencia y complejidad.
- Busqueda de alternativas de baja complejidad para la detección y decodificación de técnicas MIMO combinadas con códigos LDPC con el objetivo de una posible implementación real en *hardware*.

1.2 Contribuciones de la Tesis

Esta sección describe las contribuciones principales de la tesis indicando las publicaciones asociadas a las diferentes aportaciones:

- Análisis comparativo de rendimientos entre las técnicas de diversidad CDD (*cyclic delay diversity*), SFBC y MRC (*maximum ratio combining*) en escenarios de recepción fija y móvil para DVB-T.
- Estudio de las técnicas de diversidad incluidas en el estándar DVB-T2 sobre canales Rayleigh y Ricean.
- Resultados de simulación de la recepción SISO (*single-input single-output*) de señales DVB-T y DVB-T2 en redes SFN (*single frequency network*) afectada por interferencia de varios transmisores. Este trabajo ha sido publicado en [Sobron09a, Sobrón09b].
- Estudio de rendimientos del esquema MISO (*multiple-input single-output*) distribuido de DVB-T2 en una red SFN en función del retardo y atenuación de las señales transmitidas [Sobrón10d].
- Estudio y desarrollo de una apróximación *soft* MAP para códigos FRFD (*full-rate full-diversity*) SFBC en sistemas con tecnología DVB-T2 basada en listas de candidatos detectados. Se realiza una optimización del sistema en función del número de candidatos necesarios y se presenta una comparación de rendimientos entre los códigos FRFD Golden y Sezginer-Sari y el código DVB-T2 SFBC sobre escenarios de TDT. El trabajo ha sido publicado en [Sobron10c].

- Diseño de un algoritmo de ordenación para la detección *soft* de códigos FRFD empleando un decodificador esférico de complejidad fija LFSD (*list fixed-complexity sphere decoder*). Estudio de optimización del algoritmo basado en la configuración de la búsqueda en árbol y el número de candidatos. Se efectúa un análisis comparativo de rendimientos y de complejidad del decodificador LFSD propuesto y el algoritmo LSD para escenarios de televisión digital terrestre (TDT). Este trabajo está bajo revisión para su posible publicación en [Sobron10a, Sobron10b].

1.3 Estructura de la Tesis

La memoria de la tesis está estructurada en seis capítulos. Este primer capítulo ha servido para introducir al lector en el tema de la tesis y presentar la motivación que ha llevado al autor a la realización del trabajo, así como sus principales objetivos.

El capítulo 2 se centra en los dos pilares sobre los que se desarrolla este trabajo; por un lado, los estándares europeos de televisión digital terrestre y por otro, los sistemas inalámbricos multiantena. La primera parte describe los estándares DVB-T y DVB-T2, dando mayor relevancia a las etapas de codificación de canal y modulación de ambos sistemas. En la segunda parte, se detallan las características principales de la transmisión MIMO y se define el modelo matemático del sistema utilizado a lo largo de la tesis. Asimismo, se realiza una revisión bibliográfica de las técnicas de diversidad multiantena que han sido propuestas para su posible inclusión en futuros estándares de televisión digital.

El capítulo 3 analiza el rendimiento las técnicas de diversidad que mejor se ajustan a la red terrestre de televisión en diferentes ambientes de radiodifusión tanto de DVB-T como de DVB-T2. En primer lugar se define un modelo de canal multitrayecto que caracteriza los posibles escenarios de recepción dados en la red de TDT tanto para redes de frecuencia única como múltiple. Asimismo, se presentan diferentes resultados de simulación sobre escenarios estáticos y móviles de DVB-T. En el caso de DVB-T2, se analizan especialmente las técnicas de diversidad incluidas en el estándar y se describe la detección *soft* necesaria para la decodificación LDPC, ya que resultará un punto clave en los siguientes capítulos. En último lugar, se realiza un análisis de la detección en redes SFN para los sistemas SISO y MISO distribuido de DVB-T2.

El capítulo 4 se centra en el estudio de viabilidad de las técnicas de diversidad que incluyen multiplexación espacial en futuros estándares de televisión digital, tales como los códigos FRFD SFBC. Los resultados se presentarán sobre el sistema DVB-T2 ya que incluye la última tecnología en comunicaciones inalámbricas y es considerado un referente para el desarrollo de nuevos sistemas de televisión como DVB-NGH. En la primera parte, se redefinen las ecuaciones de la detección *soft* para códigos FRFD SFBC y se plantea la detección MAP basada en una lista de candidatos debido a la alta complejidad que supone una detección

exhaustiva. Un análisis comparativo de diferentes códigos SFBC, incluido el propuesto en el estándar DVB-T2, es presentado mediante curvas de BER. El capítulo finaliza analizando la reducción de complejidad de la detección basada en decodificadores esféricos de lista.

El capítulo 5 presenta el rediseño de un decodificador esférico de lista con complejidad fija LFSD para códigos FRFD SFBC incluyendo el respectivo análisis de rendimiento y complejidad. La primera parte del capítulo define el nuevo algoritmo de ordenación para los códigos FRFD donde se analiza la relación existente entre la ordenación y la estructura del código. Asimismo, se evalúa el número de candidatos necesario para obtener la máxima eficiencia del algoritmo con el menor coste. Posteriormente, se presentan los resultados de rendimiento para diferentes configuraciones y complejidades efectuando el análisis comparativo con el decodificador esférico de lista de complejidad variable. Finalmente, se realiza un estudio de complejidad considerando el número de operaciones del algoritmo propuesto.

Por último, el capítulo 6 resume el trabajo realizado y las principales conclusiones obtenidas, así como las líneas futuras que el autor plantea para ampliar el trabajo presentado en esta tesis. El apéndice A muestra un listado completo de las publicaciones realizadas a lo largo del periodo de investigación.

Chapter 2

Background and Related Work

2.1 Introduction

Due to the well-known potential of multiple-input multiple-output (MIMO) techniques, the inclusion of multi-antenna processing in digital television (DTV) systems has been a constant research topic since the launch of the first European standard of Digital Video Broadcasting - Terrestrial (DVB-T) [ETSI97]. Diversity techniques and their combination with spatial multiplexing are some of the transmission strategies that have been considered on the development of DTV standards. Moreover, one of the main current topics is the trade-off between performance and implementation complexity, since the addition of space-time coding involves a higher computational cost for detection at the receiver, which must be justified by a performance increase. Therefore, the analysis of these schemes over terrestrial DTV scenarios and the corresponding detection complexity, which are the aim of this thesis, are of great importance in order to get to a feasible and efficient multi-antenna implementation.

As a starting point, this chapter offers a theoretical background on the aforementioned topics, concretely terrestrial digital television (TDT) systems and multi-antenna diversity techniques. The first part of the chapter introduces the European TDT standards, DVB-T and the second generation of Digital Video Broadcasting - Terrestrial (DVB-T2), which have been the main scenarios for the transmission and detection techniques analyzed in this thesis.

In the second part of the chapter, we define the MIMO channel model and review the multi-antenna channel capacity properties, paying special attention to two of the potential benefits of multi-antenna transmission, spatial multiplexing and diversity. Finally, the last part of the chapter focuses on the kinds of diversity and discusses the most important transmission schemes, both with and without spatial multiplexing.

2.2 Terrestrial Digital Television

The delivery of DTV services can be given through multiple means of transmission such as cable or satellite networks. However, one of the most extended is the TDT system, prob-

ably due to the direct evolution of analogue television (TV). Currently, there exist several standards of TDT broadcasting in the world, being the following four considered the most important: the American ASTC (Advanced Television System Committee) [ATSC05], the Japanese ISDB-T (Integrated Services Digital Broadcasting - Terrestrial) [ARIB01], the Chinese DTMB (Digital Terrestrial Multimedia Broadcast) [SAC06] and the European DVB-T [ETSI97]. In this research we have focused on the European standard DVB-T and its second generation DVB-T2, both based on the orthogonal frequency-division multiplexing (OFDM) technique. However, the rest of the physical layer specification is completely different, since the aim of DVB-T2 is to provide a robust reception with an increment of the capacity under similar channel conditions used by DVB-T. Therefore, DVB-T2 changes drastically the physical layer of DVB-T and includes the latest techniques of wireless communications and signal processing at the present. Both European standards are summarized in the following sections so as to introduce the reader to the terrestrial DTV systems.

2.2.1 DVB-T

The DVB-T system [ETSI97] is the first generation standard of terrestrial digital television broadcasting in Europe. It was created by the European Digital Video Broadcasting (DVB) consortium in 1997 and has been adopted by all the European countries and many others worldwide. Although DVB-T is a consolidated system in western Europe, there are still countries that are in the analogue-to-digital transition and others that have not even launched it yet. Therefore, the deployment of DVB-T networks is still a topic of interest in many places of the world.

The system is structured in two layers: data link layer and physical layer. On one hand, the data link layer acts on the digital video, audio and data of different programmes, which are compressed as Moving Picture Experts Group 2 (MPEG-2), and multiplexed into a transport stream (TS). On the other hand, the physical layer adapts the information for aerial terrestrial transmission by means of coding and modulation, resulting in a coded orthogonal frequency-division multiplexing (COFDM) system. Figure 2.1 shows the block diagram of DVB-T, whose three main stages are explained below.

2.2.1.1 MPEG-2 Source Coding and Multiplexing

As we have already stated, every programme contains digital video, audio and data. The information of each programme is compressed in MPEG-2 format [ISO00] and then several programmes are multiplexed generating a bit stream called MPEG-2 TS.

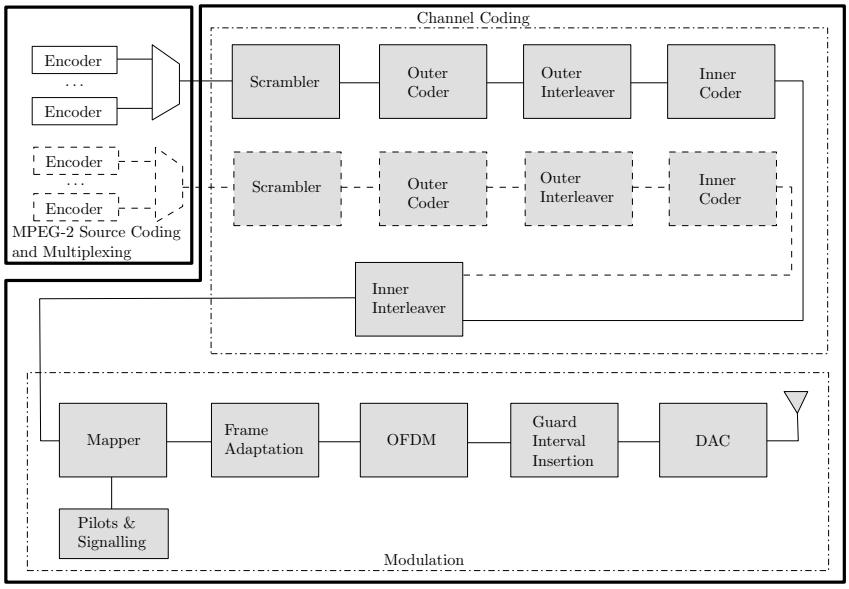

Figure 2.1: The DVB-T transmission scheme.

2.2.1.2 Channel Coding

This stage adds redundant information for error correction at the receiver side and consists of several concatenated steps, as it is shown in Figure 2.1.

- Scrambler: the TS signal is randomized for energy dispersal.
- Reed-Solomon (RS) code: the shortened code RS(204,188,t=8) generates an error protected packet that can detect and correct up to 8 wrong bytes per packet. The RS code removes the error floor of the inner code at high signal to noise ratio (SNR).
- Outer interleaver: it consists of convolutional byte-wise interleaving with a depth of 12 branches.
- Convolutional code: it is based on a mother convolutional code of rate 1/2 with 64 states that allows several rates using puncturing.
- Inner interleaver: its structure is formed by bit-wise and symbol interleaving.

DVB-T allows hierarchical transmission of two input stream (solid and dashed blocks in Figure 2.1) with different code rates and modulation. However, no country has implemented this kind of system at the present.

2.2.1.3 Modulation

The modulation stage is based on OFDM, making it robust against severe channel conditions such as fading, and simplifying the channel equalization at reception. The input bits

from channel coding stage are mapped onto complex constellations using Gray mapping in such a way that all data carriers of the OFDM symbol bear either quadrature phase shift keying (QPSK), 16-quadrature amplitude modulation (QAM) or 64-QAM signals. In addition to the data symbol carriers, the OFDM symbol contains scattered pilots, continual pilots and transmission parameter signalling (TPS) carriers. Pilots are basically used for synchronization, channel estimation and transmission mode identification. Each OFDM symbol can consist of 6817 and 1705 useful carriers in 8K and 2K modes, respectively. The reminder of carriers are filled with zeros in order to allow for frequency guard bands. Finally, the guard interval (GI), which consists of a cyclic prefix of the signal, is added before the digital to analogue conversion (DAC).

2.2.2 DVB-T2

The second generation of DVB-T was released in 2009 [ETSI09]. DVB-T2 completely modifies the physical layer of its predecessor and includes technologies that have been added in other last-generation wireless communication standards such as the second generation of satellite DTV broadcasting DVB-S2 [ETSI06] or IEEE 802.16e (WiMAX).

Based on recent research results and a set of commercial requirements, the DVB consortium concluded that there were suitable technologies which could provide increased capacity and robustness in the terrestrial environment, mainly for high definition television (HDTV) transmission. DVB-T2 has been primarily designed for fixed receptors, although it must allow for some mobility with the same spectrum characteristics as DVB-T. Figure 2.2 shows the main stages of a DVB-T2 transmitter, where dashed lines represent optional blocks. DVB-T2 contains other previous stages before the represented system, but they are not described since they are not relevant for our research, which focuses on baseband algorithms.

The system is structured in three parts: bit interleaved coded modulation (BICM), frame building and finally, OFDM generation. The system inputs are called physical layer pipes (PLPs) and consist of one or more logical data streams from TS de-multiplexing.

2.2.2.1 Bit Interleaved Coded Modulation

The first remarkable novelty lies on the error correction strategy. The concatenation of low-density parity check (LDPC) [Gallager63] and Bose-Chaudhuri-Hocquenghem (BCH) codes offers a significant improvement compared to the convolutional error correcting scheme used in DVB-T.

The output bits of the LDPC encoder are bit-interleaved by parity and column twist interleavers. The bit stream is then de-multiplexed in order to create cell words that are Gray mapped using either QPSK, 16-QAM, 64-QAM or 256-QAM constellations. Notice that the highest constellation size has been increased to 256 symbols rising the maximum

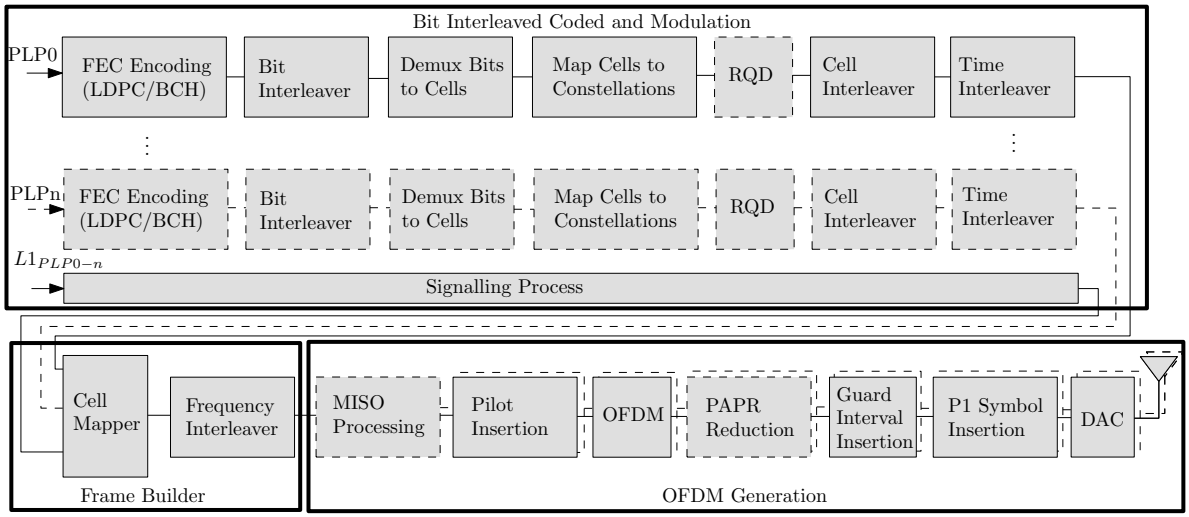

Figure 2.2: The DVB-T2 transmission scheme.

capacity of the system. On the other hand, binary phase shift keying (BPSK) is used for L1 signalling where the transmission mode information is borne.

A new technique called constellation rotation and cyclic Q-delay (RQD) is provided as optional [Nour08] after the mapping process. This technique rotates the constellation correlating the in-phase (I) and quadrature (Q) components, which are transmitted in different carriers thanks to the Q-delay as we can observe in Figure 2.3. This offers additional diversity and consequently, robustness in fading scenarios.

Next, a pseudo-random cell interleaver spreads the cells uniformly in the forward error correction (FEC) codeword in order to ensure an uncorrelated distribution of channel distortions. The BICM stage ends with a time interleaver, which operates at PLP level and, depending on the length of the frames, in a different way for each PLP. This interleaver is the main agent that allows DVB-T2 to support mobile scenarios, obtaining diversity from the temporal variations of the channel.

2.2.2.2 Frame Builder

In this stage, modulated cells are combined in order to generate the next OFDM symbols. The cell mapper of the frame builder assembles cells of PLPs and L1 signalling into data cell arrays corresponding to OFDM carriers, which are then mapped by the frequency interleaver onto each OFDM symbol.

2.2.2.3 OFDM Generation

In the same way as DVB-T, the second-generation standard uses OFDM maintaining the DVB-T 2K and 8K modes, and including longer symbols with 16K and 32K carriers in order to increase the length of the guard interval without decreasing the spectral efficiency of the

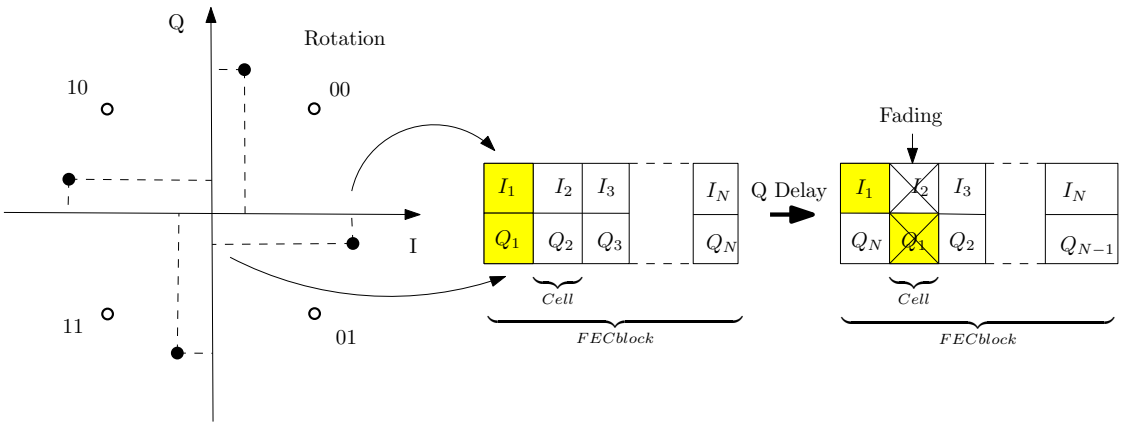

Figure 2.3: Constellation rotation and cyclic Q-delay.

system. The new specification offers a large set of transmission modes by combining different numbers of carriers and guard interval lengths, making it very flexible for different scenarios. Another interesting novelty is the addition of eight different scattered pilot patterns, whose election will depend on the transmission environment. At the end of the OFDM generation process, the preamble symbol P1 is inserted for fast recognition of DVB-T2 signals [ETSI09]. This preamble carries basic transmission parameters and synchronization patterns.

Besides the fixed blocks of this stage, two optional techniques have been included. On one hand, DVB-T2 takes into account one of the main drawbacks of OFDM, the peak-to-average power ratio (PAPR) of the signal and its effects on the transmitter equipments. High power peaks are usually generated by OFDM transmission leading to distortions at the power amplifiers. Two techniques limit the PAPR without degrading the transmitted signal: carrier reservation and active constellation extension. The former reserves some subcarriers that can be used to correct the PAPR level of the transmitted signal whereas the latter achieves the same effects modifying the QAM constellation without degrading the signal recovery at reception. On the other hand, DVB-T2 also specifies a multi-antenna diversity method based on the well-known Alamouti code [Alamouti98], focused on improving the coverage in small scale single-frequency networks. This method directly concerns with our research work and will be described in further sections, which will introduce the reader to multi-antenna processing.

2.3 Multi-Antenna Wireless Systems

The use of multiple transmit and receive antennas in a scattering wireless communication link is one of the most promising means for achieving a high data rate transmission with good quality of service [Foschini98, Telatar99]. As we will explain later, that capacity increment can be exploited in two main ways: spatial multiplexing (SM) and space-time coding (STC) [Gesbert03]. The first one splits the information sequence into M parallel streams that are

transmitted independently from the M transmit antennas, maximizing the transmission rate, whereas the second one uses the spatial and time domains to introduce redundancy. Thus, transmission errors are minimized at the receiver exploiting the MIMO fading channel.

2.3.1 System and Channel Model

First of all, we define a narrowband MIMO channel model as shown in Figure 2.4, which depicts a wireless communication link with M transmit and N receive antennas. At each time instant, M signals $x_1, \ldots, x_M$ are transmitted by M antennas satisfying an overall transmit power constraint. Here, combinations of the transmitted signals are received at each of the N antennas. If we consider a code length T that is shorter than the coherence time[1] T_C of the channel, i.e. $T < T_C$, we can rewrite the MIMO transmission model in matrix form as

$$\begin{bmatrix} y_{11} & \cdots & y_{1T} \\ y_{21} & \cdots & y_{2T} \\ \vdots & \ddots & \vdots \\ y_{N1} & \cdots & y_{NT} \end{bmatrix} = \begin{bmatrix} h_{11} & \cdots & h_{1M} \\ h_{21} & \cdots & h_{2M} \\ \vdots & \ddots & \vdots \\ h_{N1} & \cdots & h_{NM} \end{bmatrix} \begin{bmatrix} x_{11} & \cdots & x_{1T} \\ x_{21} & \cdots & x_{2T} \\ \vdots & \ddots & \vdots \\ x_{M1} & \cdots & x_{MT} \end{bmatrix} + \begin{bmatrix} z_{11} & \cdots & z_{1T} \\ z_{21} & \cdots & z_{2T} \\ \vdots & \ddots & \vdots \\ z_{N1} & \cdots & z_{NT} \end{bmatrix}, \quad (2.1)$$

which is equivalent to

$$\boldsymbol{Y} = \boldsymbol{H}\boldsymbol{X} + \boldsymbol{Z}, \quad (2.2)$$

where $\boldsymbol{H}$ denotes the $N \times M$ complex channel matrix whose coefficient h_{ij} represents the channel between transmit antenna j and receive antenna i, $\boldsymbol{X}$ is the $M \times T$ transmit signal or codeword matrix, $\boldsymbol{Z}$ represents the independent and identically distributed (IID) additive

[1] **Coherence time**: the time interval over which the channel may be considered constant.

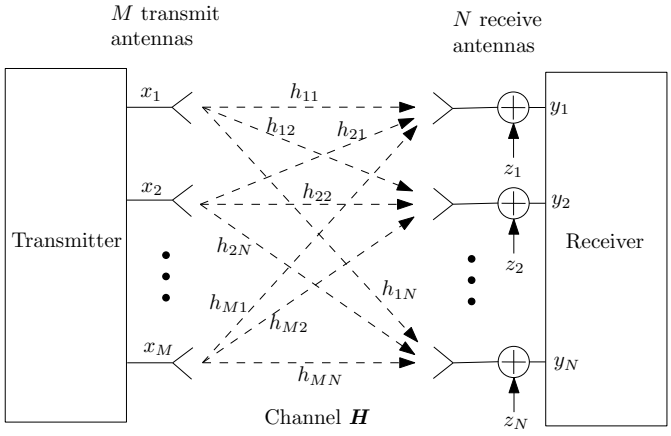

Figure 2.4: MIMO channel with M transmit and N receive antennas.

white Gaussian noise (AWGN) matrix with zero mean and variance per dimension σ^2, i.e. $z_{ij} \in \mathcal{CN}(0, 2\sigma^2)$ $1 \leq i \leq N$ and $1 \leq j \leq T$, and $\boldsymbol{Y}$ is the received signal matrix. Note that each column of the matrix $\boldsymbol{X}$ is the vector $\boldsymbol{x}$ of symbols transmitted simultaneously by all the transmit antennas; and each row corresponds to the signal transmitted by one antenna over time. Performing coding across rows of $\boldsymbol{X}$ is considered spatial coding, whereas it is referred to as time-domain coding when is carried out across columns. In other words, $\boldsymbol{X}$ is considered the codeword of a space-time code formed by a linear combination of Q data symbols where $Q \leq \min(M, N)T$. The channel matrix $\boldsymbol{H}$ and the transmitted signal matrix $\boldsymbol{X}$ obey the power constraints

$$\mathrm{E}\left[\mathrm{Tr}\left(\boldsymbol{H}\boldsymbol{H}^H\right)\right] = MN \quad \text{and} \quad \mathrm{E}\left[\mathrm{Tr}\left(\boldsymbol{X}\boldsymbol{X}^H\right)\right] = E_s T = MT, \tag{2.3}$$

where $(\cdot)^H$ denotes conjugate transpose of a matrix and $\mathrm{Tr}(\cdot)$ is the trace of a matrix. Note that we have considered the average total transmitted energy per time instant as $E_s = M$.

When we work with STC, Equation (2.2) is often rewritten for simplicity. This way, our system can be rearranged as an equivalent $NT \times MT$ MIMO channel where there is no channel interference between the different time slots $t = 1, \ldots, T$. Thus, the equivalent channel can be expressed as

$$\breve{\boldsymbol{H}} = \begin{bmatrix} \boldsymbol{H}_1 & \boldsymbol{0} & \ldots & \boldsymbol{0} \\ \boldsymbol{0} & \boldsymbol{H}_2 & \ldots & \boldsymbol{0} \\ \vdots & \vdots & \ddots & \vdots \\ \boldsymbol{0} & \boldsymbol{0} & \ldots & \boldsymbol{H}_T \end{bmatrix}, \tag{2.4}$$

where we have a block diagonal of channel realizations $\boldsymbol{H}_t$ at time instants $t = 1, \ldots, T$ and the off-diagonal entries are zero matrices with dimensions $N \times M$. Note that we have distinguished $\boldsymbol{H}_t$ for $t = 1, \ldots, T$ since they are equal if and only if $T < T_C$. In that case, $\boldsymbol{H}_t = \boldsymbol{H}\ \forall t$.

Now, we restructure matrices $\boldsymbol{X}$, $\boldsymbol{Y}$ and $\boldsymbol{Z}$ taking the elements column-wise into the column vectors $\boldsymbol{x} = [x_{11}, x_{21}, \ldots, x_{M-1T}, x_{MT}]^T$, $\boldsymbol{y} = [y_{11}, y_{21}, \ldots, y_{N-1T}, y_{NT}]^T$ and $\boldsymbol{z} = [z_{11}, z_{21}, \ldots, z_{N-1T}, z_{NT}]^T$, respectively. Thus, if we consider that $\boldsymbol{G}$ is the complex code generator matrix of the rearranged codeword $\boldsymbol{x}$, (2.2) can be given as

$$\boldsymbol{y} = \breve{\boldsymbol{H}}\boldsymbol{G}\boldsymbol{s} + \boldsymbol{z} = \boldsymbol{H}_{eq}\boldsymbol{s} + \boldsymbol{z}, \tag{2.5}$$

where $\breve{\boldsymbol{H}}\boldsymbol{G}$ forms the equivalent channel matrix $\boldsymbol{H}_{eq}$ and $\boldsymbol{s}$ corresponds to the data symbol column vector $[s_1, s_2, \ldots, s_Q]^T$.

Finally, let us define the average SNR of the wireless system per antenna and symbol time as

$$\rho = \frac{E_s}{2\sigma^2}. \tag{2.6}$$

2.3.2 Channel Capacity

The channel capacity is the theoretical limit of the amount of data we can transmit through a channel with reliability, i.e. with arbitrarily low error rate. This was first derived by Shannon for a single antenna narrowband channel [Shannon48]. For such a system, the channel capacity per Hz can be written as

$$C_{SISO} = \log_2 \left(\det \left(1 + \rho \left| h \right|^2 \right) \right) \text{ b/s/Hz}, \tag{2.7}$$

where $\det(\cdot)$ denotes the determinant function and h is the complex single-input single-output (SISO) channel.

For the capacity analysis of MIMO systems, we assume perfect channel knowledge at the receiver. This assumption is sensible since training or pilot signals are always transmitted in order to learn the channel in the DTV systems. In order to simplify notation, we consider $T = 1$ and the transmitted signal as a column vector $\boldsymbol{s}$. Hence, the capacity of a flat deterministic MIMO channel is given by [Foschini96, Telatar99]

$$C_{MIMO} = \max_{\mathrm{Tr}(\boldsymbol{R_{ss}})=E_s} \log_2 \left(\det \left(\boldsymbol{I}_N + \frac{\rho}{M} \boldsymbol{H} \boldsymbol{R_{ss}} \boldsymbol{H}^H \right) \right) \text{ b/s/Hz}, \tag{2.8}$$

where $\boldsymbol{I}_N$ is the identity matrix of dimensions $N \times N$ and $\boldsymbol{R_{ss}}$ is the covariance matrix of the transmitted signal $\boldsymbol{s}$. The covariance matrix $\boldsymbol{R_{ss}}$ must satisfy $\mathrm{Tr}(\boldsymbol{R_{ss}}) = E_s$ in order to constrain the total average energy transmitted over a symbol period, while $\boldsymbol{s}$ is assumed to have zero mean [Paulraj03].

Given that our system's channel has no preferred direction and is completely unknown to the transmitter, the best solution is to distribute the input power equally among the transmit antennas, i.e. $\boldsymbol{R_{ss}} = \boldsymbol{I}_M$. Therefore, the channel capacity of (2.8) can be rewritten as

$$C_{MIMO} = \log_2 \left(\det \left(\boldsymbol{I}_N + \frac{\rho}{M} \boldsymbol{H} \boldsymbol{H}^H \right) \right) \text{ b/s/Hz}. \tag{2.9}$$

If the channel was known at the transmitter side, it would be possible to choose a better input distribution $\boldsymbol{R_{ss}}$ and improve the channel capacity. Nevertheless, this is not the aim of this research, since it is not possible in TDT broadcasting scenarios.

2.3.3 Diversity-Multiplexing Trade-Off

The use of a MIMO channel can provide us of both data rate gain and increased robustness. However, there is a trade-off between these two types of gains; achieving more of one kind requires sacrifice of the other. This trade-off was defined and analyzed in [Zheng03]. First of all, we introduce the definition of diversity and multiplexing gains and then review the two transmit and two receive antenna case, which is the most significant case for our research.

For a given SNR ρ, let $R(\rho)$ be the transmission data rate and $P_e(\rho)$ the error probability at that rate. Thus, the diversity gain d and the spatial multiplexing gain r are defined as

$$d = -\limsup_{\rho\to\infty} \frac{\log P_e(\rho)}{\log \rho}, \tag{2.10}$$

and

$$r = \lim_{\rho\to\infty} \frac{R(\rho)}{\log \rho} \tag{2.11}$$

where sup denotes the supremum of the diversity advantage achieved over all the schemes for each r.

Therefore, the diversity gain describes how fast error probability decays asymptotically with SNR and will be directly related to the slope of the error probability curves. On the other hand, multiplexing gain offers information about how fast the data rate grows with SNR. The relation between these two parameters give us the diversity-multiplexing trade-off and can be used to evaluate and compare coding schemes.

In order to simplify calculation, [Zheng03] uses $\doteq$ to denote *exponential equality*, such that $f(\rho) \doteq \rho^b$ denotes

$$b = \limsup_{\rho\to\infty} \frac{\log f(\rho)}{\log \rho}. \tag{2.12}$$

Thus, (2.10) can be written as

$$P_e(\rho) \doteq \rho^{-d}. \tag{2.13}$$

With these definitions, we recall the main theorem of [Zheng03] for a system of M transmit and N receive antennas:

Theorem 1 *Assume $T > M + N - 1$. The optimal trade-off curve $d_{out}(r)$ is given by the piece-wise linear function connecting the points $(k, d_{out}(k)), k = 0, \ldots, K$ where $K = \min(M, N)$ and*

$$d_{out}(k) = (M - k)(N - k). \tag{2.14}$$

Note that the trade-off $d_{out}(r)$ is associated with the outage probability instead of the error probability and, consequently, this is an upper bound of the optimal trade-off achievable

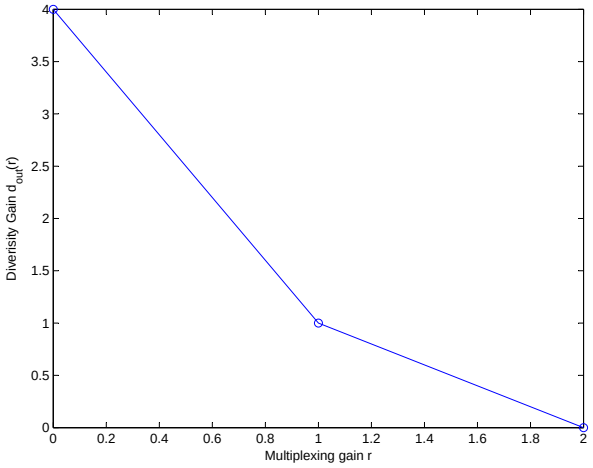

Figure 2.5: Optimal diversity-multiplexing trade-off curve for a two transmit and two receive antenna transmission.

by any system. The diversity-multiplexing trade-off $d_{out}(r)$ is represented in Figure 2.5 for the case of two transmit and two receive antennas. We can observe that the maximum diversity of this system is $MN = 4$ when $r = 0$, i.e. error probability decays with upper bound ρ^{-4} when data rate is kept constant and, on the other hand, there is a multiplexing gain of 2 b/s/Hz per 3 dB of SNR with zero diversity gain. Therefore, a bit rate increase of 2 bits leads to a shift of 3 dB in SNR for the same error probability.

In section 2.3.5, we present the diversity-multiplexing trade-off curve for orthogonal space-time block coding (OSTBC) and we see how this repetition code is sub-optimal.

2.3.4 Diversity Types

As has been stated, diversity is seen as how fast error probability decays and is represented by the slope of the bit error rate (BER) curve at high SNR. Diversity is related to the robustness of the system and depends on the number of transmit-receive antennas and the information redundancy, which can be generated in many different ways.

Different criteria appear in the literature in order to enumerate kinds of diversity. Nevertheless, all of them follow a similar pattern, classifying them according to a main parameter that represents the application area of the diversity. The three main criteria of classification are according to:

- The physical magnitude where the redundancy is generated.
- The algorithm which is used.
- The channel side, i.e. transmission or reception.

Any of the options will be used in order to specify the diversity class throughout this work. However, the classification regarding the physical magnitude will be used in general form to define the diversity classes.

2.3.4.1 Spatial Diversity

As we have mentioned, diversity depends on the number of antennas at both transmitter and receiver side. Therefore, the name of this kind of diversity comes from the own location of the antennas. The different subchannels between several transmit and receive antennas allow to obtain different observations of the same transmitted signal increasing the reliability of the wireless link. If subchannels are uncorrelated to each other, they fade independently. This allows to complement a faded signal with an enhanced one reducing the error rate in reception. Several works have proved that the distance between antennas is directly related to the subchannel correlation [Sanchez-Varela01]. Furthermore, it has to be longer than half a wavelength in order to consider complete uncorrelation.

The selective combining (SC) [Rinne00] or equal gain combining (EGC) techniques are some of the receive diversity methods that improve the reception quality. Nevertheless, the technique known as maximum ratio combining (MRC) [Proakis95] is considered the best solution at reception. Assuming perfect channel knowledge at the receiver, MRC combines N received signals (independent faded versions of the same transmitted signal x) according to

$$y_{MRC}(t) = \sum_{i=1}^{N} \left(\sum_{j=1}^{M} h_{ij}(t) \right)^{*} y_i(t), \tag{2.15}$$

where $(\cdot)^{*}$ denotes complex conjugate. Thus, the post-processing SNR, ρ_{MRC}, is maximized at the time instant t becoming

$$\rho_{MRC} = \frac{1}{N} \sum_{i=1}^{N} \left| \sum_{j=1}^{M} h_{ij} \right|^2 \rho. \tag{2.16}$$

Most of MIMO techniques present spatial diversity gain and often exploit other dimension in order to achieve more degrees of freedom. For instance, the techniques based on STC or space-frequency coding (SFC), that are the most studied in DTV, combine spatial diversity with time or frequency diversity, respectively.

2.3.4.2 Time Diversity

The information is sent repeatedly over time in such a way that each repetition is separated by the coherence time T_C in order to undergo different fading channels. This redundancy reduces the data rate and increases the latency of the system. Therefore, this kind of diversity

is rarely used individually and is combined mainly with spatial diversity.

2.3.4.3 Frequency Diversity

In the case of frequency diversity, the same information is shared in different carriers separated the coherence bandwidth[2], B_C. Its utilization is very common in frequency-division multiplexing (FDM) systems where the frequency diversity is achieved through coding and interleaving. Another example is the RQD technique of DVB-T2 (see Figure 2.3) that shares correlated information of the I and Q components of a QAM symbol in different carriers. The frequency diversity can also be combined with multi-antenna processing through SFC with the same methodology as STC.

2.3.4.4 Polarization Diversity

Polarization diversity is based on the signal transmission using antennas with different polarization (usually orthogonal polarization). The uncorrelation among different polarized signals allows us to implement this multi-antenna technique in small devices without taking into account the minimum antenna distance of half a wavelength. This technology has been widely studied in DTV systems such as DVB-T [Sanchez-Varela00, Guena04, Corre05, Fluerasu05, Mitchell06, Moss08] or Digital Video Broadcasting - Handheld (DVB-H) [ETSI04] for handheld terminals [Kyro07], and is currently an area of analysis [Gomez-Calero09] in the standardization process of the next generation of DVB-H, known as DVB-NGH.

2.3.4.5 Angular Diversity

This sort of diversity is related to the beam pattern of the antennas. The replicas of the transmitted signal can undergo different channels according to the main beams of the transmit and/or receive antenna arrays. In this way, mechanisms such as scattering or reflection give rise to different uncorrelated paths that allow the receiver to obtain diversity.

2.3.5 Space-Time and Space-Frequency Diversity Techniques

STC is an effective and practical way to approach the capacity of MIMO channels. Using several transmit/receive antennas, they achieve transmit diversity without sacrificing the bandwidth. There are various coding schemes, having been some of them analyzed and considered of interest for the development of broadcasting systems. Concretely, the well-known Alamouti technique [Alamouti98] and some delay diversity schemes have been the main candidates in last years. However, the inclusion of full rate STCs, which increase the

[2] **Coherence bandwidth**: the average frequency range over which channel can be considered flat, $B_C = \frac{1}{T_C}$.

data rate besides the diversity order, has recently taken more relevance in the standardization process of future DTV systems [Nasser08c], as we will see in the ensuing section.

This section revises some pure diversity schemes studied in TDT systems. First off, the OSTBC structure for 2×1 and 2×2 antenna setups is analyzed. Later, we discuss space-frequency block coding (SFBC) in OFDM systems and its equivalence to space-time block coding (STBC). Finally, we conclude with a simple space-frequency diversity scheme called cyclic delay diversity (CDD).

2.3.5.1 Orthogonal Space-Time Block Coding

The Alamouti code [Alamouti98] was the first OSTBC code, designed for two transmit antennas and extended to more general cases in [Tarokh99]. OSTBC encodes a two symbol vector $\boldsymbol{s} = [s_1, s_2]$ into a 2×2 transmitted signal matrix $\boldsymbol{X}$ as follows:

$$\boldsymbol{X}_{al} = \begin{bmatrix} s_1 & -s_2^* \\ s_2 & s_1^* \end{bmatrix}. \tag{2.17}$$

Thus, the vector $\boldsymbol{s}$ is sent from two antennas ($M = 2$) in two time slots ($T = 2$). Any number of receive antennas can be used. Nevertheless, we analyze the cases with $N = 1$ and 2, which are the most interesting for the considered broadcasting scenarios.

2.3.5.1.1 One Receive Antenna Assuming that the channel is quasi-static for two time slots, the resulting receive signal for $N = 1$ is

$$\begin{bmatrix} y_1 & y_2 \end{bmatrix} = \begin{bmatrix} h_1 & h_2 \end{bmatrix} \begin{bmatrix} s_1 & -s_2^* \\ s_2 & s_1^* \end{bmatrix} + \begin{bmatrix} z_1 & z_2 \end{bmatrix}. \tag{2.18}$$

Rearranging terms, this can be rewritten as

$$\begin{bmatrix} y_1 \\ y_2^* \end{bmatrix} = \underbrace{\begin{bmatrix} h_1 & h_2 \\ h_2^* & -h_1^* \end{bmatrix}}_{\boldsymbol{H}_{eq}} \begin{bmatrix} s_1 \\ s_2 \end{bmatrix} + \begin{bmatrix} z_1 \\ z_2^* \end{bmatrix}, \tag{2.19}$$

where we have obtained an equivalent channel matrix $\boldsymbol{H}_{eq}$ in the same way as in (2.5). The column vectors of $\boldsymbol{H}_{eq}$ are orthogonal to each other, so s_1 and s_2 can be decoupled, i.e. there is no interference between them, and component-wise decoding can be easily done.

This scheme achieves the full channel capacity of a 2×1 system [Hassibi02]. However, as we see later, this is not fulfilled for $N > 1$. On the other hand, OSTBC achieves the maximum diversity, i.e. $d = 2$ for $M = 2$ and $N = 1$, according to the rank criterion for STC in Rayleigh fading channels [Guey96, Tarokh98], that says:

Criterion 1 *(Rank criterion): In order to achieve maximum diversity, the matrix* $\boldsymbol{\Delta} =$

$\boldsymbol{X} - \hat{\boldsymbol{X}}$ has to be full rank for any codewords $\boldsymbol{X}$ and $\hat{\boldsymbol{X}}$. Then, the code is said to have full diversity. Otherwise, a diversity gain of $N\kappa$ is achieved being κ, the rank of $\boldsymbol{\Delta}$.

The rank criterion and the determinant criterion, which will be analyzed later, are relevant in order to maximize the gain of STC codes.

2.3.5.1.2 Two Receive Antennas For the case of $M = 2$ and $N = 2$, the resulting receive signal is

$$\begin{bmatrix} y_{11} & y_{12} \\ y_{21} & y_{22} \end{bmatrix} = \begin{bmatrix} h_{11} & h_{12} \\ h_{21} & h_{22} \end{bmatrix} \begin{bmatrix} s_1 & -s_2^* \\ s_2 & s_1^* \end{bmatrix} + \begin{bmatrix} z_{11} & z_{12} \\ z_{21} & z_{22} \end{bmatrix}, \tag{2.20}$$

which can be rewritten as

$$\begin{bmatrix} y_{11} \\ y_{21} \\ y_{12}^* \\ y_{22}^* \end{bmatrix} = \underbrace{\begin{bmatrix} h_{11} & h_{12} \\ h_{21} & h_{22} \\ h_{12}^* & -h_{11}^* \\ h_{22}^* & -h_{21}^* \end{bmatrix}}_{\boldsymbol{H}_{eq}} \begin{bmatrix} s_1 \\ s_2 \end{bmatrix} + \begin{bmatrix} z_{11} \\ z_{21} \\ z_{12}^* \\ z_{22}^* \end{bmatrix}, \tag{2.21}$$

where the orthogonality of the column vectors of $\boldsymbol{H}_{eq}$ is maintained. Therefore, low complexity decoding can also be done.

Using (2.8), the capacity of this system can be given as

$$\begin{aligned} C_{OSTBC}(\rho) &= \max_{\mathrm{Tr}(\boldsymbol{R_{ss}})=2} \frac{1}{2} \log_2 \left(\det \left(\boldsymbol{I}_2 + \frac{\rho}{2} \boldsymbol{H}_{eq} \boldsymbol{R_{ss}} \boldsymbol{H}_{eq}^H \right) \right) \\ &= \max_{\mathrm{Tr}(\boldsymbol{R_{ss}})=2} \frac{1}{2} \log_2 \left(\det \left(\boldsymbol{I}_2 + \frac{\rho}{2} \boldsymbol{H}_{eq}^H \boldsymbol{H}_{eq} \boldsymbol{R_{ss}} \right) \right), \end{aligned} \tag{2.22}$$

where the factor $\frac{1}{2}$ before the logarithm normalizes the extended equivalent channel $\boldsymbol{H}_{eq}$ due to the orthogonal design [Hassibi02]. Considering no channel information at the transmitter, i.e. $\boldsymbol{R_{ss}} = \boldsymbol{I}_2$, Equation (2.22) becomes

$$\begin{aligned} C_{OSTBC}(\rho) &= \max_{\mathrm{Tr}(\boldsymbol{R_{ss}})=2} \frac{1}{2} \log_2 \left(\det \left(\boldsymbol{I}_2 + \frac{\rho}{2} \left(|h_{11}|^2 + |h_{21}|^2 + |h_{12}|^2 + |h_{22}|^2 \right) \boldsymbol{I}_2 \right) \right) \\ &= \log_2 \left(1 + \frac{2\rho}{4} \left(|h_{11}|^2 + |h_{21}|^2 + |h_{12}|^2 + |h_{22}|^2 \right) \right) \\ &= C(2\rho, M = 4, N = 1) \\ &< C(\rho, M = 2, N = 2). \end{aligned} \tag{2.23}$$

The inequality in (2.23) implies that OSTBC does not reach the full channel capacity of a system with $M = 2$ and $N = 2$ but rather the capacity of a system with $M = 4$, $N = 1$

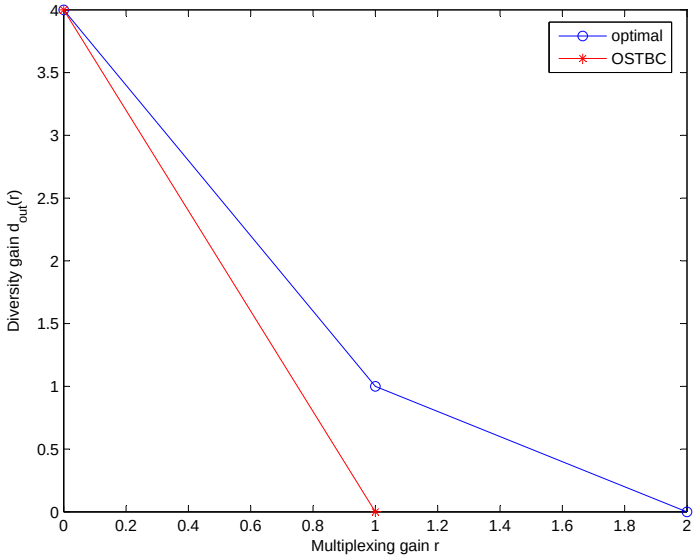

Figure 2.6: Comparison of optimal diversity-multiplexing trade-off curve and diversity-multiplexing trade-off achieved by OSTBC for two transmit and two receive antennas.

and doubled SNR. Although OSTBC does not achieve full channel capacity, this scheme is one of the most extended STC in wireless communication systems due to its low decoding complexity based on linear detection techniques.

If we examine the diversity-multiplexing trade-off of OSTBC with $M = 2$ and $N = 2$, we can see that, as for the previous case, it achieves the maximum diversity of $MN = 4$ when $r = 0$. Nevertheless, due to the code redundancy, only one new symbol is transmitted at each time slot and thus, it can only achieve $r = 1$ when $d = 0$ [Zheng03]. Therefore, as it can be seen in Figure 2.6, OSTBC does not provide optimal diversity-multiplexing trade-off and high SNR is essential for high data rate.

We now show below some of the simplest decoding and detection algorithms that can be used to decode OSTBC transmissions.

2.3.5.1.3 Linear Detection Techniques Due to the property of orthogonality, we have seen that symbols s_1 and s_2 of OSTBC are decoupled in (2.19) and (2.21). Therefore, they can be detected independently with an equivalent MRC [Alamouti98]. However, variations of channel throughout the transmission of $\boldsymbol{X}$ lead to a loss of orthogonality and consequently, a coupling between the symbols to be detected. Other low complexity decoding techniques can be used that do not require the orthogonality property. The simplest detection algorithms are the linear techniques, where the detected symbol vector $\hat{\boldsymbol{s}}$ is obtained by multiplying the received signal $\boldsymbol{y}$ in (2.5) by an equalization matrix $\boldsymbol{C}$ as follows

$$\hat{\boldsymbol{s}} = \boldsymbol{C}\boldsymbol{y}. \tag{2.24}$$

The two most common algorithms are the following:

1. **zero forcing (ZF)**: the elimination of the intersymbol interference requires the use of a channel-inverting filter, which is given by

$$\boldsymbol{C}_{ZF} = \boldsymbol{H}_{eq}^{\dagger} = \left(\boldsymbol{H}_{eq}^{H}\boldsymbol{H}_{eq}\right)^{-1}\boldsymbol{H}_{eq}^{H}, \tag{2.25}$$

   where $(\cdot)^{\dagger}$ denotes the pseudoinverse matrix. If $\boldsymbol{H}_{eq}$ is invertible, then $\boldsymbol{C}_{ZF} = \boldsymbol{H}_{eq}^{-1}$. This method is the easiest to implement but it has a limited performance due to the noise enhancement.

2. **minimum mean squared error (MMSE)**: This method minimizes the overall error taking into account the SNR for the calculation of the filter matrix $\boldsymbol{C}$ and thus, the noise enhancement is reduced. The matrix $\boldsymbol{C}_{MMSE}$ is obtained according to

$$\boldsymbol{C}_{MMSE} = \left(\boldsymbol{H}_{eq}^{H}\boldsymbol{H}_{eq} + \frac{M}{\rho}\boldsymbol{I}_{M}\right)^{-1}\boldsymbol{H}_{eq}^{H}. \tag{2.26}$$

2.3.5.2 Space-Frequency Block Coding

When systems are based on multi-carrier modulation schemes such as OFDM, coding is carried out in space and frequency domains. Since OFDM converts frequency-selective channels into multiple flat fading channels, the detection is simplified in the frequency domain, where the received signal is simply the product between the channel and the transmitted signal plus the noise term as in (2.2). Hence, codewords are fed into carriers of OFDM symbols which are transformed later to the time domain through the inverse fast Fourier transform (IFFT). At the receiver, the opposite process is carried out; the received signal is captured in time domain and is transformed to the frequency domain through fast Fourier transform (FFT) before being detected.

When the codeword is transmitted at the same carrier of several consecutive OFDM symbols, it is named STBC or STBC-OFDM [Lu00]. On the other hand, if the codeword is transmitted combining adjacent carriers of one OFDM symbol, it is named SFBC [Bolcskei00]. This technique has been adopted by the DVB-T2 standard [ETSI09] as an optional diversity transmission scheme. As we can observe in Figure 2.7, the DVB-T2 multiple-input single-output (MISO) model employs two antennas to transmit the Alamouti code [Alamouti98] across OFDM carriers. Although Alamouti code has been chosen as the MISO code for DVB-T2, any other STC scheme may be implemented in the same way.

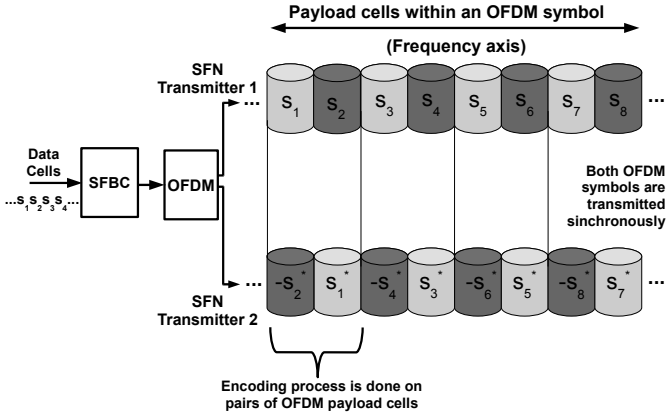

Figure 2.7: SFBC transmission scheme of DVB-T2 system.

If we pay attention to the MISO scheme of Figure 2.7, one should note that the codeword of (2.17) is slightly modified such that it is now expressed as

$$\boldsymbol{X}_{al} = \begin{bmatrix} s_1 & s_2 \\ -s_2^* & s_1^* \end{bmatrix}, \tag{2.27}$$

whose equivalent channel matrix is given by

$$\boldsymbol{H}_{eq} = \begin{bmatrix} h_1 & -h_2 \\ h_2^* & h_1^* \end{bmatrix}. \tag{2.28}$$

2.3.5.3 Cyclic Delay Diversity

This spatial and frequency diversity technique is a variation of the delay diversity (DD) scheme [Wittneben93] which was first adapted to OFDM systems in [Kaiser00] as phase diversity (PD) and later in [Dammann01] as CDD. In the DD method shown in Figure 2.8(a), the transmitted signal is identical for all transmit antennas, differing in a delay added per each antenna after the GI insertion. This simple technique generates an artificial multipath environment similar to an echo channel that achieves frequency selectivity of the signal spectrum at the receiver. The disadvantage of DD is that if the additional delays are longer than the GI, this can cause intersymbol interference and requires an extension of GI, reducing the bandwidth efficiency of the system. In contrast, CDD or its equivalent PD prevent such bandwidth efficiency reduction by using cyclic signal shifts δ before GI insertion or phase shifts in frequency domain before IFFT, respectively. Figure 2.8(b) depicts the CDD scheme. The equivalence between CDD and PD is due to the periodicity property of the discrete Fourier transform as we can see in the following equation:

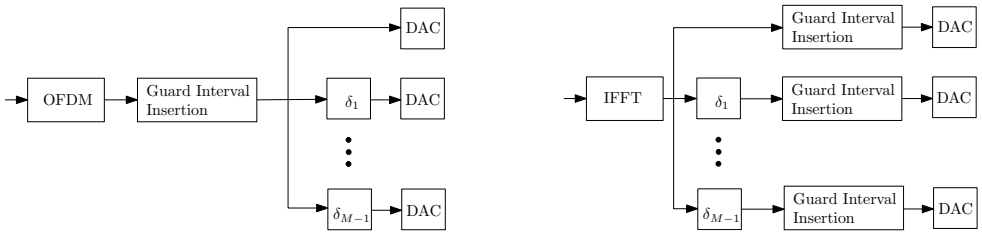

(a) DD (b) CDD

Figure 2.8: Schemes of delay diversity and cyclic delay diversity.

$$\underbrace{s((t-\delta)\mathrm{mod}N_{FFT})}_{CDD} = \frac{1}{\sqrt{N}_{FFT}} \sum_{f=0}^{N_{FFT}-1} \underbrace{e^{-i\frac{2\pi f\delta}{N_{FFT}}} S(f)}_{PD} e^{i\frac{2\pi ft}{N_{FFT}}}, \tag{2.29}$$

where $N_{FFT}, t, f, s(t)$ and $S(f)$ are number of carriers, discrete time, frequency and complex symbols in time and frequency domain, respectively.

The inclusion of CDD has been widely analyzed for different terrestrial DTV systems. For instance, in [Dammann01] for DVB-T and in [Dammann09] for DVB-T2, this diversity scheme has been assessed and compared to other techniques. On the other hand, CDD has also been tested over different channel models; in [Dammann07] this method is analyzed over Ricean channels for DVB-T and in [Zhang07], the same scheme is studied for spatial correlated channels for DVB-H. Regarding the deployment of networks, field measurements for DVB-T are presented in [Di Bari08, Di Bari09] and coverage analysis for DVB-H in [Zhang08].

2.3.6 Full-Rate Full-Diversity Techniques

So far we have focused on techniques regarding one of the benefits of MIMO systems, i.e. diversity. As we have seen in Section 2.3.3, this advantage results in robustness, in words of one syllable, reducing the error probability for a given SNR. Nonetheless, the drawback of the aforementioned diversity techniques is that they do not exploit spatial multiplexing, since such configurations preserve the SISO data rate. Consequently, they do not reach the MIMO diversity-multiplexing trade-off frontier. In this aspect, there exist multiple schemes [Tirkkonen00, Hassibi02, Ma03, Yao03] that combine those two interesting MIMO features. Hence, this section analyzes those full-rate full-diversity (FRFD) techniques that can be used in future terrestrial DTV systems.

Before starting with the review of FRFD techniques, we will comment some criteria that optimize the FRFD STC design. As we have seen in previous sections, STC must fulfill the rank criterion in order to achieve full diversity (see Criterion 1). In addition to this rule, which was derived in [Guey96, Tarokh98], Tarokh *et al.* presented in [Tarokh98] another criterion to maximize the coding gain based on the Chernoff bound analysis of pairwise error

probability (PEP) $P(\boldsymbol{X} \rightarrow \hat{\boldsymbol{X}})$, which is the probability of transmitting $\boldsymbol{X}$ and detecting $\hat{\boldsymbol{X}}$ at the receiver. The minimization of PEP for Rayleigh fading channels leads to the next criterion:

Criterion 2 *(Determinant criterion): In order to obtain maximum coding gain, the minimum of the determinants of the matrices $\boldsymbol{\Delta}^H\boldsymbol{\Delta}$ has to be maximized for all pairs of different codewords $\boldsymbol{X}$ and $\hat{\boldsymbol{X}}$.*

According to Hassibi *et al.* [Hassibi02], $\boldsymbol{X}$ can be rewritten as

$$\boldsymbol{X} = \sum_{q=1}^{Q} \left(\Re\{s_q\}\,\boldsymbol{A}_q + \Im\{s_q\}\,\boldsymbol{B}_q\right), \tag{2.30}$$

when STC is considered a linear dispersion (LD) code, being $\boldsymbol{A}_q$ and $\boldsymbol{B}_q$ for $q = 1, \ldots, Q$ the dispersion matrices. Then, the design optimization of $\boldsymbol{X}$ has to be subject to one of the following three power constraints [Hassibi02]:

$$\sum_{q=1}^{Q} \left(\mathrm{Tr}\left(\boldsymbol{A}_q^H\boldsymbol{A}_q\right) + \mathrm{Tr}\left(\boldsymbol{B}_q^H\boldsymbol{B}_q\right)\right) = 2TE_s, \tag{2.31}$$

$$\mathrm{Tr}\left(\boldsymbol{A}_q^H\boldsymbol{A}_q\right) = \mathrm{Tr}\left(\boldsymbol{B}_q^H\boldsymbol{B}_q\right) = \frac{TE_s}{Q}, \quad q = 1, \ldots, Q, \tag{2.32}$$

$$\boldsymbol{A}_q^H\boldsymbol{A}_q = \boldsymbol{B}_q^H\boldsymbol{B}_q = \frac{T}{Q}\boldsymbol{I}_M, \quad q = 1, \ldots, Q. \tag{2.33}$$

After recalling these main criteria for STC design, we review some FRFD codes which are interesting for the considered terrestrial DTV scenarios.

2.3.6.1 The Golden Code

The Golden code is the FRFD 2×2 STC which achieves the maximal coding gain [Belfiore04]. It encodes a group of four symbols $\boldsymbol{s} = (s_1, s_2, s_3, s_4)$ which are transmitted as follows:

$$\boldsymbol{X}_g = \frac{1}{\sqrt{5}}\begin{bmatrix} \alpha\left(s_1 + \theta s_3\right) & \alpha\left(s_2 + \theta s_4\right) \\ i\bar{\alpha}\left(s_2 + \bar{\theta}s_4\right) & \bar{\alpha}\left(s_1 + \bar{\theta}s_3\right) \end{bmatrix}, \tag{2.34}$$

with $\theta = \frac{1+\sqrt{5}}{2}$ (the golden number), $\bar{\theta} = \frac{1-\sqrt{5}}{2}$, $\alpha = 1 + i\left(1 - \theta\right)$ and $\bar{\alpha} = 1 + i\left(1 - \bar{\theta}\right)$.

This code fulfills the power conditions of (2.31) and (2.32), which ensure that the average transmit power corresponds to (2.3), i.e. $E\left[\mathrm{Tr}\left(\boldsymbol{X}_g\boldsymbol{X}_g^H\right)\right] = MT$, and that each of the transmitted signals x_{ij} are transmitted with the same overall power from the M antennas during the T channel uses, respectively. However, it does not obey (2.33) which involves that the symbols are dispersed with equal energy in all spatial and temporal directions.

The main drawback of the Golden code lies on the decoding complexity. In order to choose a detected vector $\hat{\boldsymbol{s}}$, we need to perform an exhaustive search for all symbol vectors $\boldsymbol{s} = (s_1, s_2, s_3, s_4)$ which form the codeword $\boldsymbol{X}_g$. This search is carried out by a maximum likelihood (ML) detector and, as we will see later, the complexity of the ML algorithm is exponential in the length of the symbol vector $\boldsymbol{s}$, i.e. $\mathcal{O}(P^4)$, which is prohibitive for large constellation sizes P. Note that we have defined $\mathcal{O}(\cdot)$ in order to quantify the detection complexity such that $\mathcal{O}(P^4)$ denotes a variable complexity upper-bounded by P^4.

2.3.6.2 Low Complexity Codes

The following STC schemes are designed in such a way that they fulfill the aforementioned STC design criteria and allow us to perform optimum detection with lower complexity. Although this sort of STC first appeared in [Tirkkonen02], their low-complexity detection property was not analyzed until [Sezginer07, Paredes07]. Despite their coding gains are lower than Golden coding gain, their reduced complexity makes them feasible candidates if MIMO techniques are considered in future broadcasting TV systems.

2.3.6.2.1 The Silver Code This 2×2 STBC code exploits the properties of the OSTBC generator matrix in order to reduce the ML decoding complexity [Paredes07, Paredes08]. This STC code belongs to the class of linear dispersion codes [Hassibi02] so they can be written as (2.30). If we rearrange the real and imaginary parts of the symbol vector $\boldsymbol{s} = [s_1, s_2, s_3, s_4]^T$ in a real-valued column vector as

$$\boldsymbol{s}_R = [\Re\{s_1\}, \Im\{s_1\}, \Re\{s_2\}, \ldots, \Im\{s_4\}], \tag{2.35}$$

and we do the same with the codeword $\boldsymbol{X}$ such that the column vector $\boldsymbol{x} = [x_{11}, x_{21}, x_{12}, x_{22}]^T$ is expressed as (2.35), $\boldsymbol{X}$ can be then written as $\boldsymbol{x}_R = \boldsymbol{G}_R\boldsymbol{s}_R$, where $\boldsymbol{G}_R$ is the real-valued code generator matrix of the STC, which is defined as

$$\boldsymbol{G}_R = \frac{1}{\sqrt{14}} \begin{bmatrix} \sqrt{7} & 0 & 0 & 0 & -1 & 1 & 1 & 2 \\ 0 & \sqrt{7} & 0 & 0 & 1 & -2 & 1 & 1 \\ 0 & 0 & \sqrt{7} & 0 & 1 & 1 & 2 & -1 \\ 0 & 0 & 0 & \sqrt{7} & 2 & 1 & -1 & 1 \\ 0 & 0 & -\sqrt{7} & 0 & 1 & 1 & 2 & -1 \\ 0 & 0 & 0 & \sqrt{7} & -2 & -1 & 1 & -1 \\ \sqrt{7} & 0 & 0 & 0 & 1 & -1 & -1 & -2 \\ 0 & -\sqrt{7} & 0 & 0 & 1 & -2 & 1 & 1 \end{bmatrix}. \tag{2.36}$$

As it is proved in [Paredes08], the detection complexity can be reduced using ML detection

for two symbols of $\boldsymbol{s}$ and symbol-by-symbol detection for the other two, thus achieving a complexity order of $\mathcal{O}(P^2) + P$.

2.3.6.2.2 The Sezginer-Sari Code This 2×2 SFBC scheme was designed so as to allow for optimum detection with a lower complexity than the Golden code. The main difference between the SS [Sezginer07] and the Silver code [Paredes07] is the larger coding gain of the Silver code.

The SS code consists of a combination of two Alamouti schemes and can be described as follows:

$$\boldsymbol{X}_{SS} = \begin{bmatrix} as_1 + bs_3 & as_2 + bs_4 \\ -cs_2^* - ds_4^* & cs_1^* + ds_3^* \end{bmatrix}, \tag{2.37}$$

with $a = c = 1/\sqrt{2}$, $b = \frac{1-\sqrt{7}+i\left(1+\sqrt{7}\right)}{4\sqrt{2}}$ and $d = -ib$. These scalars are chosen so as to fulfill the STC design criteria following the power constraints of (2.31), (2.32) and (2.33). In [Sezginer07] it is proved that optimum detection is reached with a symbol-by-symbol detector with complexity P plus an ML detector with complexity $\mathcal{O}(P^2)$. This can be further reduced by means of a sphere decoder [Sezginer09]. However, it must be taken into account that the sphere decoder complexity, which is variable, is also upper-bounded by $\mathcal{O}(P^2)$.

2.3.6.3 Detection Techniques

When orthogonal codes are used, MIMO detection can be considered as a set of parallel SISO detection problems, so it can be simplified using linear techniques such as ZF or MMSE [Paulraj03]. However, when spatial multiplexing is added to the spatial coding, non-linear detection algorithms have to be used since linear techniques reduce the diversity order in the system performance [Paulraj03]. The most common and interesting algorithms for the detection of the aforementioned FRFR codes are shown below.

2.3.6.3.1 Optimal Maximum Likelihood Detection The ML detector is considered the optimal detector since it minimizes the probability of error [Proakis95]. It chooses the transmitted symbol vector that solves

$$\hat{\boldsymbol{s}}_{ml} = \arg\min_{\boldsymbol{s}\in\mathcal{M}} \|\boldsymbol{y} - \boldsymbol{H}_{eq}\boldsymbol{s}\|^2, \tag{2.38}$$

performing an exhaustive search over all symbol vectors $\boldsymbol{s}$ which form the codeword $\boldsymbol{X}$. The complexity of computing $\hat{\boldsymbol{s}}_{ml}$ is exponential in the length of the symbol vector $\boldsymbol{s}$. In the case of the reviewed FRFD codes, this is $\mathcal{O}(P^4)$, which becomes prohibitive for large constellation orders. The detection complexity can be reduced by means of the sphere decoder (SD) algorithm whose complexity can be considered to be polynomial for moderate

numbers of antennas and constellation orders [Hassibi05], maintaining the ML performance. This algorithm is explained in detail below.

2.3.6.3.2 Sphere Decoding The SD algorithm is based on the underlying lattice structure of the received signal [Viterbo93]. The main purpose is to reduce the complexity of the ML detector by searching over only those noiseless received points, defined as $\boldsymbol{H}_{eq}\boldsymbol{s}$, that lie within a hypersphere of radius R around the received signal $\boldsymbol{y}$, instead of searching over the entire lattice. The basic principle is shown in Figure 2.9 with a simplified 2-dimensional case, where the black dots represent the noiseless received constellation or lattice and the center of the circle is the noisy received point.

The process can be described as

$$\hat{\boldsymbol{s}}_{ml} = \arg\min_{\boldsymbol{s}\in\mathcal{M}} \|\boldsymbol{y} - \boldsymbol{H}_{eq}\boldsymbol{s}\|^2 \leq R^2, \tag{2.39}$$

The Euclidean distance calculation in (2.39) can be also written as

$$\|\boldsymbol{y} - \boldsymbol{H}_{eq}\boldsymbol{s}\|^2 = \|\boldsymbol{H}_{eq}\left(\boldsymbol{s} - \hat{\boldsymbol{s}}\right)\|^2 + \left\|\left(\boldsymbol{I}_{NT} - \boldsymbol{H}_{eq}\boldsymbol{H}_{eq}^{\dagger}\right)\boldsymbol{y}\right\|^2, \tag{2.40}$$

where $\hat{\boldsymbol{s}} = \boldsymbol{H}_{eq}^{\dagger}\boldsymbol{y}$ is the unconstrained least squares estimate or Babai point [Hassibi05]. It can be observed that the second term in (2.40) is constant so it can be discarded for solving (2.39). Moreover, the sphere constraint in (2.40) can be rewritten as

$$\|\boldsymbol{U}\left(\boldsymbol{s} - \hat{\boldsymbol{s}}\right)\|^2 \leq R^2, \tag{2.41}$$

where $\boldsymbol{U}$ is an $MT \times MT$ upper triangular matrix whose coefficients u_{ij} are obtained through the Cholesky decomposition of the Gram matrix $\boldsymbol{H}_{eq}^{H}\boldsymbol{H}_{eq}$ or, equivalently, QR decomposition of $\boldsymbol{H}_{eq}$.

The solution of the sphere constraint in (2.41) can be obtained recursively using a tree search algorithm. Given the triangular structure of $\boldsymbol{U}$, it is now possible to work up to level i recursively by traversing the tree backwards from level $i = MT$ to $i = 1$. For each level,

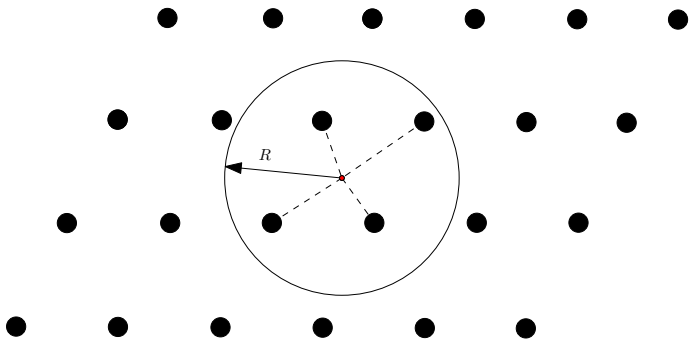

Figure 2.9: Schematic of the sphere decoder search principle for the 2-dimensional case.

the constellation points s_i that satisfy

$$|s_i - z_i|^2 \leq \frac{T_i}{u_{ii}^2}, \tag{2.42}$$

are selected as partial ML candidates, where

$$z_i = \hat{s}_i - \sum_{j=i+1}^{MT} \frac{u_{ij}}{u_{ii}}(s_j - \hat{s}_j), \tag{2.43}$$

and

$$T_i = R^2 - \sum_{j=i+1}^{MT} u_{jj} \left| s_j - z_j \right|. \tag{2.44}$$

When a new vector is found inside the hypersphere (at $i = 1$) the radius is updated with the new minimum Euclidean distance and the algorithm continues the search. This process can be seen as a tree search through MT levels where each node contains P branches. When $T_i \leq 0$ in any level i, the accumulated (squared) Euclidean distance (AED) from the root to that node has exceeded the sphere constraint and the entire branch plus all its descendants can be then discarded, yielding a speed increase compared to an exhaustive search. The search finishes when the radius has been reduced so that no more points are found inside the hypersphere, being the last point found satisfying the sphere constraint the ML solution $\hat{\boldsymbol{s}}_{ml}$.

There exist two different methods to define the order in which the points s_i are visited at each level:

- **Fincke-Pohst (FP) enumeration**: the points are visited in an arbitrary constellation order [Fincke85]. In this enumeration, the complexity of the SD is mainly determined by the radius R. The initial radius is chosen according to the noise variance per antenna [Hochwald03]. If no vectors are found inside the hypersphere, the radius would need to be increased and the detector would need to be run again.

- **Schnorr-Euchner (SE) enumeration**: in this case, the points are visited according to increasing distances to z_i [Schnorr91]. This way, the probability of finding the ML solution among the first vectors searched is incremented reducing the overall complexity of the algorithm. The initial value can be set to the end of the scale so that no estimate of the noise level is required at the receiver. However, from a simulation point of view, the initial radius still has a marginal effect on the complexity of the algorithm [Damen03].

2.4 Chapter Summary

This chapter has reviewed the two main aspects involved in this work. First, the evolution of the European DTV broadcasting standards is summarized, making a brief description of their technical key features. From the DVB-T2 standard to its predecessor DVB-T, there has been a radical change in the physical layer resulting in an increase of the system capacity and robustness. The improvement of DVB-T2 is based on the inclusion of new coding schemes, higher number of interleavers, high modulation orders and several optional techniques such as pilot patterns, RQD or MISO.

The second part of the chapter deals with the multi-antenna processing aimed at the TDT systems. As a starting point, a MIMO wireless system model has been defined. Next, a theoretical review of the potential benefits of MIMO channels has been provided, focusing on spatial multiplexing and specifically, on diversity. Due to the great variety of diversity techniques, a classification of the different kinds has been presented paying attention to those schemes used in DTV. The techniques which combine spatial with time or frequency diversity such as SFBCs, have been explained in more detail since they might become a future MIMO alternative for next generation DTV systems. A clear example is the inclusion in DVB-T2 of an optional MISO SFBC technique based on the Alamouti scheme. Although this technique offers higher robustness at the receiver, it does not fully exploit the MIMO channel properties. For that purpose, the FRFD SFBC codes are one of the most attractive possibilities for the future, because they combine spatial multiplexing and diversity getting closer to the diversity-multiplexing frontier. The last part of the chapter has shown the most interesting proposals which may be implemented in TDT networks and has reviewed the detection algorithms required for their efficient hardware implementation.

Chapter 3

Multi-Antenna Diversity Schemes in DVB-T and DVB-T2 Broadcasting

3.1 Introduction

The wide range of propagation conditions in TDT networks involves a robust and flexible physical layer in DTV standards. In order to adapt them to all possible scenarios, which can range from a strong direct component to a severe multipath channel with deep fadings, DTV standards, such as DVB-T or DVB-T2, include redundancy through channel coding. These systems are mainly based on a BICM scheme which combines coding, interleaving and modulation. When reception is given at low SNR, low code rates are necessary, resulting in a loss of throughput efficiency. Nonetheless, a solution that increases the performance while maintaining the same reception quality can be obtained based on MIMO processing.

This chapter provides a simulation analysis of diversity schemes for multiple TDT scenarios in both DVB-T and DVB-T2 systems. On one hand, we assess the state-of-the-art multi-antenna diversity techniques, such as the Alamouti code or CDD, in the DVB-T standard. On the other hand, we observe the behavior of the optional diversity techniques of DVB-T2, such as RQD and the MISO SFBC scheme.

Moreover, the inclusion of the optional SFBC technique in DVB-T2 gives rise to a new concept of transmission over single frequency networks (SFNs), called distributed MISO. In a typical MISO scheme, the transmit antennas are usually located at the same base station or transmitter. However, within the SFN network, each transmitter can be considered as one antenna in such a way that the MISO system is formed by various transmitters of the network and the receive antenna. This way, a different channel model has to be defined and the behavior of the system will also depend on the deployment of the network.

At the first part of the chapter the broadcasting channel models used throughout the thesis are defined. Next, we will see the behavior of diversity techniques over different reception environments in the DVB-T and DVB-T2 systems. Finally, the last section presents the advantages and disadvantages of the SFN deployment, both with and without multi-

antenna processing.

3.2 Fading Channels

The characterization of TDT channels is essential for the analysis of diversity schemes. DVB-T is a broadcasting system which can form either a multiple frequency network (MFN) or an SFN. The transmitters of the network are usually stationary and the reception can take place in very different scenarios: urban, rural, indoor, mobile, etc. As a result, various mathematical models with different statistical properties are necessary according to the propagation conditions.

Due to the reflections of transmitted waves from buildings, ground or other obstacles, multiple replicas of the transmitted signal arrive at the receiver. This effect is known as multipath propagation. If the maximum path delay is longer than the symbol period, the channel is said to be frequency selective and the longer the difference, the more selective the channel is, involving more and deeper fadings in the frequency domain. Rayleigh and Rice distributions are the most common statistical processes for characterizing the multipath propagation [Patzold02].

As we have mentioned, the DTV transmission can be deployed over MFN or SFN. The MFN corresponds to the typical analogue TV transmission systems where every transmitter of the network uses a different carrier frequency in order to transmit the same information. With the deployment of an SFN, all the transmitters broadcast the same program synchronously at the same carrier frequency. This means that the TV signal is transmitted at the same frequency covering the whole area of the network, which can be formed by multiple transmitters. This allows an efficient use of the radio spectrum, yielding a higher number of TV programs compared to MFN. Therefore, the SFN model represents the multipath propagation from two or more transmitters of the network in such a way that the distances from transmitters to the receiver are taken into account.

3.2.1 Rayleigh and Ricean Channels

The sum of all multipath gains of the transmitted signal can be described in the equivalent complex baseband as a zero-mean complex Gaussian random process if we consider a frequency-non-selective or flat fading channel

$$\mu(t) = \mu_1(t) + i\mu_2(t), \tag{3.1}$$

where the real-valued Gaussian random processes $\mu_1(t)$ and $\mu_2(t)$ are assumed statistically uncorrelated corresponding to $\mathcal{CN}(0, \sigma^2)$ each. Thus, the variance of $\mu(t)$ is given by $2\sigma^2$.

The envelope of (3.1), which is given by the absolute value $|\mu(t)|$, follows a Rayleigh distribution.

If there is a line-of-sight (LOS) component in the received signal, the new component can be described as $m(t) = m_1(t) + im_2(t)$ with mean value $\bar{m}$. At the receiver antenna, the received signal $\mu_\rho(t)$ is the superposition of the scattered and the LOS component such that

$$\mu_\rho(t) = \mu_{\rho_1}(t) + i\mu_{\rho_2}(t) = \mu(t) + m(t), \tag{3.2}$$

where the envelope $|\mu_\rho(t)|$ is now a Ricean distribution. Note that we have taken into account the time variable in all equations in order to represent both stationary and mobile environments.

So as to model the mobile channels, we have used a real-valued coloured Gaussian random process called the Rice method. The procedure consists of the generation of a Gaussian deterministic process μ_i from the superposition of a finite number N_i of harmonic functions with different weights $c_{i,n}$, equidistant frequencies $f_{i,n}$ and random phases $\theta_{i,n}$ with uniform distribution [Patzold02]. The generated channel for $i = 1, 2$ can be described mathematically as

$$\mu_i(t) = \sum_{n=1}^{N_i} c_{i,n} cos(2\pi f_{i,n} t + \theta_{i,n}), \tag{3.3}$$

where $c_{i,n}$, $f_{i,n}$ y $\theta_{i,n}$ are the Doppler coefficients, discrete frequencies and phases, respectively, calculated from the Doppler power spectral densities. For a process $\mu(t)$, the power spectral density $S_{\mu\mu}$ can be separated as $S_{\mu\mu} = S_{\mu_1\mu_1} + S_{\mu_2\mu_2}$ following (3.1). By modelling the mobile channel, we frequently simplify matters. Thus, assuming that the propagation of electromagnetic waves occurs in a two-dimensional plane, the angles of incidence of the waves are uniformly distributed from 0 to 2π and the receive antenna is omnidirectional, one finds the expression first derived by [Clarke89] and named Jakes spectrum [Jakes94] for the Doppler power spectral density $S_{\mu\mu}$ of a flat fading channel $\mu(t)$ as

$$S_{\mu_i\mu_i} = \frac{\sigma^2}{\pi f_{max}\sqrt{1-(f/f_{max})^2}} \qquad |f| \leq f_{max}, \tag{3.4}$$

where $i = 1, 2$ and f_{max} denotes the maximum Doppler frequency.

It has been proved that the Doppler power spectral density of the far echoes deviates considerably from the shape of the Jakes expression [Cox73], which is approximately Gaussian shaped and can be mathematically represented by the so-called Gaussian power spectral density

$$S_{\mu_i\mu_i} = \frac{\sigma^2}{f_c}\sqrt{\frac{ln2}{\pi}} e^{-ln2(\frac{f}{f_c})^2}, \tag{3.5}$$

where f_c denotes the 3-dB-cut-off frequency. The Gaussian power spectral densities are generally shifted from the origin of the frequency plane because far echoes mostly dominate from a certain direction of preference.

Finally, assuming a wide-sense stationary uncorrelated scattering (WSSUS) channel according to [Bello63, Hoeher92], a representation of a frequency-selective and time-variant SISO channel in the equivalent complex baseband can be given by a sum of a finite number L of taps as

$$h(\tau, t) = \sum_{l=0}^{L-1} a_l \mu_l(t) \delta(\tau - \tau_l), \tag{3.6}$$

where a_l and τ_l are the tap coefficients and delays, respectively. It is noteworthy that (3.6) is the instantaneous channel impulse response (CIR) of the channel and each path is characterized by an independent and uncorrelated process, $\mu_l = \mu_{1,l} + i\mu_{2,l}$. For a MIMO channel, there are as many CIR as subchannels, i.e. MN, and the corresponding translation of (3.6) to each OFDM carrier would correspond to the entries of the channel matrix $\boldsymbol{H}$ in (2.2).

In order to measure the multipath degree of the channel, let us define the delay spread as

$$\tau_{rms} = \sqrt{\frac{\sum_{l=0}^{L-1} (\tau_l - \bar{\tau})^2 a_l \mu_l(t)}{\sum_{l=0}^{L-1} a_l \mu_l(t)}}, \tag{3.7}$$

where $\bar{\tau}$ is the mean delay of the channel, expressed as

$$\bar{\tau} = \frac{\sum_{l=0}^{L-1} \tau_l a_l \mu_l(t)}{\sum_{l=0}^{L-1} a_l \mu_l(t)}. \tag{3.8}$$

3.2.2 Multipath Channel Models

Radio channel models are usually derived from field measurements of the channel parameters in reference scenarios. This allows us to create realistic models according to the reception environment under study (e.g. outdoor, indoor, rooftop, etc.). In TDT, due to the variety of scenarios, multiple models have been used to assess the performance at the receiver. TDT standards, such as DVB-T or DVB-T2, define several channel models to provide simulated performance results. However, some of them are not realistic and should be used only for

checking and verification tasks. For instance, some of them are considered as a snapshot of a real channel and they do not include Doppler parameters. In that case, one channel realization is only used for the assessment of the system providing probably optimistic performance results. The DVB-T specification [ETSI97] defines two channel models which describe fixed (F1) and portable (P1) reception. In addition to the DVB-T channels, the DVB-T2 implementation guidelines document [DVB09] includes a higher number of channel models that cover a wide range of reception conditions. Besides the channels presented for DVB-T and DVB-T2, there also exist several research projects where other models have been developed to simulate and analyze the performance of the DTV systems. The list below shows the most common channels used in the literature including the mentioned DVB-T and DVB-T2 channels.

1. DVB-T channels [ETSI97]
   (a) Rayleigh P1 (20 paths).
   (b) Rayleigh P1 approximation (6 paths)[EVS06].
   (c) Ricean F1 (21 paths).
2. DVB-T2 channels [DVB09]
   (a) DVB-T P1 and F1.
   (b) Mobile Channel-Typical Urban channel (6 paths) (TU6).
   (c) Simple two path profile, 0 dB echo.
   (d) MISO channels: Ricean and Rayleigh.
   (e) Memoryless Rayleigh channel with erasures.
3. COST[1] 207 channels[COST20789]:
   (a) Typical Urban channel (12 paths) (TU12).
   (b) TU6.
   (c) Rural Area channel (6 paths) (RA6).
   (d) Bad Urban channel (6 paths) (BA6).
4. Eureka Celtic Wing TV project channels [ITU06, Hakala07]:
   (a) Pedestrian Indoor channel (PI).
   (b) Pedestrian Outdoor channel (PO).

[1]COST: *European Cooperation in the Field of Scientific and Technical Research.*

Type	Doppler power spectral density $S_{\mu\mu}(f)$
Jakes	$\frac{1}{\pi f_{max}\sqrt{1-(f/f_{max})^2}}$
Gauss 1	$\frac{50}{3\sqrt{2\pi}f_{max}}e^{-\frac{(f+0.8f_{max})^2}{2(0.05f_{max})^2}} + \frac{5}{3\sqrt{2\pi}f_{max}}e^{-\frac{(f-0.4f_{max})^2}{2(0.1f_{max})^2}}$
Gauss 2	$\frac{10\sqrt{10}}{\sqrt{2\pi}(\sqrt{10}+0.15)f_{max}}e^{-\frac{(f-0.7f_{max})^2}{2(0.1f_{max})^2}} + \frac{1}{\sqrt{2\pi}(\sqrt{10}+0.15)f_{max}}e^{-\frac{(f+0.4f_{max})^2}{2(0.15f_{max})^2}}$
Rice	$\frac{0.41^2}{\pi f_{max}\sqrt{1-(f/f_{max})^2}} + 0.91^2\delta(f-0.7f_{max})$

Table 3.1: Specification of Doppler power spectral densities according to the COST 207 project.

5. Channels used in Pluto project [ist07]:

   (a) Outdoor Residential-High Antenna (Channel B) [JTC93].

   (b) Indoor Commercial (Channel B) [JTC93].

In this work, we have chosen some of the mentioned channel models in order to study and analyze the multi-antenna diversity techniques and the corresponding detection algorithms paying special attention to the COST 207 TU6 and RA6 channels [COST20789].

3.2.2.1 TU6 and RA6 Channels

TU6 and RA6 channel models were first developed for Global System for Mobile Communications (GSM) systems. Nonetheless, some channel profiles from [COST20789], such as TU6 and RA6, were adapted to mobile DVB-T due to similar propagation conditions of GSM and TDT systems [Motivate00]. In fact, the TU6 channel has been included in the DVB-T2 specifications [DVB09] and it is one of the most extended models for simulation tests in DTV systems.

The Doppler characterization of TU6 and RA6 is based on the Doppler power spectral densities $S_{\mu\mu}(f)$ of the different paths of the channels. According to the statistical properties of the received echoes, four types of Doppler power spectral densities have been specified in Table 3.1. Note that the Doppler power spectrum called Rice is the sum of the classical or Jakes Doppler spectrum and one direct path. Besides TU6 and RA6, these Doppler spectra have been used for other channels defined in [COST20789] such as Bad Urban or Hilly Terrain. The characterization of the mobile TU6 channel in [DVB09] has been modified using only the classical Doppler spectrum.

The TU6 channel represents an urban environment with reflexions from buildings and without LOS from the transmitter to the receiver. Consequently, it is a Rayleigh channel.

Path number l	Propagation delay τ_l (μs)	Path power(dB)	Category of the Doppler power spectral density $S_{\mu\mu}$	
			COST 207	DVB-T2
0	0.0	-3	Jakes	Jakes
1	0.2	0	Jakes	Jakes
2	0.5	-2	Gauss 1	Jakes
3	1.6	-6	Gauss 1	Jakes
4	2.3	-8	Gauss 2	Jakes
5	5.0	-10	Gauss 2	Jakes

Table 3.2: Definitions of the mobile TU6 channel by the COST 207 project and the DVB-T2 standard.

Path number l	Propagation delay τ_l (μs)	Path power(dB)	Category of the Doppler power spectral density $S_{\mu\mu}$
0	0.0	0	Rice (LOS) / Jakes (NLOS)
1	0.1	-4	Jakes
2	0.2	-8	Jakes
3	0.3	-12	Jakes
4	0.4	-16	Jakes
5	0.5	-20	Jakes

Table 3.3: Definition of the RA6 channel by the COST 207 project.

The power delay profile is given in Table 3.2. As we have mentioned, the Doppler spectra of the longer paths are different depending on the chosen model. In Figure 3.1(a), the Doppler power spectral spectra of the six taps for COST 207 are shown. Figures 3.1(c) and 3.1(d) depict in detail the type 1 and 2 Gaussian spectra for taps 4 and 6, respectively.

The RA6 channel is a typical rural area channel for non hilly terrain. This channel considers LOS and non line-of-sight (NLOS), resulting in a Ricean or Rayleigh channel model, respectively. The power delay profile is defined in Table 3.3. Figure 3.1(b) shows the Doppler spectra for all echoes when LOS is considered. In Figures 3.1(e) and 3.1(f), the Ricean and classical spectra of paths 1 and 4 are shown, respectively. Most of the results on the literature are carried out using one channel realization composed of the fixed taps defined in the tables, without considering the Doppler spectrum.

3.2.3 Single-Frequency Networks

Due to the OFDM modulation adopted by TDT systems, TV broadcasting networks can be deployed using both MFN and SFN. Unlike MFN, where each of the transmitter uses a different carrier frequency to transmit the same program, the transmitters in the SFN

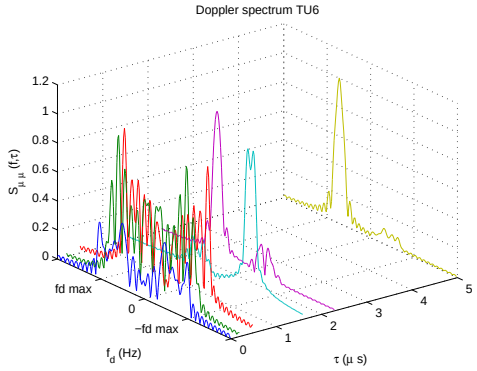

(a) $S_{\mu\mu}(f,\tau)$ of channel TU6

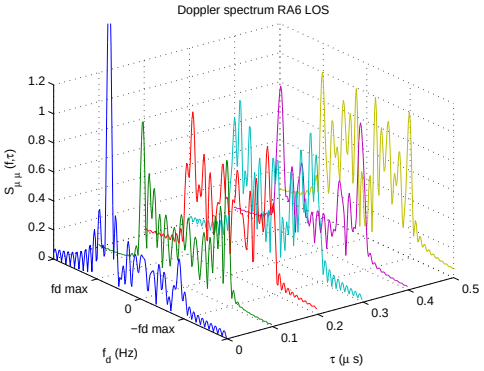

(b) $S_{\mu\mu}(f,\tau)$ of channel RA6 LOS

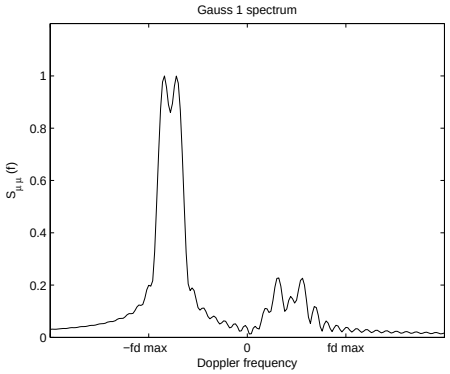

(c) Gauss spectrum type 1 of path 4 in channel TU6

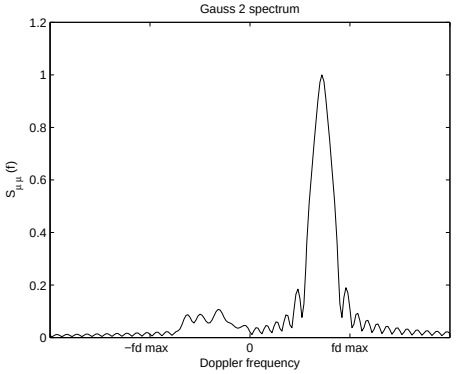

(d) Gauss spectrum type 2 of path 6 in channel TU6

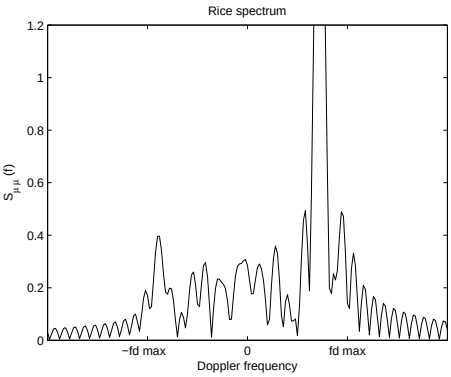

(e) Rice spectrum of path 1 in channel RA6

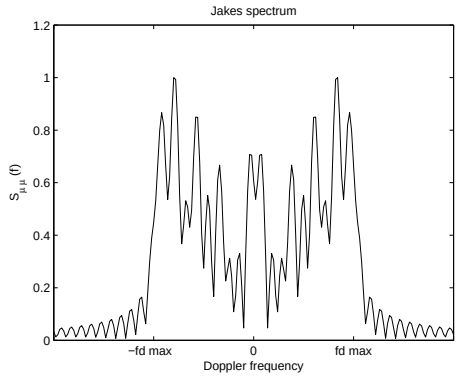

(f) Jakes spectrum of path 4 in channel RA6

Figure 3.1: Doppler power spectrum densities of channels TU6 and RA6 LOS.

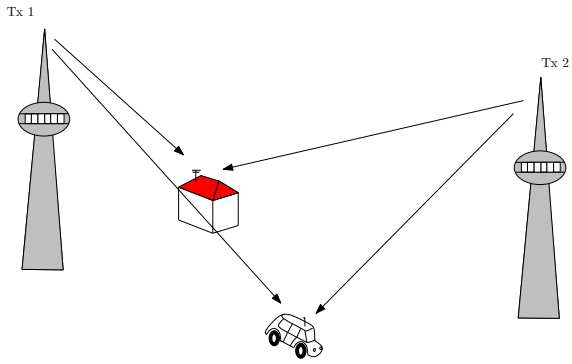

Figure 3.2: Distributed MISO scheme in SFN.

broadcast the same program synchronously at the same carrier frequency. The coverage area of every transmitter is called cell and the network can be composed of two or more cells which are deployed to cover wide areas with an unique frequency band exploiting the TV spectrum more efficiently by allowing a higher number of TV programs [Penttinen08]. Currently, SISO communication links between transmitter and receiver are used in the existing SFN architectures. However, due to the increase of demanded services, the deployment of SFN with new MIMO techniques, which ensure high spectrum efficiency as well as high diversity gain, is one of the objectives for the future and last-generation DTV systems.

As we have seen in the previous chapter, the inclusion of MIMO schemes has been first studied in DVB-T and DVB-H [ETSI04]. However, MIMO transmission is basically considered as an intra-cell transmission. This means that transmit antennas are located on the transmitter of one cell and the receiver is in the same cell. The SFN channel model in DVB-T/H was focused on the mobile reception or self-interference scenarios [Santella04]. The simultaneous transmission from several sources of the SFN could be considered as multipath propagation since the received echoes of the same signal form constructive and destructive interference which results in fading. This model was used in [MBRAI07] in order to define a mobile SFN channel from two transmitters based on two independent TU6 channels, the first six taps belong to the first transmitter of the network and the last six taps correspond to the second transmitter.

The idea of the deployment of SFN with multi-antenna techniques appears with the DVB-T2 standard [ETSI09]. This defines a distributed MISO scheme where every transmit antenna of the MISO system is a transmitter of the SFN network as it is shown in Figure 3.2. The channel model of this inter-cell configuration requires at least two independent fading channels, one for each transmitter. As a result, two SFN channel models, one Ricean and one Rayleigh, have been defined in the implementation guidelines document of DVB-T2 [DVB09]. Nevertheless, the distributed MISO is not the unique proposed configuration for future DTV systems. In the standardization process of the second generation of DVB-H, known as Digital Video Broadcasting - Next Generation Handheld (DVB-NGH), various

MIMO techniques are being analyzed. Dual polarizated MIMO [Moss08] or 3D space-time-space block codes [Nasser08b, Nasser08c], for instance, involve different SFN models.

The SFN channel model we have used in the thesis is based on two independent multi-path fading channels which suffer different attenuations α_k and delays t_k according to the distance between the transmitter k and the receiver. In general form, the model can be mathematically described as

$$h_{SFN} = \sum_{k=1}^{M} \alpha_k \sum_{l=1}^{L} h(\tau_l + t_k). \tag{3.9}$$

3.3 Diversity Techniques in DVB-T

Chapter 2 has shown the advantages provided by multi-antenna processing in wireless communications systems. Due to the architecture of a TDT network, MIMO processing is initially proposed through multi-antenna transmit diversity techniques since they increase the coverage area and the robustness of the transmitted signal against the channel conditions. The reason of using multi-antenna techniques at the transmitter side aims at a reduced cost at the terminals and backward compatibility. On one hand, the inclusion of a second antenna at the receiver would result in an additional cost for the users in such a way that diversity would be only achieved by those that had upgraded their domestic installations. However, when diversity techniques with backward compatibility are used at the transmitter, their potential benefits will be available for any user within the MISO network.

This section analyzes the 2×1 Alamouti SFBC scheme and the 2×1 CDD technique, which can be easily applied to the OFDM systems, and compares their performances with the 1×2 MRC solution over static and mobile environments.

First of all, some simulation aspects, which have been taken into account throughout the whole research work, are defined. The system performance has been mainly measured through BER curves using Monte Carlo simulations. In order to ensure reliable results, the number of channel realisations depends on the number of transmitted symbols in every channel realization and the target BER. For instance in DVB-T, unless otherwise stated, $N_{OFDM} = 5$ OFDM symbols are transmitted in every channel realisation fulfilling the following relation:

$$\text{target BER} = \frac{1000 \text{ erroneous bits}}{N_{MC} N_{OFDM} N_C R_c \log_2 P}, \tag{3.10}$$

where N_{MC} and N_C are the number of channel realisations and payload carriers, respectively, and R_c corresponds to the code rate. Since simulation results are usually obtained after the convolutional decoder, the quasi-error free (QEF)[2] corresponds to BER=$2 \cdot 10^{-4}$. Therefore,

[2]In DVB-T, QEF means less than one uncorrected error event per hour, corresponding to BER=10^{-11}

we have considered a target BER=10^{-5}.

The simulations have been carried out maintaining the overall transmit power equal to the unity in the time domain, i.e. after the IFFT. Due to the fact that both DVB-T and DVB-T2 are OFDM systems, we can consider each of carrier as a narrowband channel. In this way, the SNR ρ defined in Chapter 2 corresponds now to the relation between the carrier and noise power in the frequency domain, which is called carrier to noise ratio (CN). Thus, the relation between the SNR of the OFDM system and the CN is given by

$$\text{SNR} = \frac{N_C \rho}{N_{FFT}}. \tag{3.11}$$

where N_{FFT} denotes the transmission mode. Hence, the parameter ρ will be considered as the CN in OFDM systems in the following.

3.3.1 Static Environments

The most common scenario in a TDT network corresponds to the rooftop reception. The reception is mostly static and, as a result, the channel probably varies slowly or does not vary in accordance to external agents of the reception environment such as weather, mobile obstacles, etc. If the receive antenna has a direct sight of the transmitter, i.e. there exists a LOS component, the channel will be a Ricean channel whereas, if the reception is only due to reflexions of the transmitted signal, the channel will follow a Rayleigh distribution.

In this section, we analyze how CDD, the Alamouti code and MRC affect the quality of the reception compared to the SISO case. The multi-antenna techniques have been implemented using the simplest antenna setups, i.e. 2×1, 1×2 or 2×2. The detection is based on the ZF algorithm for SISO, 2×1 CDD and 2×1 SFBC. When the 2×2 setup is used, ZF and MRC detectors are combined. The DVB-T parameters which have been used correspond to the current Spanish configuration:

- Convolutional code rate: $R_c = 2/3$
- Constellation size: 64-QAM
- FFT size: 8192 carriers (8K)
- Guard interval: 1/4

3.3.1.1 Previous Considerations About the CDD Technique

As we have seen in Section 2.3.5.3, CDD provides additional diversity through the constructive and destructive superposition of the transmitted signals, which generates an artificial

at the input of the MPEG-2 demultiplexer [ETSI97].

equivalent frequency selective channel. This technique, combined with a coding stage, is specially advantageous over flat fading environments since some carriers of the OFDM symbol can be enhanced through the frequency selectivity. For the 2×1 system, the equivalent channel corresponds to

$$H_{eq}(f,t) = H_0(f,t) + e^{-i\frac{2\pi f \delta_1}{N_{FFT}}} H_1(f,t), \tag{3.12}$$

where δ_1 is the cyclic delay added in the second antenna. In order to get a reduction of the bandwidth coherence equivalent, the delay δ_1 (in samples) has to fulfill

$$\delta_1 \geq \frac{1}{T_s B}, \tag{3.13}$$

where T_s and B denote the sampling period and the OFDM bandwidth, respectively. In DVB-T, these values correspond to $T_s = 7/64$ μs and $B = 8$ MHz in such a way that $\delta_1 \geq 1.14$. In [Dammann01], it is proved that there is a saturation effect on the performance improvement in terms of the cyclic delay increment. The minumum delay which offers the maximum gain depends on the delay spread of the channel τ_{rms} and the higher the delay spread is, the smaller the necessary delay is. In Figure 3.3, we provide simulation results of CDD for different cyclic delays over channels with different delay spread. On one hand, we can observe that CDD obtains a higher gain when the delay spread is shorter. As in [Dammann01], we have taken $\delta_1 = 20$, which maximizes the gain for the tested configurations.

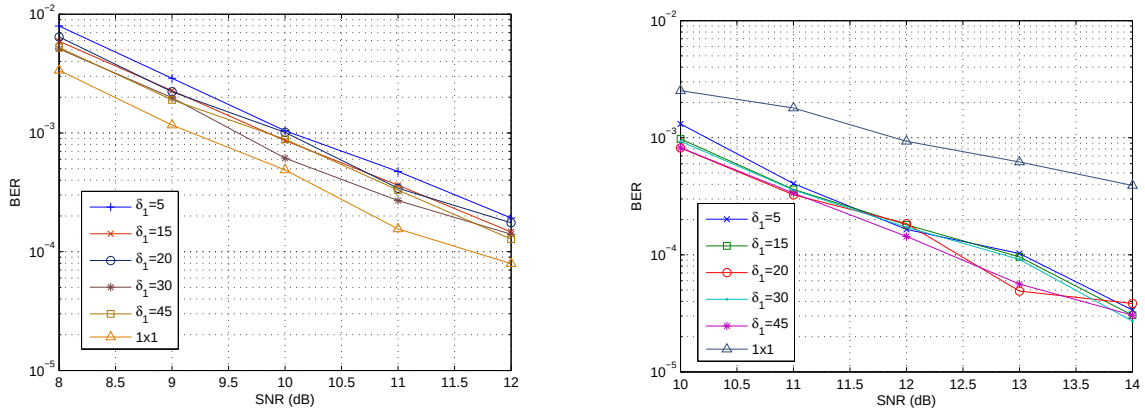

(a) Outdoor channel $\tau_{rms} = 3.58\mu$s

(b) Indoor channel $\tau_{rms} = 0.18\mu$s

Figure 3.3: Comparison of 2×1 CDD schemes in the DVB-T system over the channels defined in [JTC93] varying the cyclic delay δ_1 of the second antenna.

Figure 3.4 depicts the effect of CDD over TU12 and RA6 NLOS channels with $f_d = 30$ Hz compared to the SISO case. One can observe in Figure 3.4(a) that the SISO TU12 is a highly frequency selective channel due to its long replicas. However, SISO RA6 results in a more flat channel due to its shorter delay spread as Figure 3.4(c) shows. When CDD is added, its effect is more remarkable over the RA6 channel than the TU12 channel. The aim

of CDD is to generate frequency selectivity in order to be beneficial to the decoding process. Nonetheless, due to the inherent frequency selectivity of TU12, CDD does not apparently vary its bandwidth coherence and consequently, its performance benefit vanishes.

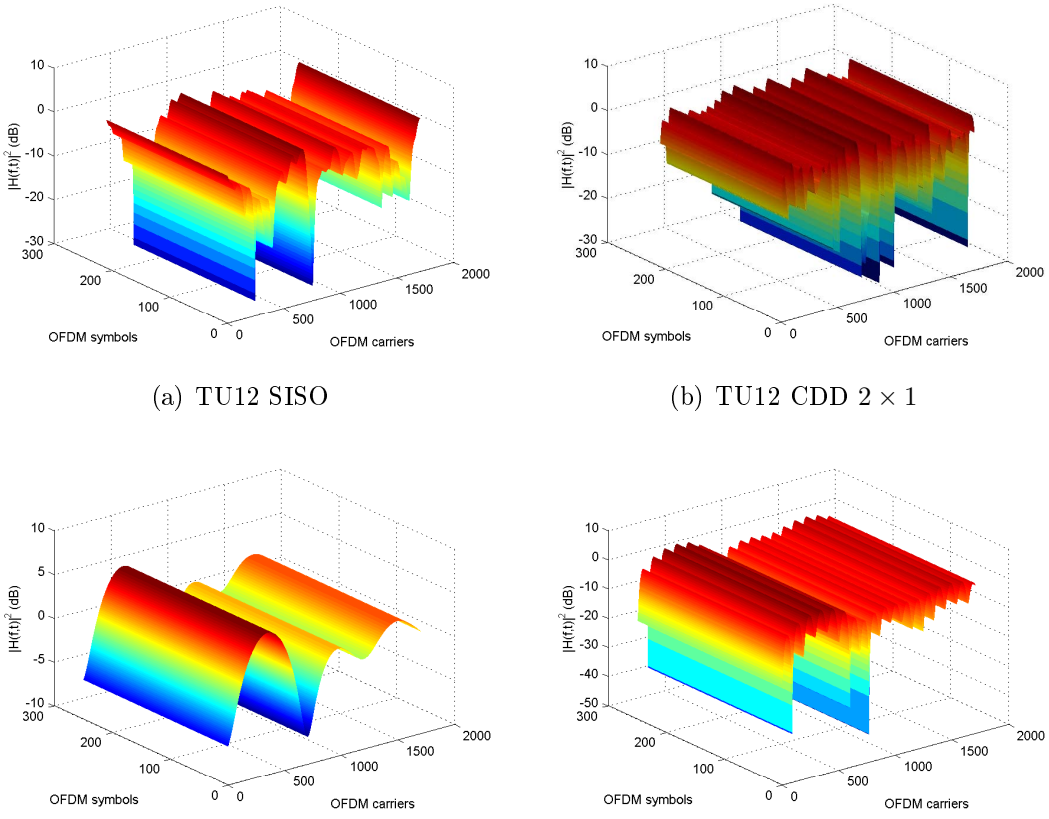

(a) TU12 SISO

(b) TU12 CDD 2×1

(c) RA6 SISO

(d) RA6 CDD 2×1

Figure 3.4: TU12 and RA6 channel snapshots for single antenna and CDD systems with $f_d = 30$ Hz.

3.3.1.2 Simulation Results

Figure 3.5 shows simulation results for 2×1 CDD, 2×1 orthogonal space-frequency block coding (OSFBC), 1×2 MRC and 2×2 CDD plus MRC over the DVB-T P1 Rayleigh channel. As it has been stated previously, one can observe that the CDD gain is negligible due to the frequency selectivity of the channel or in other words, the high delay spread. On the other hand, the SFBC based on the Alamouti scheme offers a gain of 4 dB at BER$=2 \cdot 10^{-4}$. It is noteworthy how 2×1 OSFBC and 1×2 MRC obtain the same diversity gain as it was demonstrated in [Alamouti98] even though MRC achieves other 3 dB else due to the array gain. Moreover, the combination of CDD and MRC does not offer any gain versus the 1×2 MRC configuration.

When simulations are carried out over RA6 NLOS and TU6 channels, as shown in Figures

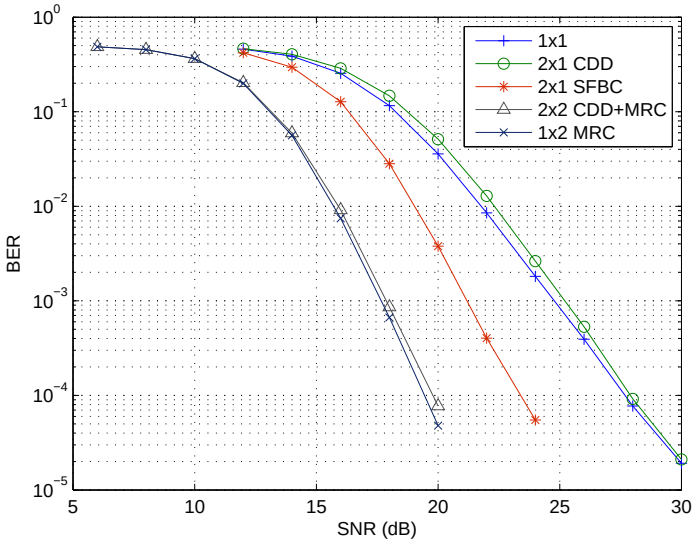

Figure 3.5: Performance comparison of diversity techniques for the DVB-T P1 channel.

3.6(a) and 3.6(b), respectively, we can see that diversity techniques offer higher gains over the RA6 channel without LOS that the TU6 channel. Furthermore, one should note that the behavior of CDD over RA6 obtains a gain of 2 dB whereas there is no gain in a TU6 channel. This is due to the fact that *extra* frequency selectivity added artificially by CDD does not result advantageous in high frequency selective channels such as TU6 or TU12 (See Figure 3.4). However, an enhancement of the performance can be given when properties of the fading channel are more similar to the RA6 channel case. On the other hand, we can observe that the SFBC scheme offers a high gain compared to the SISO case in both scenarios.

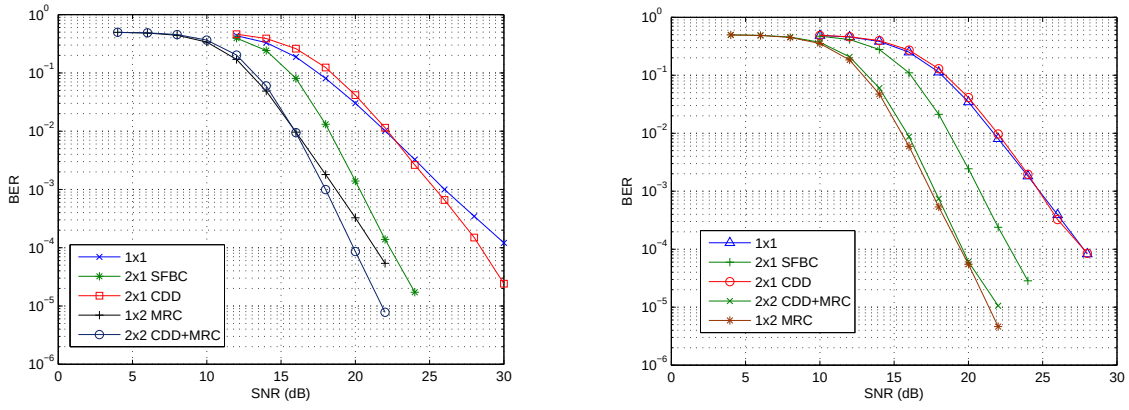

(a) RA6 NLOS

(b) TU6

Figure 3.6: BER performances of multi-antenna schemes over RA6 with NLOS and TU6 static channels.

If we now consider the Ricean channel RA6 with LOS, we observe in Figure 3.7 that

the performance of CDD decreases being 1 dB with respect to the SISO case for the 2×1 scheme. The gain becomes negative when CDD is combined with MRC. This behavior can be given in LOS conditions when the Ricean factor reaches certain threshold as it is proved in [Dammann07]. For the SFBC technique, we can notice that the LOS propagation slightly decreases the gain in comparison to the NLOS case since the direct component of the channel decreases the diversity of the system.

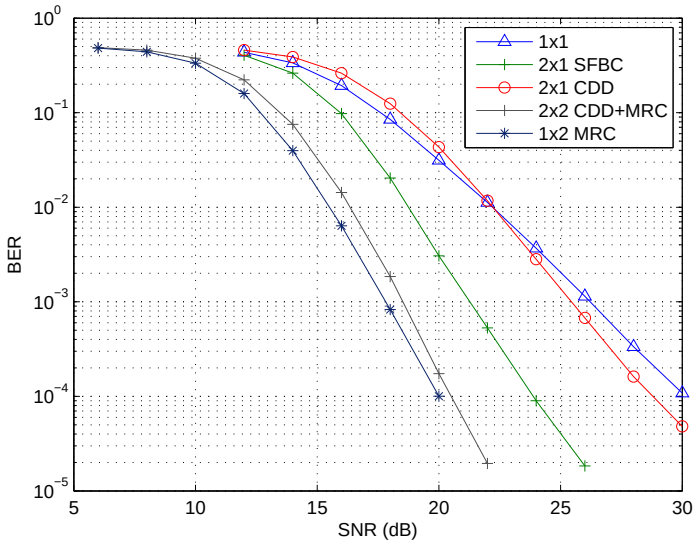

Figure 3.7: Performance comparison of diversity techniques for the RA6 channel with LOS component.

3.3.2 Mobile Environments

Despite the fact that DVB-T was not initially focused on mobile receivers[3], simulation results are provided to analyze the behavior of the system with the addition of diversity techniques. The Doppler frequency f_d has been set to 100 Hz, which corresponds to speeds of 228 km/h and 126 km/h at the limits of the ultra-high frequency (UHF) band, i.e. 474 and 858 MHz, respectively.

Figure 3.8 shows the BER performance as a function of SNR for the previously assessed diversity techniques over the TU6 channel. We can notice that DVB-T does not reach the QEF value of BER=$2 \cdot 10^{-4}$ for the SISO case since the BER curve has an error floor starting around SNR=30 dB. When multi-antenna techniques are used, the error floor is reduced up to BER=$2 \cdot 10^{-5}$ with the 2×1 SFBC configuration, making the QEF reception possible at SNR=24 dB. For 2×2 configuration with CDD and MRC techniques, the QEF reception

[3]The DVB-T standard [ETSI97] considers the portable mode as an available reception mode. However, portable reception should be considered as an static indoor or outdoor reception through portable devices with antenna. For reception in motion, the DVB-H standard [ETSI04], whose physical layer is shared by both systems, should be used.

is at SNR=19.5 dB. Note that the contribution of CDD technique affects negatively in the 2×2 configuration since 1×2 MRC obtains a gain around 0.5 dB greater.

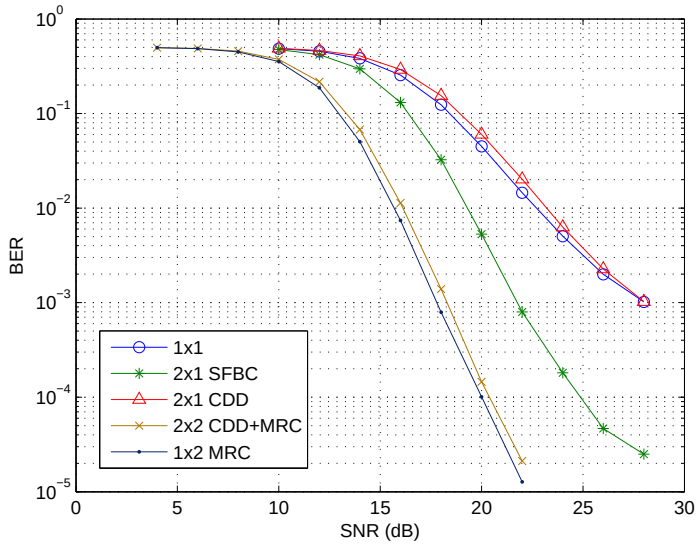

Figure 3.8: Comparison of diversity techniques performances for a mobile TU6 channel with $f_d = 100Hz$.

For the RA6 channels, we can see an improvement of the reception when there is a LOS component. Although 2×1 CDD reduces the error floor of the SISO performance, neither SISO case nor CDD schemes reach the QEF in any case. However, if the Alamouti SFBC code is used, good reception conditions are given for SNRs of 25 and 27.5 dB with LOS and NLOS, respectively. For mobility, 1×2 MRC reception obtains the best performance since the error floor is fully avoided up to the level of BER=$3 \cdot 10^{-5}$. On the other hand, one can observe that the LOS component reduces the gain of CDD technique as it is proved in [Dammann07].

As a conclusion, the SFBC technique offers good results in different broadcasting scenarios maintaining the diversity gain. On the other hand, CDD obtains lower gains than SFBC in any reception case. Furthermore, the CDD gain can be negligible or even negative for some channel conditions. Therefore, its implementation does not offer any advantage in comparison to the SFBC scheme from a performance point of view apart from the full backward compatibility.

3.4 Diversity and Coding in DVB-T2

This section present simulation results of the diversity techniques aimed at DVB-T2 over broadcasting scenarios. Concretely, the DVB-T2 SFBC scheme based on the Alamouti code [Alamouti98] and the RQD technique have been analyzed. As we have seen in Chapter 2, the

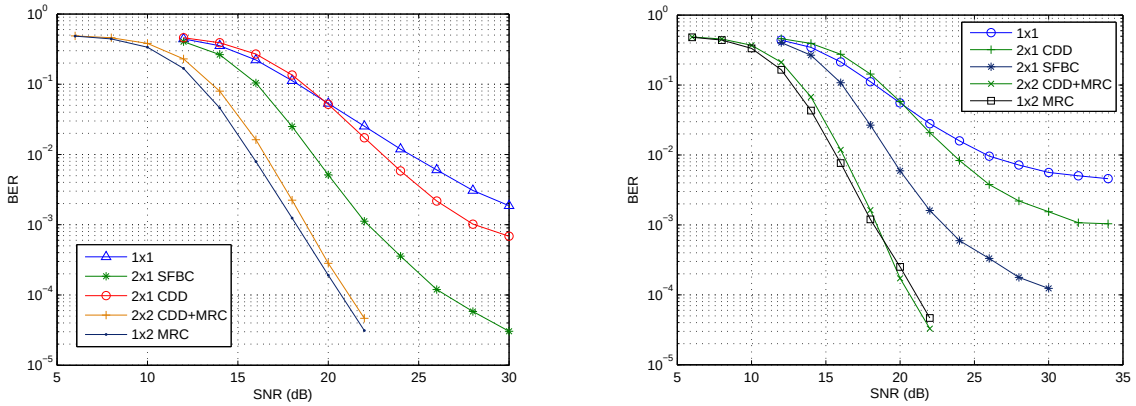

(a) RA6 LOS $f_d = 100$ Hz

(b) RA6 NLOS $f_d = 100$ Hz

Figure 3.9: BER performances of multi-antenna schemes over 100 Hz mobile RA6 channel with and without LOS.

former consist of a 2×1 multi-antenna system which achieves the full channel capacity and the latter is a frequency diversity technique which copes with deep fading scenarios. Both techniques have been included as optional in the DVB-T2 specifications in order to increase the robustness of the reception compared to its predecessor DVB-T.

We will analyze the performance of the DVB-T2 system with the mentioned techniques and we will compare them to other schemes studied in DVB-T and the SISO case. Moreover, we will briefly describe the necessary soft detection in DVB-T2 since it is a key reception issue which we will treat in detail in the ensuing chapters.

In the case of DVB-T2 system, the number of Monte Carlo realisations have been obtained as follows:

$$\text{target BER} = \frac{100 \text{ erroneous bits}}{N_{MC} N_{FEC} N_{IF} L_{FEC} R_c}, \tag{3.14}$$

where N_{FEC} corresponds to the number of FEC blocks per interleaving frame, N_{IF} denotes the number of interleaving frames and L_{FEC} is the length of the LDPC block. In DVB-T2, the QEF value after the LDPC decoder corresponds to BER=10^{-7} [4]. Reaching this value involves a very long simulation time and a smaller value is often assumed in the literature to keep simulation time reasonable. Since the performance of DVB-T2 is perfectly proved in [DVB09], we have considered different values of BER throughout this work depending on a reference target. When it is assumed that QEF is actually reached, BER values of 10^{-3} or 10^{-4} have been used for evaluation considering a target BER of 10^{-6} for the Monte Carlo realisations. Otherwise, the value of 10^{-7} is used considering the target BER of 10^{-8}.

[4] A BER rate of 10^{-7} after LDPC decoder corresponds to approximately 10^{-11} after BCH decoder.

3.4.1 Soft Detection: The Maximum a Posteriori Detection

LDPC decoding requires soft estimates of the transmitted information bits. This is usually carried out through the calculation of the *a posteriori* probabilities (APPs) of the received symbols using the maximum a posteriori (MAP) detector. This method expresses this information in the form of log-likelihood ratios (LLRs) (i.e. L-values [Hagenauer96]). The LLR of a bit b_k is defined as the logarithm of the ratio of the probabilities of the bit taking its two possible values and can be expressed as

$$L(b_k) = \ln \frac{\Pr[b_k = +1]}{\Pr[b_k = -1]}, \tag{3.15}$$

where the values of the bits are taken to be +1 and -1, representing logical '1' and '0', respectively. From one constellation symbol, there are $\log_2 P$ LLRs. Therefore, $k = \{0, \ldots, \log_2 P\}$. We can assume that the information bits are scrambled by means of several interleavers in such a way that the bits within the received symbol y may be considered statistically independent. Therefore, using Bayes' rule in (3.15), the *a posteriori* information $L_D(b_k|y)$ can be expressed as follows:

$$L_D(b_k|y) = \ln \frac{\Pr[b_k = +1|y]}{\Pr[b_k = -1|y]} = L_A(b_k) + L_E(b_k|y), \tag{3.16}$$

where $L_A(b_k)$ and $L_E(b_k|y)$ denote the *a priori* and extrinsic information, respectively. The extrinsic information conditioned to the received symbol y can be written as

$$L_E(b_k|y) = \ln \frac{\sum\limits_{\boldsymbol{b} \in \mathbb{X}_{k,+1}} p(y|\boldsymbol{b}) \exp\left(\sum\limits_{j \neq k \text{ and } b_j = +1} L_A(b_j) \right)}{\sum\limits_{\boldsymbol{b} \in \mathbb{X}_{k,-1}} p(y|\boldsymbol{b}) \exp\left(\sum\limits_{j \neq k \text{ and } b_j = +1} L_A(b_j) \right)}, \tag{3.17}$$

where $s = \text{map}(\boldsymbol{b}), s \in \mathcal{M}$ is the mapping of the bit vector $\boldsymbol{b}$ into the symbol s of the constellation $\mathcal{M}$. The set $\mathbb{X}$ represents the set of all bit vectors with length $\log_2 P$, i.e. the demapped set of $\mathcal{M}$. The expression $\mathbb{X}_{k,+1}$ and $\mathbb{X}_{k,-1}$ denote the subsets of $\mathbb{X}$ with the k-th bit to $+1$ or -1, respectively.

Multiplying the numerator and denominator in (3.17) by $\exp\left(-\sum_{k=0}^{\log_2 P - 1} L_A(b_k)/2\right)$, we obtain

$$L_E(b_k|y) = \ln \frac{\sum\limits_{\boldsymbol{b} \in \mathbb{X}_{k,+1}} p(y|\boldsymbol{b}) \exp\left(\frac{1}{2} \boldsymbol{b}_{[k]}^T \boldsymbol{L}_{A,[k]}\right)}{\sum\limits_{\boldsymbol{b} \in \mathbb{X}_{k,-1}} p(y|\boldsymbol{b}) \exp\left(\frac{1}{2} \boldsymbol{b}_{[k]}^T \boldsymbol{L}_{A,[k]}\right)}, \tag{3.18}$$

where $\boldsymbol{b}_{[k]}$ is the sub-vector of $\boldsymbol{b}$ obtained by omitting the k-th bit b_k and $\boldsymbol{L}_{A,[k]}$ denotes the vector of all L_A values, also omitting $L_A(b_k)$. Now, we must calculate the likelihood function

$p(y|\boldsymbol{b})$. Due to the Gaussian nature of the noise added at the receiver, the conditional probability distribution function is given by

$$p(y|\boldsymbol{b}) = p(y|s = \text{map}(\boldsymbol{b})) = \frac{\exp - \frac{|y-hs|^2}{2\sigma^2}}{2\pi\sigma^2}, \tag{3.19}$$

where h is the flat fading channel which affects a specific OFDM carrier.

By replacing (3.19) in (3.18), we obtain the exact expression for the calculation of the extrinsic information. However, the computation of the LLRs is usually simplified for hardware implementation by applying the Max-log approximation, which consists of a coarse approximation of the Jacobian logarithm

$$\ln\left(e^{a_1} + e^{a_2}\right) = \max(a_1, a_2) + \ln(1 + e^{-|a_2 - a_1|}), \tag{3.20}$$

by omitting the second term at the right-hand side of the equation. This correction term can be considered negligible at the SNR range where a receiver usually operates, resulting in a small performance degradation over the Jacobian logarithm approximation of (3.20) [Robertson95]. This way, Equation (3.18) becomes

$$\begin{aligned} L_E(b_k|y) \approx \\ \frac{1}{2}\max_{\boldsymbol{b}\in\mathbb{X}_{k,+1}} \left\{ -\frac{1}{\sigma^2}\left|y - hs\right|^2 + \boldsymbol{b}_{[k]}^T \boldsymbol{L}_{A,[k]} \right\} \\ -\frac{1}{2}\max_{\boldsymbol{b}\in\mathbb{X}_{k,-1}} \left\{ -\frac{1}{\sigma^2}\left|y - hs\right|^2 + \boldsymbol{b}_{[k]}^T \boldsymbol{L}_{A,[k]} \right\}. \end{aligned} \tag{3.21}$$

When iterative demapping is not used, there is no *a priori* information and (3.21) is simplified as

$$\begin{aligned} L_E(b_k|y) \approx \\ \frac{1}{2}\max_{\boldsymbol{b}\in\mathbb{X}_{k,+1}} \left\{ -\frac{1}{\sigma^2}\left|y - hs\right|^2 \right\} \\ -\frac{1}{2}\max_{\boldsymbol{b}\in\mathbb{X}_{k,-1}} \left\{ -\frac{1}{\sigma^2}\left|y - hs\right|^2 \right\}. \end{aligned} \tag{3.22}$$

3.4.2 Rotated Constellations

The constellation rotation or RQD operation specified in DVB-T2 aims to increase the diversity order of the DVB-T2 BICM scheme. This technique is comprised of two stages: correlating the I and Q components of the transmitted signal through the rotation of the QAM constellation and making these components fade independently by means of a cyclic

delay of the Q component. The rotation of the constellation allows casting every constellation symbol over I and Q axis independently in such a way that the whole information of the QAM symbol can be taken from either the new I or Q components. The cyclic delay of the Q component makes the I and Q components fade independently using a simplified approach of the signal space diversity (SSD) technique [Al-Semari97]. The insertion of a simple delay for one of the two components avoids the loss of both I and Q signals due to the same fading event, as it was shown in Figure 2.3.

One should note that whether RQD technique is used[5], Equation (3.21) has to be slightly modified since the I (s_I) and Q (s_Q) components of the symbol s are subject to different fading channels, h_I and h_Q, respectively. Therefore, the extrinsic information is given as

$$\begin{aligned} L_E(b_k|y) \approx \\ \frac{1}{2}\max_{\boldsymbol{b}\in\mathbb{X}_{k,+1}}\left\{-\frac{1}{\sigma^2}\left|y_I-h_I s_I\right|^2+\left|y_Q-h_Q s_Q\right|^2+\boldsymbol{b}_{[k]}^T\boldsymbol{L}_{A,[k]}\right\} \\ -\frac{1}{2}\max_{\boldsymbol{b}\in\mathbb{X}_{k,-1}}\left\{-\frac{1}{\sigma^2}\left|y_I-h_I s_I\right|^2+\left|y_Q-h_Q s_Q\right|^2+\boldsymbol{b}_{[k]}^T\boldsymbol{L}_{A,[k]}\right\}, \end{aligned} \tag{3.23}$$

where y_I and y_Q are the received I and Q values of y, respectively.

In order to analyze the performance of this technique, an approach for a flat Rayleigh channel with erasures (RME) was proposed in [Nour08] and included later in [DVB09] for DVB-T2. The proposed channel model substitutes the frame builder, the OFDM generation blocks, the wireless channel and their corresponding inverse stages with an equivalent flat fading channel as depicted in Figure 3.10. This way, the BICM module of the DVB-T2 standard is only necessary for the RQD assessment. The channel samples are considered uncorrelated due to all the interleaving stages of DVB-T2. Hence, the equivalent received symbol Y at discrete time t is given by

$$Y(t) = H(t)E(t)X(t) + N(t), \tag{3.24}$$

where $X(t)$ is the complex discrete transmit symbol, $H(t)$ is a Rayleigh distributed fading channel coefficient with mean the unity, $E(t)$ is a uniform random process which takes the value of zero with probability P_E and $N(t)$ is the AWGN sample at time index t.

The work, which is presented below, was partially published in [Mendicute10]. Figure 3.11 presents the BER curves of the DVB-T2 BICM system as a function of CN over a RME channel with 20% of erasures or lost carriers for two different code rates, $R_c = 3/4$ and $2/3$. For the first case, the LDPC can not recover the lost information due to erasures and the performance of the system without RQD tends to an error floor above the QEF limit of

[5]The DVB-T2 specification [DVB09] recommends its use at all times unless other incompatible technique is in use.

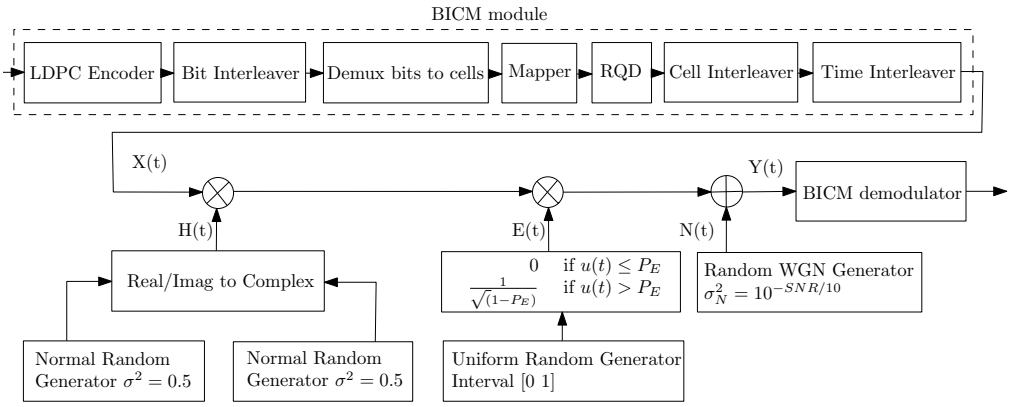

Figure 3.10: Equivalent DVB-T2 BICM system over flat fading Rayleigh channel with erasures.

10^{-7}. However, the diversity added by RQD makes LDPC correction possible providing a considerable improvement. On the other hand, when the error-correcting capacity of the code is greater, the improvement provided by RQD becomes smaller, as is shown in Figure 3.11 for the case of $R_c = 2/3$. Therefore, the gain of the system with RQD transmission results very significant over this kind of channels for high coding rates and low modulation orders.

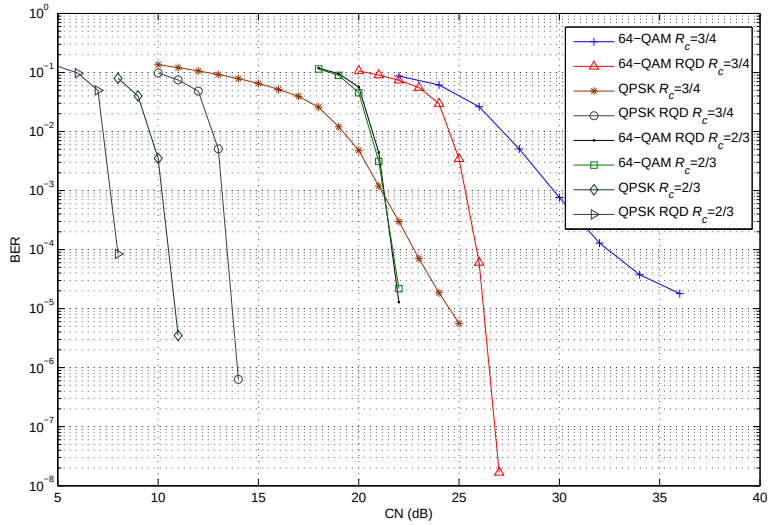

Figure 3.11: Performance of RQD in DVB-T2 BICM transmission with $L_{FEC} = 16200$ over a flat Rayleigh channel with 20% of erasures.

If we now simulate the complete DVB-T2 system model of Figure 2.2 over a frequency-selective TU6 channel, we can observe in Figure 3.12 that the gain of RQD decreases significantly in comparison to the results displayed in the previous figure. When the code rate is high, the RQD technique improves the reception thanks to the increased diversity level. Consequently, the RQD method can be taken into account for high code rates where the re-

dundancy rate of the coding is similar or even less than the loss of information. Furthermore, when high-order modulation is used such as 64-QAM, the RQD gain is almost negligible. However, if the modulation order is decreased, RQD offers an improvement of the reception. As a result, one conclusion that can be drawn from the results depicted in Figures 3.11 and 3.12, is that the Rayleigh memoryless channel with erasures is not a very realistic channel when modeling realistic hard transmission scenarios such as a TU6 channel.

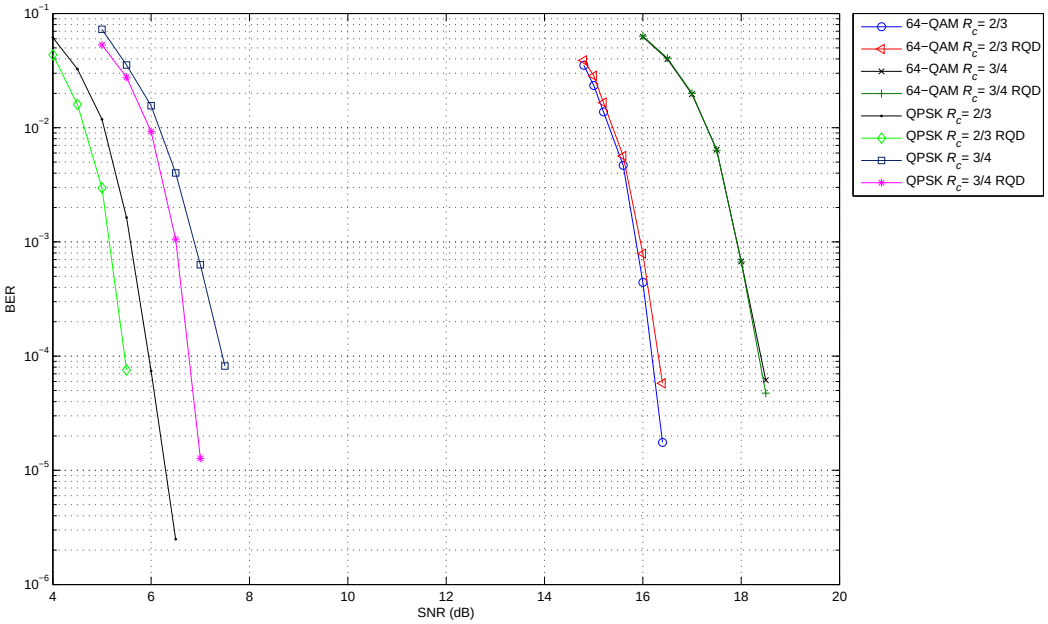

Figure 3.12: Performance of RQD in the SISO DVB-T2 system with $L_{FEC} = 64800$ over a TU6 channel.

3.4.3 The DVB-T2 SFBC

This section presents simulation results of the DVB-T2 SFBC scheme over Rayleigh TU6 and Ricean RA6 channels. The detection stage has been carried out using two methods. On one hand, the decoupling of the transmitted signals based on the quasi-static fading assumption [Alamouti98], where, by considering (2.19) for the 2×1 configuration, transmitted symbols can be detected through

$$\boldsymbol{H}_{eq}^{H} \begin{bmatrix} y_1 \\ y_2^* \end{bmatrix} = \begin{bmatrix} |h_1|^2 + |h_2|^2 & 0 \\ 0 & |h_1|^2 + |h_2|^2 \end{bmatrix} \begin{bmatrix} s_1 \\ s_2 \end{bmatrix}, \tag{3.25}$$

in such a way that s_1 and s_2 are completely decoupled. For the 2×2 case, the procedure is the same using the equivalent channel in (2.21) instead. One should note that due to the slight modification in DVB-T2 of the original Alamouti STBC, $\boldsymbol{H}_{eq}$ in (2.19) and (2.21) has

to be modified following (2.28). On the other hand, if we assume that the channel can vary in adjacent carriers, the linear ZF technique of (2.25) can be then considered. In this case, the equivalent channel $\boldsymbol{H}_{eq}$ distinguishes the channel coefficients in adjacent carriers, such that (2.28) is written for 2×1 as

$$\boldsymbol{H}_{eq} = \begin{bmatrix} h_{1,c1} & -h_{2,c1} \\ h^*_{2,c2} & h^*_{1,c1} \end{bmatrix}, \tag{3.26}$$

where the subscripts $c1$ and $c2$ denote the first and second carriers of each coded pair, respectively. The considered DVB-T2 parameters are:

- Length of LDPC block: 64800 bits
- LDPC code rate: $R_c = 2/3$
- Constellation size: 64-QAM
- FFT size: 8192 carriers (8K)
- Guard interval: 1/4

Figure 3.13 shows the BER performance of the 2×1 and 2×2 SFBC schemes compared to the SISO case over a TU6 channel. When the detection is based on ZF (denoted by adj=0 in the Figure), one can observe at the BER level of 10^{-4} that the 2×1 setup achieves a performance gain around 2 dB whereas this is 6 dB for 2×2 configuration. On the other hand, we can see how the performance gains become smaller when quasi-static channel is assumed (denoted by adj=1 in the Figure). If the channel is highly frequency selective such as TU6, the use of an small FFT size (2K) involves that the channel of adjacent carriers does not maintain invariant. As a result, the Alamouti detection based on the quasi-static fading assumption leads to a slight loss of performance. When channels are time-variant, the loss of performance could become greater.

In Figure 3.14 we show simulation results for a RA6 channel with LOS. In this case, the performance gains compared to the SISO case are greater than the previous ones. At a BER=10^{-4}, they are around 3.5 and 8 dB for 2×1 and 2×2, respectively, when ZF detection is used. One can note that the use of the detection based on the quasi-static fading assumption has a negligible loss of performance in the RA6 channel. This is because of RA6 is less frequency selective and the channel variation in adjacent carriers is much lower.

3.5 Reception in SFN Networks

The main advantages of the SFN deployment strategy are the efficient use of the television spectrum, allowing a higher number of TV programs [Penttinen08], and the coverage in-

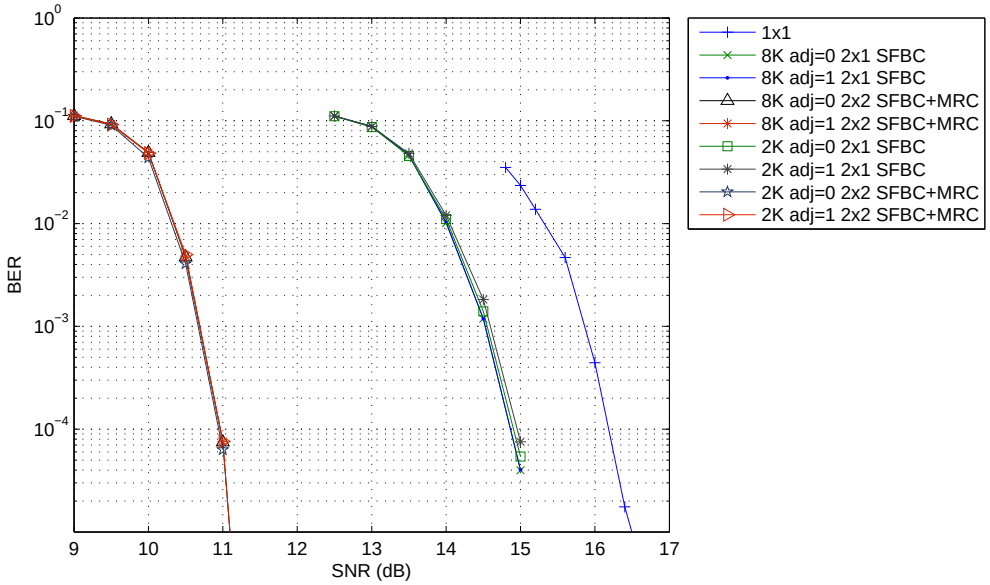

Figure 3.13: BER curves of diversity schemes in a DVB-T2 system with FFT sizes 2K and 8K, 64-QAM modulation, code rate $R_c = 2/3$, LDPC block length $L_{FEC} = 64800$ affected by a TU6 channel.

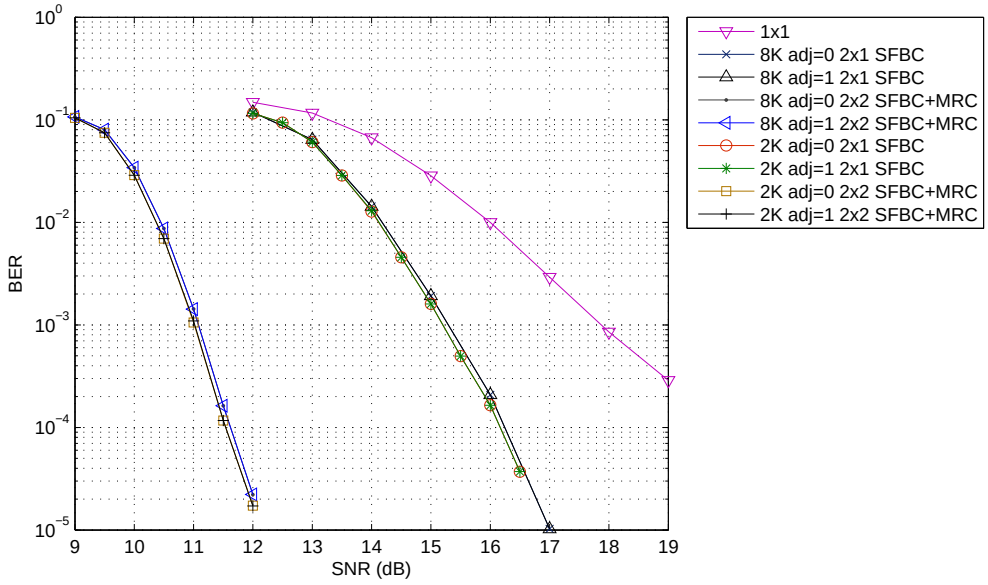

Figure 3.14: BER curves of diversity schemes affected by a RA6 channel with LOS in a DVB-T2 system with FFT sizes 2K and 8K, 64-QAM modulation, LDPC block length of 64800 bits and code rate $R_c = 2/3$

crease due to the SFN gain obtained through the positive contribution of the transmitters [Santella04]. The latter advantage is not actually true since two identical delayed signals do not only add constructively but also destructively leading to severe interference in specific locations which can make the signal unrecoverable [Sobron09a]. This effect, which is called self-interference, can be a nightmare for network planning and has been widely studied in the literature [García-Lozano10, Morgade09, Mannino08]. This section analyzes the case of self-interference for DVB-T2 SISO and the behavior of DVB-T2 system using a distributed MISO network architecture.

3.5.1 Echoes in the SFN Network or Self-Interference

SFN networks are composed by several cells which are deployed to cover wide areas with an unique frequency band. The border between cells, where receivers have sight from several transmitters, is called overlapping area. The SFN network gain is defined as the positive contribution due to constructive superposition of all received signals within the GI. However, received signals can also add destructively despite being inside the GI. In order to observe the negative effect in these areas, a simple constructive and destructive wave interference problem is stated in [Sobron09a, Mendicute10] and explained below.

Two coherent sources generate wave forms $\psi_1(x,t)$ and $\psi_2(x,t)$ with speed v and direction $+x$, so that:

$$\psi_1(x,t) = \Re(A_1 e^{i(\omega\left(t-\frac{x}{v}\right)+\varphi_1)}) = \Re(A_1 e^{i(\omega t - kx + \varphi_1)}), \tag{3.27}$$

$$\psi_2(x,t) = \Re(A_2 e^{i(\omega\left(t-\frac{x}{v}\right)+\varphi_2)}) = \Re(A_2 e^{i(\omega t - kx + \varphi_2)}), \tag{3.28}$$

where $k = \frac{\omega}{v} = \frac{2\pi}{\lambda}$ is the angular wavenumber. The resulting waveform at a point P, whose distances to the sources are d_1 and d_2, can be expressed as the real part of the sum of phasors shown in Figure 3.15 as follows:

$$\psi_T(P,t) = A_T \cos(\omega t + \varphi_T), \tag{3.29}$$

where the resultant waveform amplitude is

$$A_T = \sqrt{A_1^2 + A_2^2 + 2A_1A_2\cos(k\,(d_1 - d_2) + \varphi_1 - \varphi_2)}. \tag{3.30}$$

If τ_0 is the resulting delay due to the distances and phase differences, Equation (3.30) can be written as

$$A_T = \sqrt{A_1^2 + A_2^2 + 2A_1A_2\cos(2\pi f \tau_0)}, \tag{3.31}$$

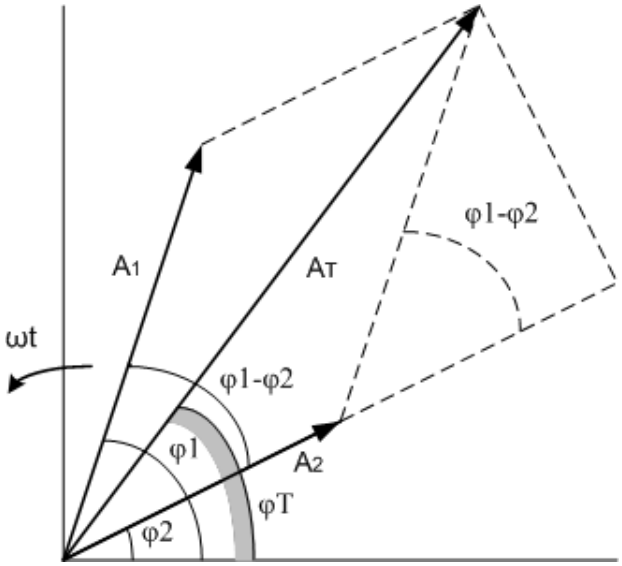

Figure 3.15: Phasor diagram of the waveforms.

where f is the carrier frequency. Equation (3.31) proves that the resultant waveform amplitude will never be zero if received signals powers are different. However, if power levels are equal, involves that $A_1 = A_2 = A$ and (3.31) can be expressed after some operations as

$$A_T = 2A\cos(\pi f \tau_0)\,. \tag{3.32}$$

In this case, resultant waveform amplitude is periodically nulled. If we now consider the wideband OFDM spectrum, A_T will be zero when carrier frequency is equal to $f = \frac{2n+1}{2\tau_0}, n \in \mathbb{Z}^+$. The number of zeros within the OFDM spectrum depends on the delay between transmitters since the distance between nulls is $\Delta f = 1/\tau_0$. Considering a DVB-T or DVB-T2 system with 8K FFT size and GI length 1/4, an echo delayed half a guard interval involves τ_0=112 μs. Therefore, there is a null every 9 KHz within 8 MHz OFDM spectrum as shows Figure 3.16(b). If the distance between carriers is 1.1 KHz, one out of nine carriers is nulled, losing its information. One should note that the previous analysis does not take into account channel considerations such as fading coefficients or noise power. However, it is enough to prove the carrier destruction in the SFN reception.

Simulation results for an AWGN channel affected by an echo are depicted in Figure 3.17 using a DVB-T2 system with parameters:

- RQD constellation
- Length of LDPC block: 16200 bits
- LDPC code rate: $R_c = 3/5$
- Constellation size: 64-QAM

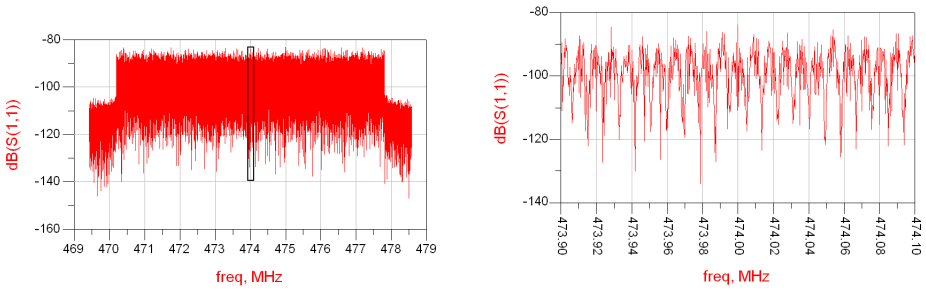

(a) 8 MHz OFDM symbol

(b) Zoom of the marked box in the left Figure

Figure 3.16: 8 MHz OFDM spectrum affected by an echo delayed half a guard interval (1024 samples for 8K).

- FFT size: 2048 carriers (2K)
- Guard interval: 1/4

The gain between the main signal and the echo powers is defined as

$$\mathrm{G} = 10\log_{10}\frac{P_{echo}}{P_{signal}}\ (\mathrm{dB}). \tag{3.33}$$

One can see that the performance gain becomes smaller when the delay between the signal and the echo is longer. Furthermore, as we have seen in (3.32), if the powers are equal (G=0 dB) the degradation for the same delay is maximum (3.8 and 7 dB for GI/2 and GI, respectively). DVB-T2 system is more robust against self-interference than DVB-T since DVB-T2 achieves good reception where DVB-T does not reach QEF as it is proved in [Sobron09a]. As can be seen, all the simulated scenarios achieve the QEF limit of 10^{-7}.

3.5.2 Distributed MISO Transmission in SFN Networks

When a distributed MISO network is deployed, we have to take into account that MISO channel antennas can be located several kilometers away from each others. Therefore, depending on the position of the receiver, the signals from the transmit antennas can be received with different attenuation and delay as expressed in (3.9). These propagation conditions are assessed in this section varying the attenuation and the delay of the second transmitter of the MISO scheme. For that purpose, we have used a TU6 SFN channel following (3.9). In order to maintain the transmitted power to the unity, attenuations of (3.9) for the MISO 2×1 scheme must fulfill the following constraints:

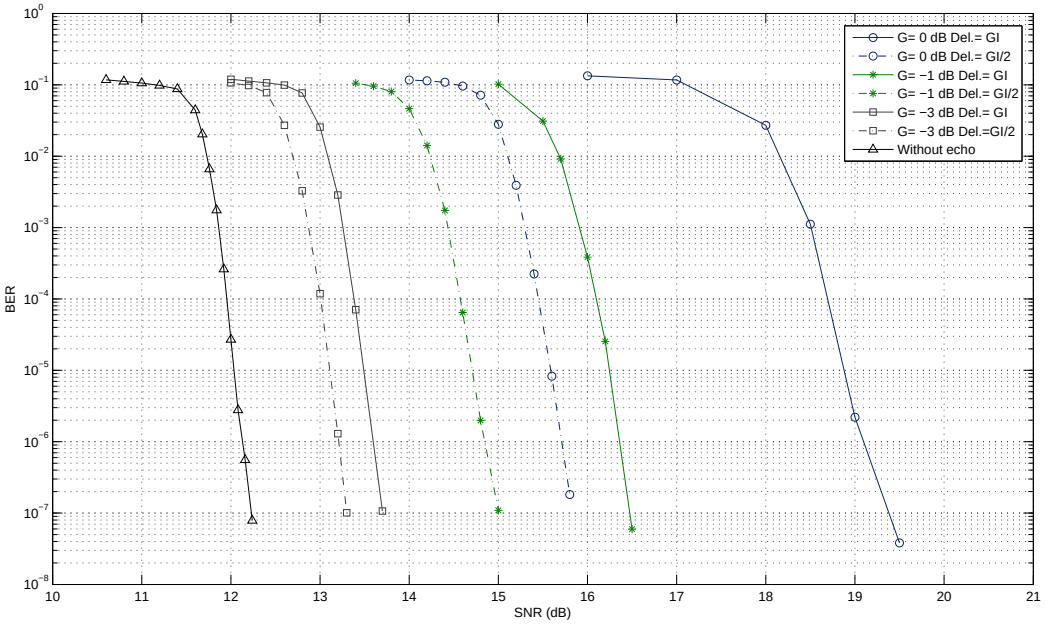

Figure 3.17: BER performance for DVB-T2 system affected by echoes of different power delayed GI and GI/2 in an AWGN channel.

$$\sum_{k=1}^{2} \alpha_k^2 = 1, \tag{3.34}$$

$$\mathrm{G} = 10 \log_{10} \frac{\alpha_2^2}{\alpha_1^2}. \tag{3.35}$$

With these considerations, simulation results are provided in Figure 3.18 for the DVB-T2 systems with the following parameters:

- Length of LDPC block: 64800 bits
- LDPC code rate: $R_c = 2/3$
- Constellation size: 64-QAM
- FFT size: 8192 carriers (8K)
- Guard interval: 1/4

Considering the delay of the first transmitter equal to zero, i.e. $t_1 = 0$, the values of the G and t_2 are shown in Table 3.4. One can observe in Figure 3.18 that delays longer than 0.75 GI do not allow a correct reception of the signal, since the BER performance has an error floor over the QEF. On the other hand, we can see that similar attenuations, i.e. $\alpha_1 \approx \alpha_2$,

Table 3.4: SFN channel parameters

Delay t_2 (samples)	0 (Synchronized)	0.45GI	0.75GI	0.9GI
G (dB)	0	-3	-6	

result in a loss of performance when $t_2 > 0.45$GI whereas we find an opposite behavior if $t_2 < 0.45$GI. As a result, the synchronous case, $t_2 = 0$, obtains the optimum performance with SNR=16.2 dB at the QEF.

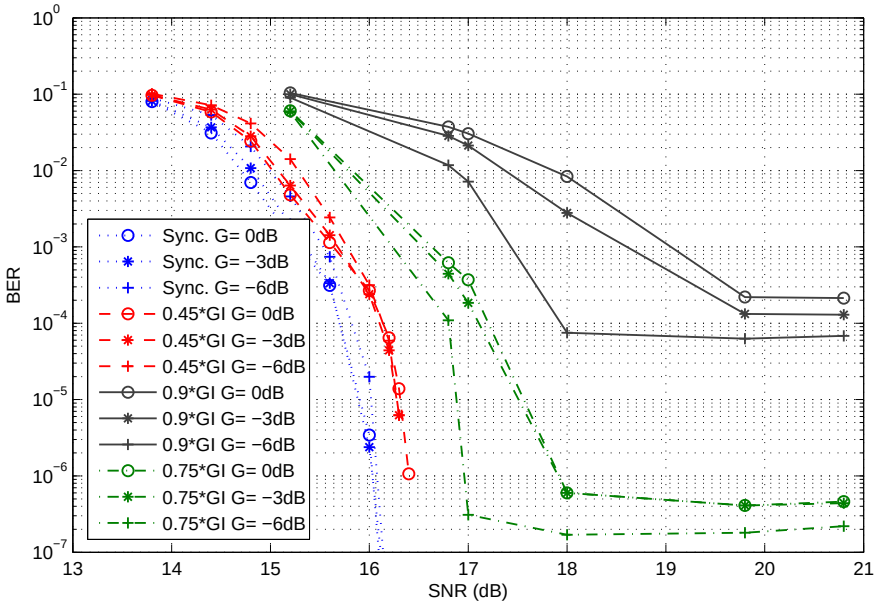

Figure 3.18: BER performance comparison for the distributed DVB-T2 MISO system affected by different TU6 SFN channel configurations.

3.6 Chapter Summary

In this chapter, we have studied the multi-antenna diversity techniques in the broadcasting environments of the TDT systems DVB-T and DVB-T2. First of all, we have defined the common propagation scenarios in the TDT networks, which are essentially multipath fading channels due to the multiple reflexions existing in broadcasting transmission. These channels follow Rayleigh or Ricean distributions depending on the NLOS or LOS component from the transmitter to the receiver, respectively.

The CDD, OSFBC and MRC diversity techniques have been assessed in the DVB-T standard. According to the simulation results and considering a viability point of view, the MISO SFBC method, which has been included in the DVB-T2 specification [ETSI09], offers

the best trade-off between performance and deployment cost. The 2×1 OSFBC achieves the same diversity gain as the 1×2 MRC. Therefore, by using transmit diversity instead of receive diversity, the cost of receivers can be reduced maintaining the diversity performance. On the other hand, although the inclusion of CDD does not need any modifications in the reception stage, its performance is negligible or even negative in scenarios such as very frequency selective channels or Ricean channels, respectively.

For the DVB-T2 system, an analysis of the standard options have been carried out from a diversity point of view. Due to the utilization of an LDPC coding, the necessary soft-output MAP detection has been previously described.

The last part of the chapter has focused on two situations which can be given in SFN networks. First, the echoes inside the SFN network due to other interfering transmitters have been analyzed. The contribution of various transmitters can affect negatively to the received signal depending on the power differences and delays among transmitters. The worst case is given when the power of different transmitters is similar at the receiver. In that case, deep fadings along the OFDM symbol completely erase the information of the affected carriers resulting in a considerable reduction of the BER performance.

The second issue has concerned with the distributed transmission of the DVB-T2 MISO scheme. The MIMO concept is usually associated to various antennas located at the same transmitter or receiver such that the power contribution of transmit antennas can be assumed the same and the delay between signals negligible. However, the distributed DVB-T2 MISO scheme consists of considering two transmitters of the SFN network as the transmit antennas of the MISO channel. Therefore, due to the large distance between transmitters and receiver, signal power and delays have to be taken into account in the channel modelling. Simulation results showed that long delays between transmitted signals lead to a loss of performance at the receiver. If the delay exceeds certain threshold value, the degradation could cause an error floor over the QEF limit. Therefore, the deployment of the SFN network results in a key point for the optimum performance.

Chapter 4

Soft-Output MIMO Detection in DVB-T2

4.1 Introduction

Multi-antenna diversity techniques offer a higher robustness maintaining the bandwidth of the system. As we have seen in the Chapter 3, the diversity gain is higher when the coding gain is lower since bit error probability curves are further from the theoretical capacity limit. In other words, when SFBC is used in DVB-T, we can observe a higher diversity gain due to the lower error correction capability of a convolutional code. However, when MISO is used in DVB-T2 which has a powerful FEC stage, the diversity gain becomes lower in comparison to the DVB-T system due to the high coding gain the LDPC encoding offers. So far, we have thought on MIMO techniques as a simple and efficient way to obtain one of their main advantages, diversity. However, MIMO channels can be exploited maximizing the diversity-multiplexing frontier.

Currently, the main objective of the MIMO inclusion in future DTV systems is based on combining diversity and spatial multiplexing, being various MIMO techniques analyzed for that purpose. Nevertheless, FRFD codes are becoming an interesting proposal, being the most remarkable the Golden code [Belfiore04]. Due to the fact that FRFD codes include spatial multiplexing, the computational cost of the detection at the receivers grows drastically. Therefore, it is important to find a trade-off between their detection complexity and performance.

This chapter studies the behavior of two FRFD codes with different detection complexity degrees over a DVB-T2 framework, since the DVB-T2 standard presents some key techniques in the BICM stage which can be adopted by next-generation systems. First of all, we will present the adaptation of the MAP detection for FRFD SFBC codes. In order to reduce the calculation of the necessary soft information for the LDPC decoder, an LLR approximation based on a list of candidates is seen, showing that the accuracy of the approximation depends on the number of candidates. The performance of the list ML detector with the FRFD codes

is shown for different broadcasting scenarios. Finally, the analysis of detection complexity is drawn.

4.2 Soft Detection of SFBCs

In the same way as SISO schemes, the LDPC decoder requires a soft estimate of each transmitted bit. However, unlike the symbol-wise detector for single-antenna transmission (see Subsection 3.4.1), the computation of the LLRs of a given symbol of the SFBC code will depend on the rest of coded symbols in the same codeword. Therefore, a soft-output MAP detector has to be designed for MIMO detection.

4.2.1 SFBC MAP Detection

In order to detect the transmitted symbols of the vector $\boldsymbol{s}$ jointly, we rewrite the equations of MAP detection considering the MIMO model in Chapter 2. Following (3.16), the *a posteriori* information conditioned to the received vector $L_D(b_k|\boldsymbol{Y})$ will depend on the *a priori* information $L_A(b_k)$ and the channel observations given by extrinsic information. The latter, which is conditioned to the received vector $\boldsymbol{Y}$, can be expressed as

$$L_E(b_k|\boldsymbol{Y}) = \ln \frac{\sum\limits_{\boldsymbol{b}\in\mathbb{B}_{k,+1}} p(\boldsymbol{Y}|\boldsymbol{b}) \exp\left(\sum\limits_{j\in\mathbb{J}_{k,\boldsymbol{b}}} L_A(b_j)\right)}{\sum\limits_{\boldsymbol{b}\in\mathbb{B}_{k,-1}} p(\boldsymbol{Y}|\boldsymbol{b}) \exp\left(\sum\limits_{j\in\mathbb{J}_{k,\boldsymbol{b}}} L_A(b_j)\right)}, \tag{4.1}$$

where $p(\boldsymbol{Y}|\boldsymbol{b})$ represents the likelihood function. Defining $K_b = MT\log_2 P$ as the number of bits mapped into the symbol vector $\boldsymbol{s}$, $\mathbb{B}_{k,+1}$ represents the set of 2^{K_b-1} bit vectors $\boldsymbol{b}$ having $b_k = +1$ so that

$$\mathbb{B}_{k,+1} = \{\boldsymbol{b}|b_k = +1\}, \mathbb{B}_{k,-1} = \{\boldsymbol{b}|b_k = -1\}, \tag{4.2}$$

and $\mathbb{J}_{k,\boldsymbol{b}}$ is the set of subindices that can be written as

$$\mathbb{J}_{k,\boldsymbol{b}} = \{j|j = 0,\ldots,K_b-1, j\neq k, b_j = +1\}. \tag{4.3}$$

4.2.2 Likelihood Function for SFBC MAP Detection

The most important part of the calculation of L_E in (4.1) is the likelihood function $p(\boldsymbol{Y}|\boldsymbol{b})$. Considering the system model in (2.2), we can rewrite $\boldsymbol{H}$ as an equivalent 4×4 MIMO channel following (2.4). Thus, the equivalent channel can be expressed as

$$\breve{\boldsymbol{H}} = \begin{bmatrix} \boldsymbol{H}_1 & \boldsymbol{0} \\ \boldsymbol{0} & \boldsymbol{H}_2 \end{bmatrix} = \begin{bmatrix} h_{11}^1 & h_{12}^1 & 0 & 0 \\ h_{21}^1 & h_{22}^1 & 0 & 0 \\ 0 & 0 & h_{11}^2 & h_{12}^2 \\ 0 & 0 & h_{21}^2 & h_{22}^2 \end{bmatrix}, \tag{4.4}$$

where h_{ij}^k is the complex channel coefficient from transmit antenna j to receive antenna i at the k-th carrier. Note that we have distinguished between $\boldsymbol{H}_1$ and $\boldsymbol{H}_2$ since they are equal if and only if the channel does not vary in adjacent carriers. By taking the elements from matrices $\boldsymbol{X}$ and $\boldsymbol{Y}$ column-wise, we obtain the vectors $\boldsymbol{x} = [x_{11}, x_{21}, x_{12}, x_{22}]^T$ and $\boldsymbol{y} = [y_{11}, y_{21}, y_{12}, y_{22}]^T$, respectively. Now, considering the generator matrix $\boldsymbol{G}$ for the corresponding SFBC, the system in (2.2) can be expressed as in (2.5) facilitating the calculation of the likelihood function. Thus, $p(\boldsymbol{Y}|\boldsymbol{b})$ can be rewritten as

$$p(\boldsymbol{Y}|\boldsymbol{s} = \text{map}(\boldsymbol{b})) = \frac{\exp\left(-\frac{\left\|\boldsymbol{y}-\breve{\boldsymbol{H}}\boldsymbol{G}\boldsymbol{s}\right\|^2}{2\sigma^2}\right)}{(2\pi\sigma^2)^{NT}}, \tag{4.5}$$

where $\boldsymbol{s} = \text{map}(\boldsymbol{b})$ is the mapping of the vector $\boldsymbol{b}$ into the symbols of column vector $\boldsymbol{s}$. In the same way as the SISO case, only the term inside the exponent in (4.5) is relevant for the calculation of L_E, and the constant factor outside the exponent can be omitted. Therefore, with the Max-log approximation, the extrinsic value L_E in (4.1) becomes

$$\begin{aligned} L_E(b_k|\boldsymbol{Y}) \approx \\ \frac{1}{2}\max_{\boldsymbol{b}\in\mathbb{B}_{k,+1}}\left\{-\frac{1}{\sigma^2}\left\|\boldsymbol{y}-\breve{\boldsymbol{H}}\boldsymbol{G}\boldsymbol{s}\right\|^2 + \boldsymbol{b}_{[k]}^T L_{A,[k]}\right\} \\ -\frac{1}{2}\max_{\boldsymbol{b}\in\mathbb{B}_{k,-1}}\left\{-\frac{1}{\sigma^2}\left\|\boldsymbol{y}-\breve{\boldsymbol{H}}\boldsymbol{G}\boldsymbol{s}\right\|^2 + \boldsymbol{b}_{[k]}^T L_{A,[k]}\right\}. \end{aligned} \tag{4.6}$$

The main difficulty in the calculation of (4.6) arises from the computation of the ML metrics

$$\left\|\boldsymbol{y}-\breve{\boldsymbol{H}}\boldsymbol{G}\boldsymbol{s}\right\|^2, \tag{4.7}$$

since a calculation of P^4 metrics is necessary for a 2×2 FRFD SFBC. This becomes unfeasible for high modulation orders unless the calculation of (4.6) can be reduced. Therefore, techniques that simplify and reduce the number of computed candidates are usually used.

4.2.3 List Detection

In order to reduce the calculation of L_E in (4.6), a good approximation based on a candidate list $\mathcal{L}$ of the ML metrics in (4.7) is proposed in [Hochwald03]. The list includes $1 \leq N_{cand} < P^4$ vectors $\boldsymbol{s}$ with the smallest ML metrics in (4.7). The number of candidates N_{cand} must be defined sufficiently large in such a way that it contains the maximizer of (4.6) with high probability [Hochwald03]. Hence, (4.6) can be approximated as

$$\begin{aligned} L_E(b_k|\boldsymbol{Y}) \approx \\ \frac{1}{2}\max_{\boldsymbol{b}\in\mathcal{L}\cap\mathbb{B}_{k,+1}}\left\{-\frac{1}{\sigma^2}\left\|\boldsymbol{y}-\breve{\boldsymbol{H}}\boldsymbol{G}\boldsymbol{s}\right\|^2+\boldsymbol{b}_{[k]}^T L_{A,[k]}\right\} \\ -\frac{1}{2}\max_{\boldsymbol{b}\in\mathcal{L}\cap\mathbb{B}_{k,-1}}\left\{-\frac{1}{\sigma^2}\left\|\boldsymbol{y}-\breve{\boldsymbol{H}}\boldsymbol{G}\boldsymbol{s}\right\|^2+\boldsymbol{b}_{[k]}^T L_{A,[k]}\right\}. \end{aligned} \tag{4.8}$$

One should note that either $\mathcal{L}\cap\mathbb{B}_{k,+1}=\emptyset$ or $\mathcal{L}\cap\mathbb{B}_{k,-1}=\emptyset$ make the computation of the extrinsic information unfeasible. To solve this problem, a simple clipping of the L_E value is proposed in [Hochwald03]. Considering $\mathcal{L}$ sufficiently large, the fact that the k-th bit for all symbol vectors of the candidate list $\mathcal{L}$ corresponds to $+1$ or -1 involves that the corresponding LLR has a certain reliability. Therefore, truncating L_E to a reliable value should yield good results. There is not any established criteria in the literature, to the best of our knowledge, to choose the suitable clipping value. Hence, several tests have been carried out using different statements. The different options proposed are:

1. L_E value truncated to ± 8 [Hochwald03].

2. L_E value truncated to ± 80. In this case, we simply consider a high value of L_E.

3. L_E value truncated to $\pm\frac{d_{min}^2}{2\sigma^2}$. Noting that the sets $\mathbb{B}_{k,+1}$ and $\mathbb{B}_{k,-1}$ are delimited by horizontal and vertical boundaries, two symbols in different sets which are closest to a received symbol always lie either on the same row (if the boundaries are vertical) or on the same column (if the boundaries are horizontal) [Surendra Raju04]. Therefore, considering the least significant bit (LSB), the most reliable L_E corresponds to the received symbol being equal to the constellation point, i.e. $L_E=\pm\frac{d_{min}^2}{2\sigma^2}$, being d_{min} the minimum distance between two adjacent points of the constellation.

4. The previous four statements give the same reliability to all bits whose extrinsic information is unable to calculate. Considering the obtained metrics for the candidate list, we use the maximal metric in order to truncate the L_E value in (4.8). Therefore,

Equation (4.8) is given by

$$
\begin{aligned}
&L_E(b_k|\boldsymbol{Y}) \approx \\
&\frac{1}{2}\min_{\boldsymbol{b}\in\mathcal{L}\cap\mathbb{B}_{k,-1}}\left\{-\frac{1}{\sigma^2}\left\|\boldsymbol{y}-\breve{\boldsymbol{H}}\boldsymbol{G}\boldsymbol{s}\right\|^2+\boldsymbol{b}_{[k]}^T L_{A,[k]}\right\} \\
&-\frac{1}{2}\max_{\boldsymbol{b}\in\mathcal{L}\cap\mathbb{B}_{k,-1}}\left\{-\frac{1}{\sigma^2}\left\|\boldsymbol{y}-\breve{\boldsymbol{H}}\boldsymbol{G}\boldsymbol{s}\right\|^2+\boldsymbol{b}_{[k]}^T L_{A,[k]}\right\} \text{ if } \mathcal{L}\cap\mathbb{B}_{k,+1}=\emptyset
\end{aligned}
\tag{4.9}
$$

$$
\begin{aligned}
&L_E(b_k|\boldsymbol{Y}) \approx \\
&\frac{1}{2}\max_{\boldsymbol{b}\in\mathcal{L}\cap\mathbb{B}_{k,+1}}\left\{-\frac{1}{\sigma^2}\left\|\boldsymbol{y}-\breve{\boldsymbol{H}}\boldsymbol{G}\boldsymbol{s}\right\|^2+\boldsymbol{b}_{[k]}^T L_{A,[k]}\right\} \\
&-\frac{1}{2}\min_{\boldsymbol{b}\in\mathcal{L}\cap\mathbb{B}_{k,+1}}\left\{-\frac{1}{\sigma^2}\left\|\boldsymbol{y}-\breve{\boldsymbol{H}}\boldsymbol{G}\boldsymbol{s}\right\|^2+\boldsymbol{b}_{[k]}^T L_{A,[k]}\right\} \text{ if } \mathcal{L}\cap\mathbb{B}_{k,-1}=\emptyset
\end{aligned}
\tag{4.10}
$$

Thus, when all metrics in the same set are similar, the reliability of L_E is lower than when the difference among metrics is higher.

Figure 4.1 shows the results with the different proposals where one can observe that options 1, 3 and 4 obtain similar BER performance being slightly better option 4. The second case, where a high value has been chosen, shows a worse performance than the others. Therefore, the 4th option has been chosen for the rest of simulations in the thesis.

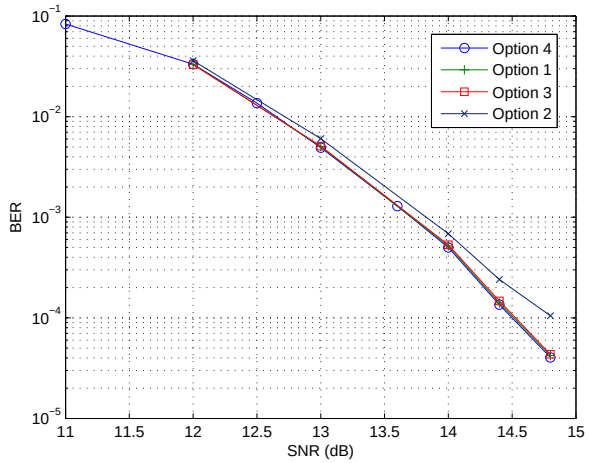

Figure 4.1: BER performances for different clipping options in a 2×2 DVB-T2 system with Golden codes and 16-QAM modulation.

The list detection approach results in a good system performance and its complexity depends on the method to obtain the candidate list $\mathcal{L}$ and on the number of candidates N_{cand}.

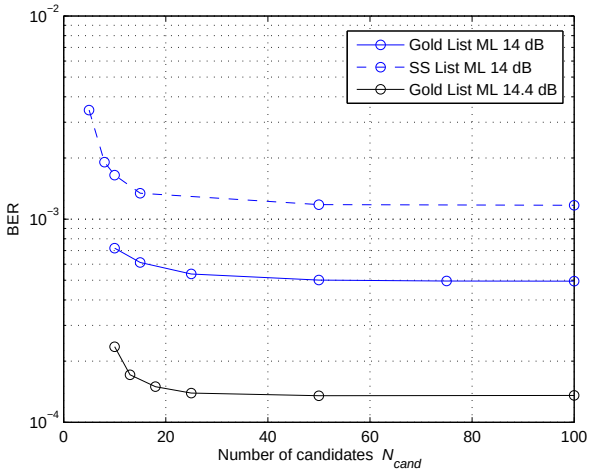

Figure 4.2: BER performances modifying the number of candidates N_{cand} for different SNR values in a 2×2 DVB-T2 system with Golden and SS codes using 16-QAM modulation.

4.2.4 Choice of Candidates Number

As we have previously mentioned, the number of candidates has to be sufficiently large to contain the maximizer of (4.6) with high likelihood since the ML estimate $\hat{\boldsymbol{s}}_{ml}$ is not necessarily the estimate that maximizes (4.6). In order to find the magnitude of N_{cand} from which the approximation (4.6) can be considered reliable, a battery of simulation have been carried out modifying the N_{cand} used to compute (4.8). All the simulations have focused on a 2×2 FRFD SFBC system with modulation order $P = 16$ over a TU6 channel. For this configuration, the exhaustive search corresponds to computing $P^4 = 65536$ metrics. In Figure 4.2, we observe that the BER performance converges for $N_{cand} > 30$ for different SNRs. This involves that a candidate list larger than $N_{cand} = 50$ does not offer any performance increase and consequently, candidate search can be reduced optimizing the computational cost of the search algorithm.

4.3 Performance Results of FRFD Schemes in DVB-T2 Broadcasting Scenarios

This section presents simulation results, based on BER curves, for FRFD SFBC codes in a DVB-T2 framework for different reception conditions, which have published in [Sobron10a]. Unlike the DVB-T2 MISO scheme where a symbol-wise soft detection is possible, the decoding of FRFD codes requires the proposed list version of the MAP detection algorithm in order to obtain the necessary soft information for the LDPC decoder. This involves a higher operation number, which increases the detection complexity. This study basically compares the performances of the Golden and the Sezginer-Sari (SS) codes, which have different detec-

tion complexities, to the DVB-T2 MISO technique combined with an MRC at the receiver. Hence, all the systems have the same diversity order. However, the FRFD codes' spatial rate is twice as the DVB-T2 MISO scheme for the same modulation order. As a result, FRFD codes allow to transmit the same data rate with lower-order modulations. In order to perform a fair comparison among the SFBC codes, we define the spatial rate S as

$$S = \frac{Q}{T}. \tag{4.11}$$

Hence, the raw bit rate η of the system is given by $\eta = SR_c \log_2 P$. Note that the raw bit rate is defined as the data bit rate before LDPC coding. On the other hand, the BER curves are presented as a function of the SNR per raw bit. As the fading channel coefficients are independent with unit variance, the signal energy per receive antenna is also the unity. Therefore, the N receive antennas collect an overall average energy of N, bearing $R_c S \log_2 P$ raw bits. Thus, considering the relation between the CN ρ and the SNR of (3.11), the SNR per raw bit $\frac{E_b}{N_0}$ can be expressed as

$$\frac{E_b}{N_0} = \frac{N_{FFT} N \rho}{N_C R_c S \log_2 P}. \tag{4.12}$$

The simulator is based on a 2×2 setup over the DVB-T2 system. Figure 4.3 depicts an schematic diagram of the system without including other different interleaving stages which have been also added (frequency, cell and time interleavers). The performance has been assessed using the same raw bit rate η and the same bit energy E_b for all SFBC schemes. The DVB-T2 parameters are the following:

- Length of LDPC block: $L_{FEC} = 64800$ bits
- LDPC code rate: $R_c = 2/3$
- Constellation sizes: QPSK, 16-QAM and 256-QAM
- FFT size: 2048 carriers (2K)
- Guard interval: 1/4

The simulations have been carried out over the Rayleigh channel TU6 and the Ricean channel RA6. We consider perfect channel state information (CSI) at the receiver and non-iterative MIMO detection. Therefore, there is no *a priori* information $L_A(b_k)$ and hence (4.8) is simplified. The BER performance has been yielded for the number of candidates $N_{cand} = 100$ using the ML algorithm and keeping the 100 symbol vectors $\boldsymbol{s}$ which provide the lowest metrics in order to compute (4.8). This method is not efficient at all since there exist low-complexity detection algorithms for that purpose, as we will see in the following chapter. Furthermore, according to Figure 4.2, we can observe that the BER performance converges

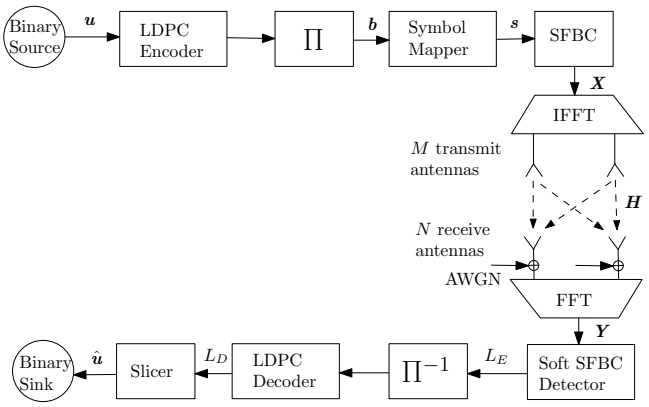

Figure 4.3: Simplified diagram of a LDPC-based SFBC MIMO transmission and reception scheme based on DVB-T2.

for $N_{cand} < 100$ being possible to optimize the detection complexity. This aspect will be further considered in the next section. However, the target of this section is to prove the viability of the FRFD SFBC codes over DTV systems and to assess their performance.

Figures 4.4 and 4.5 compare the aforementioned SFBC schemes over TU6 and RA6 channels, respectively. Two different raw bit rates have been used in the analysis, $\eta = 8/3$ and $\eta = 16/3$, which have been obtained through the configurations shown in Table 4.1.

Table 4.1: Possible configurations for different raw bit rates η.

Bit rate (η)	SFBC scheme	Spatial rate (S)	Code rate (R_c)	Constellation size (P)
16/3	Alamouti	1	2/3	256-QAM
16/3	Golden	2	2/3	16-QAM
16/3	SS	2	2/3	16-QAM
8/3	Alamouti	1	2/3	16-QAM
8/3	Golden	2	2/3	QPSK
8/3	SS	2	2/3	QPSK

As we can observe in Figure 4.4, SS and Golden codes achieve a higher gain than the DVB-T2 Alamouti scheme for $\eta = 16/3$. According to the observations, the utilization of a lower modulation order ($P = 16$) in FRFD codes results favourable in comparison to the high-order modulation ($P = 256$) used in the 2×2 DVB-T2 SFBC scheme at the same channel and noise conditions. Nonetheless, this advantage becomes smaller when the bit rate is lower. A raw bit rate of $\eta = 8/3$ involves a modulation order of $P = 16$ in DVB-T2 SFBC, which offers a better behavior than the equivalent systems with FRFD. On the other hand, the performance of SS is 0.3 dB worse than Golden code at BER=10^{-3}. This gain can be considered negligible if we take into account the reduction in detection complexity.

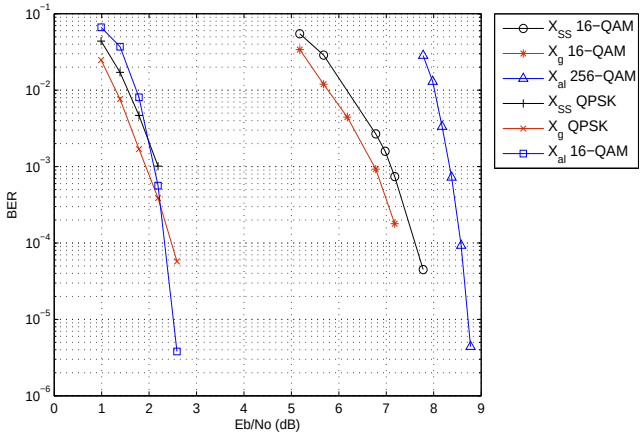

Figure 4.4: BER curves as a function of SNR per raw bit of 2×2 SFBC DVB-T2 schemes over a TU6 channel.

In Figure 4.5, where we show a RA6 channel with LOS, SS and Golden codes provide a lower performance than the DVB-T2 MIMO scheme for both $\eta = 16/3$ and $\eta = 8/3$. In this case, the gain between SS and Golden codes is also maintained. Different performance criteria can be followed when designing FRFD codes according to channel conditions. In [Tarokh98], several STBC design criteria were presented for Rayleigh, Ricean and time varying channels. However, most of FRFD codes, for instance, SS and Golden codes, have been designed for Rayleigh channels (See Criteria 1 and 2 described in Chapter 2). As a result, the performance becomes lower for Rician channels as we can observe in Figure 4.5.

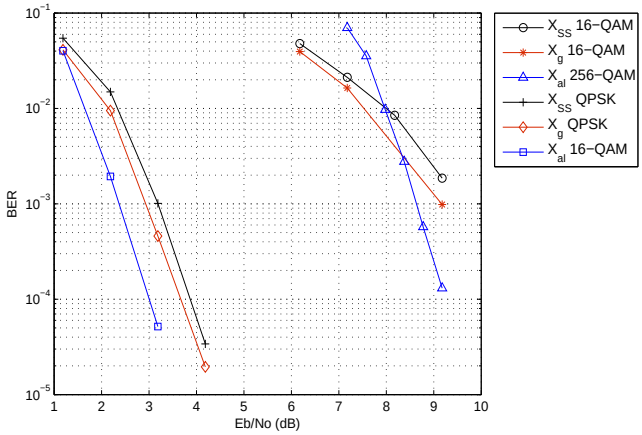

Figure 4.5: BER curves as a function of SNR per raw bit of 2×2 SFBC DVB-T2 schemes over a RA6 channel.

As a conclusion, we observe that FRFD codes obtain a higher performance than the current DVB-T2 SFBC scheme based on the Alamouti code over Rayleigh channels. However, the performance of FRFD codes decreases in a Ricean scenario. From a performance point of view, the Golden code results the best choice requiring a higher computational

cost. Nonetheless, SS codes reduce the detection complexity at the expense of sacrificing performance. Moreover, FRFD codes would allow to increase the data rate using higher modulation orders such as 64-QAM. For that purpose, it would be necessary the utilization of low-complexity soft detection algorithms as the ones proposed in the following sections.

4.4 Complexity of List Sphere Decoder-Based Soft Detectors

The main disadvantage of the implementation of 2×2 FRFD codes in DTV systems is the high computational cost of the detection stage. When computing (4.6), the calculation of P^4 Euclidean distances would be necessary, which would result unfeasible for a realistic implementation. For the complexity reduction, we can approximate (4.6) to (4.8) with a list of candidates instead of computing all Euclidean distances. Different algorithms can be used when considering the candidate list. The list sphere decoder (LSD) algorithm [Hochwald03] is considered in the literature as the most promising approach to provide soft information. However, we review some low-complexity soft-detection algorithms analyzing their advantages and disadvantages for the DTV system under consideration.

4.4.1 List Sphere Decoder

The LSD was proposed in [Hochwald03] as a means of obtaining soft information in MIMO detection. Basically, the functionality of SD is extended to generate a list of candidates which maximizes (4.8) such that the extrinsic information L_E is approximated without having to consider the entire set of possible transmitted symbol vectors. Instead, the information about the demapped bits from the list of candidate vectors is only considered. The complexity of the algorithm and the accuracy of the soft information will depend on the size of the list. Hence, a good trade-off must be found. If a large number of candidates is considered, the approximated L-value will be closer to the exact solution but the LSD will require a larger number of operations to generate the complete list.

The LSD proposed in [Hochwald03] is based on the FP enumeration. Consequently, the choice of the initial radius R is extremely important to limit the complexity. Furthermore, its calculation may result in a non-deterministic polynomial-time hard (NP-hard) problem if we use the covering radius of the lattice [Conway88] for that purpose. Apart from the disadvantages of the FP enumeration, the LSD presents the same problems of the SD from an implementation point of view: its variable complexity depending on the noise level and the channel conditions and its sequential nature. Different modifications have been proposed for the original LSD, although most of them still use the FP enumeration. In [Boutros03], a modification of the LSD has been proposed combining the original SD with SE enumeration

and a double FP enumeration. The SE-SD is used to obtain the ML solution and then the double FP enumeration generates a list of candidates around the ML solution instead of the received vector. Although the performance of the LSD is improved, this solution has different problems such as the complexity increment, the irregular structure of the algorithm and the possible re-enumeration of the same vectors in the SE-SD and the double FP enumeration. Other solutions based on the addition of the *a priori* information [Vikalo04, Park05, Sumii05] have been proposed to improve the soft value computation and to reduce the complexity. However, they have been proposed from a theoretical point of view and their additional number of operations would represent a problem for a realistic implementation.

With the utilization of the SE enumeration in [Lee06], a feasible LSD was proposed from an implementation point of view. It consists of taking a very large initial radius following the SE enumeration so that it is maintained until the list of candidates is full. Then, the initial radius is set to the largest distance among the candidates on the list and the operation continues replacing the candidate with the largest distance on the list if new candidates are found satisfying the new sphere constraint.

4.4.1.1 Complexity Results

Simulation results are here presented to analyze the complexity reduction of the SE-LSD compared to the computation of P^4 Euclidean distances in a previously used list ML. In addition, we will observe the behavior of the SE-LSD as a function of either the noise level or the size of the list. The simulations have been carried out for the Golden code scheme with 16-QAM modulation in the DVB-T2 framework and over a TU6 channel. If the complex-valued version of the LSD is considered, the number of nodes per tree level is $\boldsymbol{n}_{tree} = [P^4\ P^3\ P^2\ P]$ considering the level $i = 1$ at the bottom of the tree. Note that the number of levels corresponds to the $Q = 4$ symbols coded in any 2×2 FRFD code and the number of nodes in the level $i = 1$ is the overall Euclidean distances.

Figure 4.6 shows the average number of visited nodes per tree level as a function of the SNR for a LSD decoder with $N_{cand} = 50$ candidates. One can observe that the behavior of the LSD does not notably vary in that range of noise power. Unlike the SD, where the highest average number of visited nodes arises at the intermediate levels due to the pruning generated by the reduction of the hypersphere radius, the LSD has the greatest average number of visited nodes at the last level, due to the necessary updating of the list of candidates.

If we analyze the complexity of the tree search as a function of the number of list candidates, Table 4.2 shows us that the average number of visited nodes per tree level becomes greater when N_{cand} increases, being the higher difference at level $i = 1$. The last level requires a larger number of operations than the rest of levels. Therefore, an increment of visited nodes in that level involves a much higher computational cost. As a result, consider-

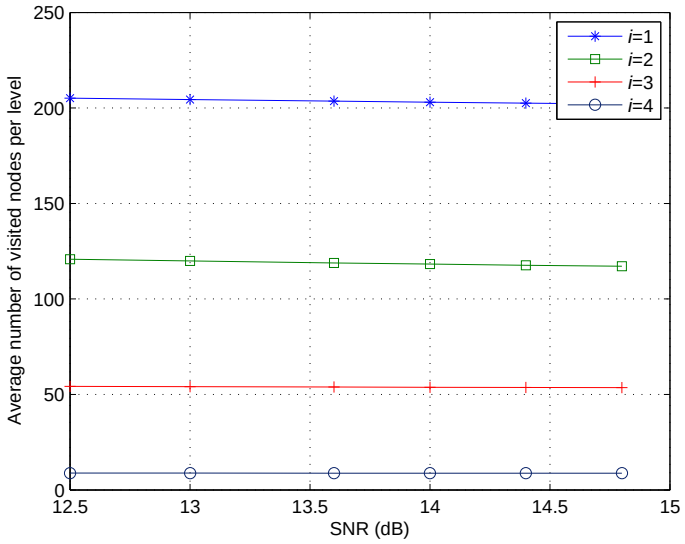

Figure 4.6: Average number of visited nodes per tree level as a function of SNR for SE-LSD detection of Golden codes with 16-QAM modulation and $N_{cand} = 50$.

ing the simulation results of Figure 4.2 for a TU6 channel, the choice of $N_{cand} = 50$ offers a trade-off between accuracy and complexity. Note that we have measured the average number of visited nodes at the highest SNR value (14.8 dB) of Figure 4.6 so that the average values correspond to the most optimistic situation for the studied range of SNR.

Table 4.2: Average number of visited nodes for LSD detection of Golden codes with 16-QAM modulation using different number of candidates at SNR=14.8 dB.

Number of candidates (N_{cand}) / Tree level	25	50	100
$i = 1$	97.27	201.80	409.73
$i = 2$	77.26	118.67	183.71
$i = 3$	42.38	54.35	69.23
$i = 4$	7.78	8.76	9.81

As we have mentioned before, one of the two main drawbacks of the LSD algorithm is the variable nature according to the channel and noise conditions. This feature can be depicted in Figures 4.7 and 4.8 for $N_{cand} = 50$ and 100, respectively, where the histograms of the number of visited node are shown. The overall number of channel realisations has been 502260, while the number of realizations per number of visited nodes has been normalized to the unity and expressed as percentage. Despite the average figures shown in the Table 4.2, one can notice that the number of visited nodes for some channel realisations is higher

than the average values resulting in a problem for the detection process and verifying the characteristic upper-bound equal to the ML detection complexity. For instance, in the level $i = 3$ of Figures 4.7(c) and 4.8(c), we can observe that the 0.2 and 0.4 per cent of channel realisations exceed 900 visited nodes even though the average values are 118.67 and 183.71 (dashed lines), respectively. This behavior can be seen at all levels reaching the entire number of nodes at the levels $i = 2$ and 1.

4.4.2 Review of Fixed-Complexity Implementations

The variable computational cost of the LSD algorithm and its sequential nature negatively affect the complexity of the architecture and the achievable throughput of the implementation. In order to overcome that problem, although it is not strictly based on the LSD, the K-Best [deJong05] and QRD-M [Dai05] algorithms were proposed as soft-MIMO detectors that have a fixed complexity and can be fully pipelined in a hardware implementation. However, the algorithms suffer from high computational complexities depending on the parameter M. The K-Best lattice decoder has been implemented in practice to obtain soft-information proving its fixed complexity and its fully-pipelined architecture [Guo06]. However, the implementation shows that the sorting procedure required in each level represents a significant percentage of the overall complexity. Other algorithms exist with comparable performance to that of the LSD. In [Radosavljevic09], bounded soft sphere detection (BSSD) with probabilistically determined and variable search bounds per search level is proposed, being also suitable for the pipelining of search levels. In [Barbero08], an extension of the fixed-complexity sphere decoder (FSD) [Barbero06b] for turbo-MIMO detection called list fixed-complexity sphere decoder (LFSD) was proposed with interesting results. In accordance to [Jaldén07], the FSD maintains the diversity of the ML while searching over only a very small number of candidates. Therefore, given the lower complexity of the LFSD and its quasi-ML performance, we will show in next chapter that the same concept can be applied to the FRFD detection with a redesign of the ordering procedure, resulting in a more optimized implementation of the algorithm.

4.5 Chapter Summary

In the development groups of forthcoming DTV standards such as DVB-NGH, the inclusion of MIMO technologies based on FRFD codes have been proposed. This chapter has presented a performance analysis of FRFD codes in last-generation DTV systems, such as DVB-T2, and has discussed the complexity issues related to soft detection.

First of all, soft detection has been described rewriting the equations of the MAP detector for FRFD SFBC codes. Furthermore, a MAP algorithm approximation based on a list

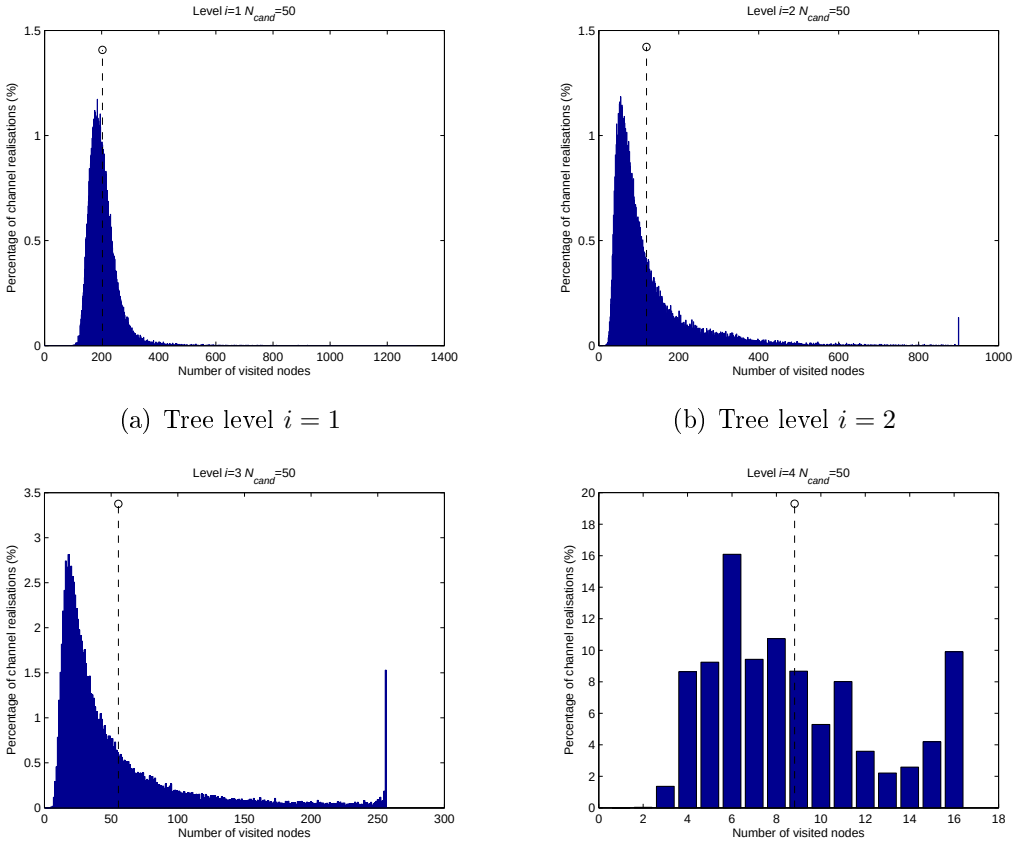

(a) Tree level $i = 1$

(b) Tree level $i = 2$

(c) Tree level $i = 3$

(d) Tree level $i = 4$

Figure 4.7: Histograms of the percentage of channel realisations as a function of the visited nodes per each level for the Golden code decoding using the SE-LSD with $N_{cand} = 50$ and 16-QAM modulation.

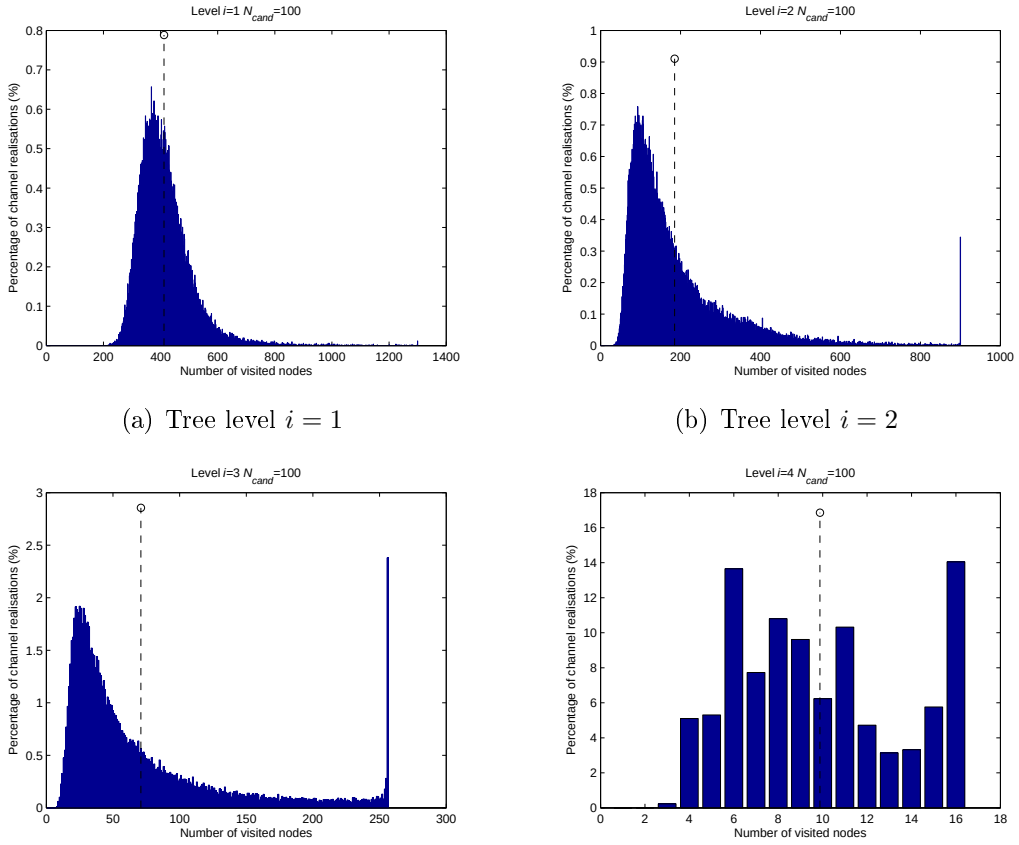

(a) Tree level $i = 1$

(b) Tree level $i = 2$

(c) Tree level $i = 3$

(d) Tree level $i = 4$

Figure 4.8: Histograms of the percentage of channel realisations as a function of the visited nodes per each level for the Golden code decoding using the SE-LSD with $N_{cand} = 100$ and 16-QAM modulation.

of candidates is given. In order to find the trade-off between complexity and accuracy, simulations results have been presented for different sizes of the list of candidates. Next, performance simulation results have been shown for the Golden code and the low-complexity SS code using different data bit rates and broadcasting scenarios. The FRFD codes have been compared to a 2×2 DVB-T2 SFBC scheme with MRC detection at the receiver. The drawback of multi-strata codes [Samuel07], such as the SS code, is their worse performance in comparison to codes designed using number theory like the Golden code. However, due to its multi-strata structure, they can be decoded with lower complexity sacrificing the performance.

In the last part of the chapter, detection complexity considerations have taken into account. Several low-complexity detection algorithms have been reviewed paying special attention to the LSD algorithm. This method is considered as the most promising approach to provide soft-information. However, as we have proved in the complexity results, its variable complexity depending on the noise level and the channel conditions and its sequential nature can affect its practical implementation. As a result, after reviewing some fixed-complexity algorithms, a solution based on the LFSD of [Barbero08] for turbo-MIMO systems will be proposed in the following chapter.

Chapter 5

List Fixed-Complexity Sphere Decoder for FRFD Codes

5.1 Introduction

A redesign of the previously proposed LFSD for turbo-MIMO systems in [Barbero06a, Barbero08] is developed in this chapter and adapted to SFBC-LDPC scenarios. Initially, the LFSD algorithm was proposed to provide soft outputs in spatially multiplexed MIMO systems. For that purpose, LFSD generates a subset or list of candidates from the entire possible transmit constellation approaching the LSD performance with a fixed complexity and resulting in a good option for hardware implementation. Before starting with the tree search, the LFSD performs a channel ordering procedure which maximizes the algorithm performance. In [Barbero06a], the ordering process is aimed at the spatially multiplexed transmission where the subchannels which affect the transmitted symbols are uncorrelated to each other. However, the equivalent subchannels of the FRFD SFBC coded symbols are correlated through the code generator matrix $\boldsymbol{G}$. Therefore, the channel ordering procedure can follow a pattern which optimizes the performance of the LFSD algorithm. For that purpose, the 2×2 SFBC system is transformed to an equivalent 4×4 MIMO system where we take into account the mentioned correlation between subchannels.

A new version of the channel ordering stage is presented in this chapter for FRFD SFBC coding. First, a theoretical revision of the previously proposed LFSD is performed and the novel ordering algorithm is then introduced. The effect of the number of candidates is analyzed in the DVB-T2 platform finding a trade-off between complexity reduction and performance maximization. Simulation results are provided in order to show the performance and complexity of the new algorithm compared to the original LFSD and the LSD. Finally, further complexity considerations about number of operations are drawn.

5.2 The LFSD Algorithm

In order to limit the complexity and to facilitate the computation of the detected symbols, a fixed-complexity tree-search-based algorithm was proposed in [Barbero06b] for spatial multiplexing schemes, named FSD. The FSD was developed with the purpose of overcoming the two main drawbacks of the SD detection scheme in MIMO systems, first, the variable complexity and second, the sequential nature of the algorithm. As in the case of the SD, the distance calculations are performed following a tree-search fashion. The main feature of the FSD is that, instead of constraining the search to those nodes whose accumulated Euclidean distances are within a certain radius from the received signal, the search is performed in an unconstrained fashion. The tree search is defined instead by a tree configuration vector $\boldsymbol{n} = [n_1, \ldots, n_{MT}]$, which determines the number of child nodes (n_i) to be considered at each level. Therefore, the tree is traversed level by level regardless of the sphere constraints. Once the bottom of the tree is reached, the path leading to the smallest Euclidean distance is selected as the FSD solution.

An extension to the FSD was proposed in [Barbero06a] for systems with soft symbol information requirements. This soft-output algorithm, coined LFSD, performs an unconstrained tree search based on a certain tree configuration vector $\boldsymbol{n}$ but, as opposed to the FSD, retrieves a list of N_{cand} candidate symbol vectors. It is worth noting that the set $\mathfrak{G}$ composed of the N_{cand} selected symbol vectors may not correspond to the vectors of the $\mathcal{L}$ set with the smallest metrics given by the LSD, but provides sufficiently small metrics and diversity of bit values to obtain accurate soft information [Barbero08]. A representation of an LFSD tree search is depicted in Figure 5.1 for a 2×2 FRFD SFBC with QPSK modulation and a tree configuration vector of $\boldsymbol{n} = [1, 1, 2, 4]$. We can observe that at level $i = 4$, all nodes are visited, whereas two nodes per branch are visited at the next levels, which sum eight nodes in total. For the remainder levels, $i = 2$ and 1, the same overall number of nodes, i.e. 8, is maintained since one child node is only chosen for each of the parent nodes of the upper level.

For the sake of simplicity, the equations for the aforementioned FRFD codes will be rearranged so that Euclidean distance can be given by

$$\left\| \bar{\boldsymbol{y}} - \boldsymbol{H}_{eq} \bar{\boldsymbol{s}} \right\|^2 . \tag{5.1}$$

where $\bar{\boldsymbol{y}}$ and $\bar{\boldsymbol{s}}$ are the received and transmitted signals reorganized according to the corresponding code and $\boldsymbol{H}_{eq} = \breve{\boldsymbol{H}}\boldsymbol{G}$ is the effective equivalent channel as defined in (2.5). For the previously studied codes, the corresponding complex-valued code generator matrices $\boldsymbol{G}$ are the following:

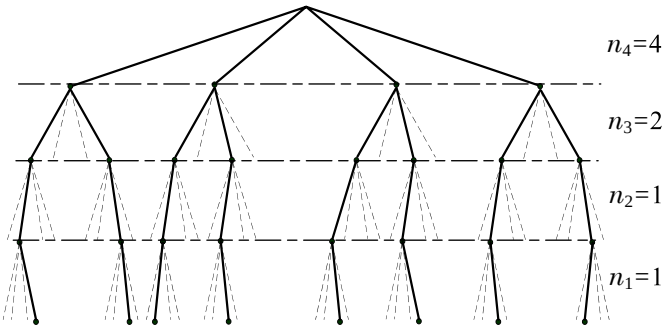

Figure 5.1: Fixed-complexity tree search of a QPSK-modulated signal using a tree configuration vector of $\boldsymbol{n} = [1, 1, 2, 4]$

$$\boldsymbol{G}_G = \begin{bmatrix} 1+i\bar{\theta} & 0 & \theta - i & 0 \\ 0 & -\theta + i & 0 & 1 - i\bar{\theta} \\ 0 & 1+i\bar{\theta} & 0 & \theta - i \\ 1+i\theta & 0 & \bar{\theta} - i & 0 \end{bmatrix}, \qquad \boldsymbol{G}_{SS} = \begin{bmatrix} a & 0 & b & 0 \\ 0 & -c & 0 & -d \\ 0 & a^* & 0 & b^* \\ c^* & 0 & d^* & 0 \end{bmatrix}. \tag{5.2}$$

A level-by-level computation of the metrics in (5.1) requires the conversion to the following equivalent system

$$\left\| \boldsymbol{U}(\bar{\boldsymbol{s}} - \hat{\bar{\boldsymbol{s}}}) \right\|_2^2, \tag{5.3}$$

where $\boldsymbol{U}$ is obtained through the Cholesky decomposition of $\boldsymbol{H}_{eq}^H \boldsymbol{H}_{eq}$ and $\hat{\bar{\boldsymbol{s}}} = \boldsymbol{H}_{eq}^{\dagger} \bar{\boldsymbol{y}}$. Given the triangular structure of $\boldsymbol{U}$, it is now possible to compute the AED up to level i recursively by traversing the tree backwards from level $i = MT$ downto $i = 1$. The Euclidean distances that must be minimized in the cost function in (2.40) can be equivalently represented in a tree search fashion as

$$D_i = u_{ii}^2 \left| \bar{s}_i - z_i \right|^2 + \sum_{j=i+1}^{MT} u_{jj}^2 \left| \bar{s}_j - z_j \right|^2 = d_i + D_{i+1}, \tag{5.4}$$

and

$$z_i = \hat{\bar{s}}_i - \sum_{j=i+1}^{MT} \frac{u_{ij}}{u_{ii}} (\bar{s}_j - \hat{\bar{s}}_j), \tag{5.5}$$

where D_i and d_i are the AED and the partial (squared) Euclidean distance (PED) at level i, respectively, and z_i corresponds to the centre of the hypersphere.

Therefore, at each level i the n_i symbols to be selected are chosen in accordance with the SE enumeration [Schnorr91] and their corresponding PEDs d_i are computed and accumulated to the previous level's AED, that is, D_{i+1}. Once the bottom of the tree has been reached, a sorting operation is performed on the $n_T = \prod_{i=1}^{MT} n_i$ Euclidean distances in order to select

the N_{cand} symbol vectors with the smallest metrics. This latter sorting procedure can be avoided if the tree configuration vector $\boldsymbol{n}$ is selected so as to yield $n_T = N_{cand}$. In such a case, the complexity of the algorithm is reduced but the quality of the soft information is also degraded as the selected metrics are higher in value.

5.2.1 The Ordering Algorithm for FRFD SFBC

The performance of the LFSD soft-detector in uncoded scenarios is strongly dependent on the ordering algorithm of the channel matrix and the choice of the tree configuration vector [Barbero06a]. However, in the specific case of FRFD SFBC systems the effect of the ordering algorithm on the overall performance relies on the type of code utilized [Sobron10a]. For a spatial multiplexed configuration, the ordering algorithm proposed in [Barbero06a] to enhance the performance of the LFSD and the FSD detectors was based on the fact that it was possible to mitigate the error propagation derived from ruling out several tree branches by ordering the several columns of the channel matrix depending on their *quality*. More precisely, the FSD ordering dictates that the subchannel with the worst norm of all needs to be processed first given that in that level all the constellation symbols are evaluated (see Figure 5.1), and therefore, there is no error propagation to the other levels.

In the case of spatial multiplexing, each data symbol is transmitted from one transmit antenna of the MIMO system such that their corresponding subchannels are completely uncorrelated assuming that the distance between antennas is longer than half a wavelength. Therefore, the columns of the channel matrix can be ordered independently. However, when FRFD SFBCs are used, data symbols are usually transmitted in pairs (s_1, s_3) and (s_2, s_4) through both spatial and frequency directions (see Chapter 2) such that the symbols of each pair are affected by the same channel conditions. This feature as well as the power conditions defined in (2.31), (2.32) and (2.33) make the ordering of the equivalent channel columns, i.e. the subchannels of the coded symbols, to depend on the tree configuration. Let us see this assertions for SS and Golden codes in the sequel.

5.2.1.1 SS Code

When considering the equivalent system in (2.40) for the SS code, it is worthy noting that the equivalent subchannels for the symbol pairs (s_1, s_3) and (s_2, s_4) have equal norms. This is due to two main factors: on one hand, both symbol pairs undergo the same channel conditions as they are assigned to adjacent carriers, and on the other hand, the code weights a, b, c and d imposed by the SS code fulfill the power constraint (2.33), which forces the symbols to be dispersed with equal energy in all spatial and temporal directions. Let us see it mathematically. If we represent the equivalent channel matrix $\boldsymbol{H}_{eq} = \breve{\boldsymbol{H}}\boldsymbol{G}$ in matrix form, we obtain that

$$\boldsymbol{H}_{eq} = \begin{bmatrix} ah_{11}^1 & -ch_{12}^1 & bh_{11}^1 & -dh_{12}^1 \\ ah_{21}^1 & -ch_{22}^1 & bh_{21}^1 & -dh_{22}^1 \\ (ch_{12}^2)^* & (ah_{11}^2)^* & (dh_{12}^2)^* & (bh_{11}^2)^* \\ (ch_{22}^2)^* & (ah_{21}^2)^* & (dh_{22}^2)^* & (bh_{21}^2)^* \end{bmatrix} = [\boldsymbol{h}_1\ \boldsymbol{h}_2\ \boldsymbol{h}_3\ \boldsymbol{h}_4], \tag{5.6}$$

with $\boldsymbol{h}_j$ denoting the j-th column vector of $\boldsymbol{H}_{eq}$, which corresponds to the symbol s_j. One should note that if the channel is quasi-static over adjacent carriers, i.e. $\boldsymbol{H}_1 \approx \boldsymbol{H}_2$, the norms of columns follow $\|\boldsymbol{h}_1\|^2 \approx \|\boldsymbol{h}_2\|^2$ and $\|\boldsymbol{h}_3\|^2 \approx \|\boldsymbol{h}_4\|^2$. Furthermore, due to the fact that SS code fulfills (2.33), $|a| = |b| = |c| = |d| = 1/\sqrt{2}$, which involves that the norms of columns obey $\|\boldsymbol{h}_1\|^2 = \|\boldsymbol{h}_3\|^2$ and $\|\boldsymbol{h}_2\|^2 = \|\boldsymbol{h}_4\|^2$. By combining these two properties, we can say that all norms are equal if the channel is flat in adjacent carriers. The consequence of employing such an SFBC code is that the difference in the subchannels' qualities is negligible and therefore, performing a matrix ordering stage does not provide any remarkable performance enhancement. This behavior is actually observed in all codes that fulfill (2.33), such as the Silver code [Paredes08].

5.2.1.2 Golden Code

The fact that Golden code does not fulfill (2.33) generates an unbalanced power distribution of the transmitted symbols. Thus, given the difference in the absolute values of the code weights, one of the symbols in each pair (s_1, s_3) and (s_2, s_4) is always transmitted with a higher power. This results in a certain difference in the norms of the equivalent subchannels, which allows for the implementation of an ordering procedure in order to improve the overall system's performance.

In this case, the equivalent channel matrix $\boldsymbol{H}_{eq}$ is

$$\boldsymbol{H}_{eq} = \begin{bmatrix} h_{11}^1\left(1+i\bar{\theta}\right) & h_{12}^1\left(-\theta+i\right) & h_{11}^1\left(\theta-i\right) & h_{12}^1\left(1-i\bar{\theta}\right) \\ h_{21}^1\left(1+i\bar{\theta}\right) & h_{22}^1\left(-\theta+i\right) & h_{21}^1\left(\theta-i\right) & h_{22}^1\left(1-i\bar{\theta}\right) \\ h_{12}^2\left(1+i\theta\right) & h_{11}^2\left(1+i\bar{\theta}\right) & h_{12}^2\left(\bar{\theta}-i\right) & h_{11}^2\left(\theta-i\right) \\ h_{22}^2\left(1+i\theta\right) & h_{21}^2\left(1+i\bar{\theta}\right) & h_{22}^2\left(\bar{\theta}-i\right) & h_{21}^2\left(\theta-i\right) \end{bmatrix}, \tag{5.7}$$

where we can observe the unbalanced power distribution since the norms of the code weights are not equal, i.e. $1+\theta^2 \neq 1+\bar{\theta}^2$. Therefore, $\|\boldsymbol{h}_1\|^2 \neq \|\boldsymbol{h}_3\|^2$ and $\|\boldsymbol{h}_2\|^2 \neq \|\boldsymbol{h}_4\|^2$ in any case. On the other hand, if the channel is again assumed quasi-static over adjacent carriers, $\|\boldsymbol{h}_1\|^2 \approx \|\boldsymbol{h}_2\|^2$ and $\|\boldsymbol{h}_3\|^2 \approx \|\boldsymbol{h}_4\|^2$.

An important feature when considering the optimum ordering approach is the tree configuration vector that will shape the search tree. As opposed to the LFSD detector presented in [Barbero06a] for spatial multiplexing MIMO transmission, the tree configuration vector for the detection of the Golden Code has been set to $\boldsymbol{n} = [k, k, P, P]$, where $k < P$ [Sobron10a]. With such a tree structure, an exact ML search is performed in the first two levels of the

tree, and therefore, there is no error propagation down to the next levels. Consequently, by ordering the equivalent channel matrix in such a way that the *worst* subchannel is processed in the first two levels of the tree, the probability of finding vectors with smaller metrics is increased. Moreover, it has to be taken into account that in the non-ML part of the tree search the symbols belonging to the same symbol pair need to be detected together for a better performance of the algorithm. The equivalent ordered channel matrix $\boldsymbol{H}_{eq}^{ord}$ to be used in the detection of the Golden Code can then be described as

$$\boldsymbol{H}_{eq}^{ord} = [\boldsymbol{h}_{\widetilde{b}}\ \boldsymbol{h}_b\ \boldsymbol{h}_{\widetilde{w}}\ \boldsymbol{h}_w], \tag{5.8}$$

where

$$w = \arg\min_{j\in\mathbb{S}} \|\boldsymbol{h}_j\|_2^2, \tag{5.9}$$

and

$$b = \arg\max_{j\in\mathbb{S}, j\neq w,\widetilde{w}} \|\boldsymbol{h}_j\|_2^2, \tag{5.10}$$

The two symbols that compose a symbol pair are represented as $(a, \widetilde{a})$ and the set of symbol indices is $\mathbb{S} = \{1, \cdots, MT\}$. Given the chosen tree configuration vector, one can notice that the order of the first two selected symbols can be switched without having any impact on the system's final performance.

As it will be shown in the next section, the proposed ordering approach yields close-to-optimum performance when combined with the suggested tree configuration vector. Moreover, the matrix ordering process only requires the computation of MT vector norms as opposed to other ordering algorithms such as FSD [Barbero06a] or V-BLAST [Wolniansky98], which need to perform $MT - 1$ matrix inversion operations.

5.2.2 Bit LLR Generation for the Proposed List Fixed-Complexity Detector

Once we have defined the equivalent system model for the FRFD codes, the expression for the LLRs in (4.8) can be rewritten to comply with the equivalent system in (2.40) where the list of candidates $\mathcal{L}$ of the ML/LSD detector has been substituted by the set $\mathfrak{G}$ of the LFSD so that

$$\begin{aligned} L_E(b_k|\boldsymbol{Y}) \approx & \frac{1}{2}\min_{\boldsymbol{b}\in\mathfrak{G}\cap\mathbb{B}_{k,+1}} \left\{ \frac{1}{\sigma^2}\left\|\bar{\boldsymbol{y}} - \boldsymbol{H}_{eq}\bar{\boldsymbol{s}}\right\|^2 + \boldsymbol{b}_{[k]}^T L_{A,[k]} \right\} \\ & - \frac{1}{2}\min_{\boldsymbol{b}\in\mathfrak{G}\cap\mathbb{B}_{k,-1}} \left\{ \frac{1}{\sigma^2}\left\|\bar{\boldsymbol{y}} - \boldsymbol{H}_{eq}\bar{\boldsymbol{s}}\right\|^2 + \boldsymbol{b}_{[k]}^T L_{A,[k]} \right\}. \end{aligned} \tag{5.11}$$

In the case of the Golden code, the column vectors $\bar{\boldsymbol{y}}$ and $\bar{\boldsymbol{s}}$ correspond to $\boldsymbol{y}$ and $\boldsymbol{s}$,

respectively and the equivalent channel is $\boldsymbol{H}_{eq} = \breve{\boldsymbol{H}}\boldsymbol{G}_G$ where $\boldsymbol{H}^1 = \boldsymbol{H}^2 = \boldsymbol{H}$ if the channel is invariant in two adjacent carriers. For the SS code, the received and transmitted signals are rearranged as $\bar{\boldsymbol{y}} = [y_{11}, y_{21}, y_{12}^*, y_{22}^*]^T$ and $\bar{\boldsymbol{s}} = [s_1, s_2^*, s_3, s_4^*]^T$, respectively. The equivalent channel is the product $\breve{\boldsymbol{H}}\boldsymbol{G}_{SS}$ where $\boldsymbol{H}^1 = \left(\boldsymbol{H}^2\right)^* = \boldsymbol{H}$ when the channel is flat in the two consecutive carriers of the codeword.

5.3 Simulation Results

This section presents the performance assessment of the new list fixed-complexity soft FRFD SFBC detector in DVB-T2 broadcasting scenarios. The performance of the overall system has been assessed by means of the BER after the LDPC decoder. The DVB-T2 parameters which have been used for simulation are the following:

- Length of LDPC block: 64800 bits
- LDPC code rate: $R = 2/3$
- Number of LDPC blocks per realisation: $N_{FEC} = 2$
- Constellation size: 16-QAM
- FFT size: 2048 carriers (2K)
- Guard interval: 1/4

The simulations have been carried out over a TU6 Rayleigh and RA6 Ricean channels. The *a priori* information of (5.11) has been removed since we have considered that the DVB-T2 system depicted in Figure 4.3 is not iterative at the receiver, which is also assumed to have perfect CSI. When comparing results, the gain between BER curves is evaluated at the level of BER=10^{-3}.

5.3.1 Effect of the Number of Candidates on the System Performance

As has been previously stated, the calculation of the extrinsic information L_E can be approximated using a list $\mathcal{L}$ or $\mathfrak{G}$ with N_{cand} symbol vectors, respectively. When working with the ML metrics, i.e. the list $\mathcal{L}$, the higher the number of candidates is, the more accurate the L_E approximation results. Nevertheless, when considering the $\mathfrak{G}$ list, the optimum value for N_{cand} will depend on the tree configuration vector $\boldsymbol{n}$. Thus, the higher the value of n_T, the better the approximation is. In order to choose a suitable number of candidates for the detection algorithm, a battery of tests have been carried out.

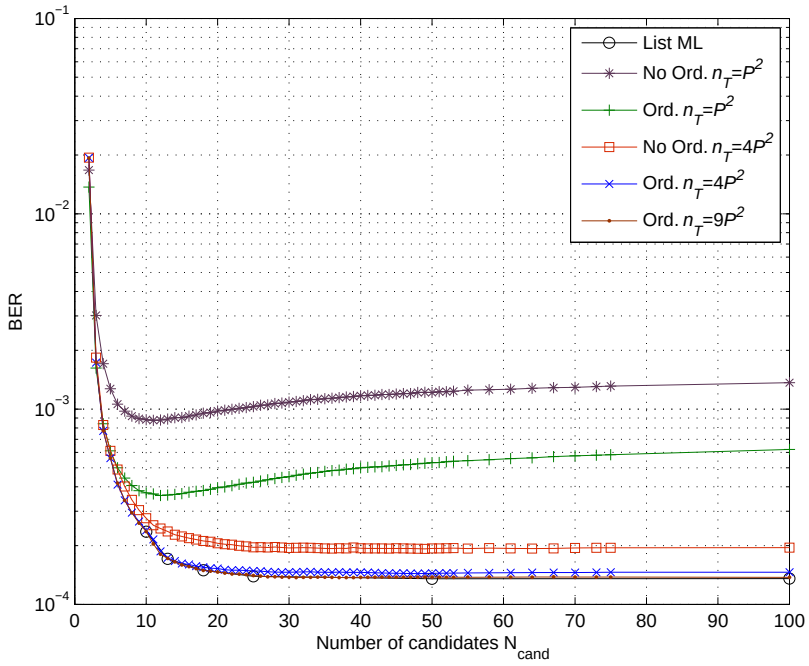

Figure 5.2: BER performance of the Golden code with different number of candidates and fixed-complexity tree search levels at 14.4 dB of SNR over a TU6 channel.

Considering the simulation results provided in Chapter 4, we have analyzed the behavior of the algorithm for certain values of SNR. Figure 5.2 depicts the BER performance of the Golden code reception after the LDPC decoding stage for a given SNR of 14.4 dB, several values of N_{cand} and tree search configurations. The effect of the preprocessing stage is also depicted in this figure. The analyzed tree search configuration vectors $\boldsymbol{n}$ have been obtained by setting $k = 1, 2, 3$, which is equivalent to calculating $n_T = P^2, 4P^2, 9P^2$ Euclidean distances, respectively. As we could see in the previous chapter, the list ML or LSD approximation in (4.8) converges for $N_{cand} > 30$.

If we now pay attention to the fixed-complexity detector, a similar behavior can be noticed for the different configurations, where the higher the value of k, the better the performance we obtain. Furthermore, it is noticeable that the ordering algorithm provides a performance enhancement such that the $k = 2$ LFSD approximates the BER values for the exhaustive ML detector. On the other hand, note that the BER degrades for a higher number of candidates with the tree search configuration $k = 1$. This is due to the fact that if we choose a large N_{cand} value from $n_T = P^2$ Euclidean distances, the probability of achieving the smallest or close to the smallest metrics is reduced. For that reason, the LFSD provides a better performance when the number of candidates is lower. If $k > 1$, this effect is mitigated. Moreover, the ordering stage offers a higher gain when n_T is minimum for the proposed tree search configuration based on $\boldsymbol{n} = [k\ k\ P\ P]$.

In Figure 5.3, BER performance comparisons are shown for the ordered detection of

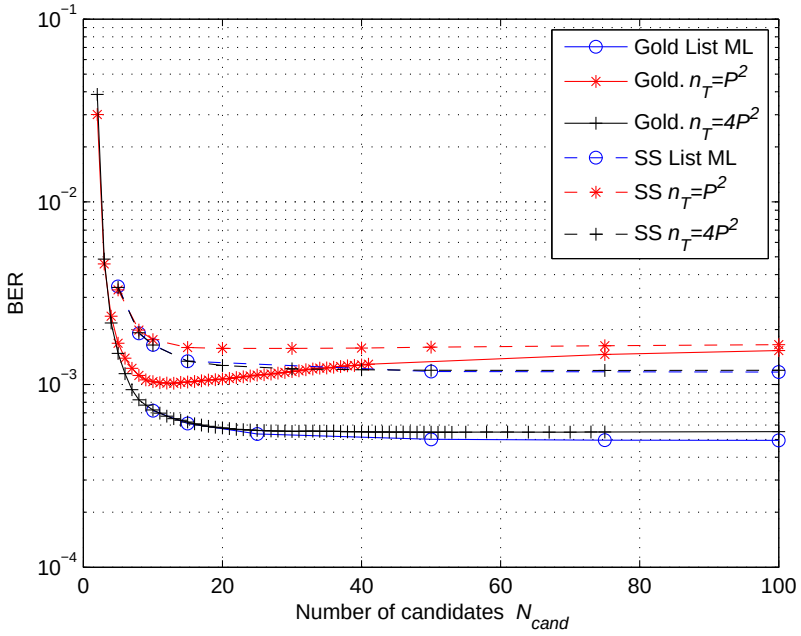

Figure 5.3: BER performance of the Golden code with ordering stage and SS code for different number of candidates and fixed-complexity tree search levels at 14 dB of SNR over a TU6 channel.

Golden code and the unordered detection of SS code as a function of different number of candidates at SNR=14 dB over a TU6 channel. As has been stated in Section 5.2, the SS code achieves a close-to-optimum performance without using the ordering preprocessing for tree search configurations with $k = 1$ and 2. However, an increment from $k = 1$ to $k = 2$ improves considerably the results of the Golden code. One should note that Golden and SS codes obtain a similar BER performance for $k = 1$ if the number of candidates is higher than 30. When $N_{cand} < 30$, the Golden code provides a better performance than the list ML solution.

As a conclusion, a correct design of the number of candidates and the tree search configuration results in a better performance for the Golden codes than for the low-complexity FRFD codes with a great reduction of the detection complexity.

5.3.2 Comparative Analysis Between List Sphere Decoder and List Fixed-Complexity Sphere Decoder

Figure 5.4 shows the BER versus SNR curves for different configurations of the proposed algorithm in the detection of Golden and SS codes with $N_{cand} = 50$. For the Golden code, it is noteworthy that the ordering algorithm provides a gain of 0.4 and 0.05 dB compared to the non-ordering case for $n_T = P^2$ and $n_T = 4P^2$, respectively. However, as previously stated, the ordering algorithm does not have any performance improvement on the SS code

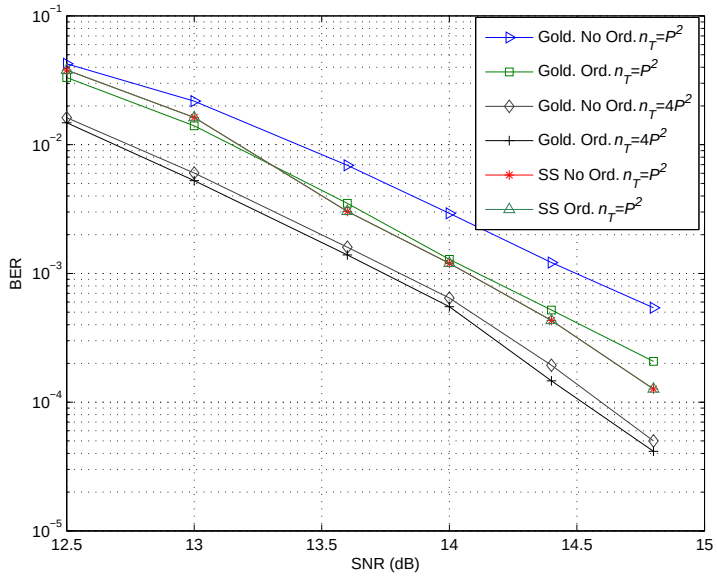

Figure 5.4: BER performance comparison of LFSD detection with and without ordering stage for different complexity orders of the tree search configuration $\boldsymbol{n} = [k\ k\ P\ P]$ and 16-QAM modulation.

due to the inherent power constraints of the code. In this case, the subchannel norms of the symbol pair $(a, \widetilde{a})$ are completely equal, i.e. $\|\boldsymbol{h}_b\|^2 = \left\|\boldsymbol{h}_{\widetilde{b}}\right\|^2$ and $\|\boldsymbol{h}_w\|^2 = \|\boldsymbol{h}_{\widetilde{w}}\|^2$, being the enhancement provided by the ordering procedure negligible. As a result, we can observe that the ordering stage provides a higher enhancement when the algorithm has a lower complexity, i.e. a smaller number of Euclidean distances have been computed at the bottom of the tree.

The BER performances of the ordering algorithms and the list ML or LSD solution are depicted in Figure 5.5 for $N_{cand} = 50$. One can observe that the proposed fixed-complexity detection algorithm achieves a similar performance result with a substantial reduction in complexity. For the SS code, the fixed algorithm with complexity P^2 obtains the same BER performance as the algorithm proposed in [Sezginer09], which has a complexity of $\mathcal{O}(P^3)$. For the Golden code, if the fixed tree of P^2 branches is considered, the performance is 0.4 dB worse than the LSD with complexity $\mathcal{O}(P^4)$. However, if the complexity is increased to $4P^2$, the performance difference is negligible. Furthermore, Figure 5.5 shows how the proposed algorithm obtains a higher performance than the previous LFSD introduced in [Barbero06a] for both Golden and SS codes. Even though both algorithms compute the same number of Euclidean distances at the last level, the number of visited nodes per level is different due to the tree configuration vector $\boldsymbol{n}$, resulting in a more reliable list of candidates for our case. The gain between both algorithms becomes 0.65 and 0.9 dB for the Golden and the SS codes, respectively.

Figure 5.6 shows the BER curve comparison as a function of SNR for configurations of the proposed algorithm and the LSD with different complexities. In this simulations, we

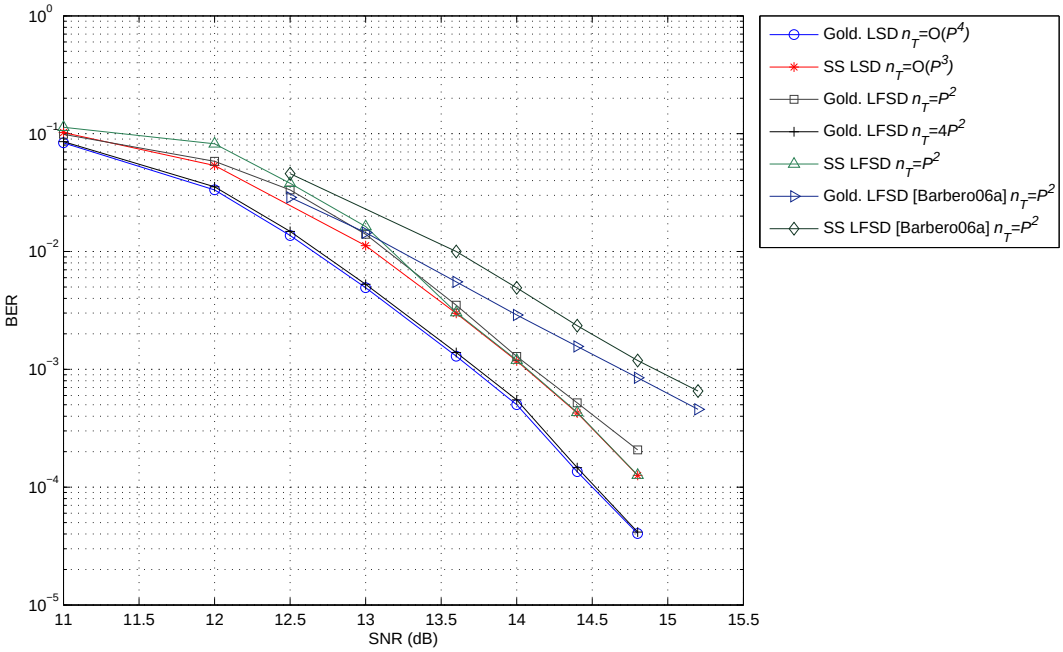

Figure 5.5: BER performance comparison of the proposed FRFD SFBC codes with LSD and ordered LFSD detectors for DVB-T2 transmission.

have stated a more general tree configuration vector so that $\boldsymbol{n} = [k, k, p, p]$, where $k < P$, $p \leq P$ and $k < p$. When $p = P$, we obtain the previously tested structure where there is no error propagation at the first two levels. In addition, simulations have been carried out using $N_{cand} = 25$,50 and 100. For the LSD algorithm, one can see that there is no noticeable performance difference if the number of candidates is reduced from 100 to 50, following the results obtained in Figure 4.2. The performance difference between LSD and ordered LFSD is 0.3 dB for the LFSD configuration $k = 1$, $p = P$ and $N_{cand} = 25$. It is noteworthy that LFSD achieves a better performance with a lower number of candidates. This is due to the fact that the Euclidean distances of a much reduced LFSD list are more likely to be the list ML distances. On the other hand, if a tree configuration with $p < P$ is used, the performance decreases (up to 1.3 dB for $k = 2$ and $p = 8$) when the number of visited nodes at the first level is reduced. Note that with $k = 1$ and $p = 14$ we can obtain a reduction of the overall complexity of the algorithm without an important performance loss.

5.3.3 Complexity Considerations

In order to analyze the complexity of the detection algorithms, the cumulative distribution functions (CDFs) of the visited nodes in the tree search have been computed. For instance, Figure 5.7 depicts the CDF of the overall visited nodes where one can see that the reduction of N_{cand} decreases the complexity of the LSD decoder compared to the LFSD. If we compare

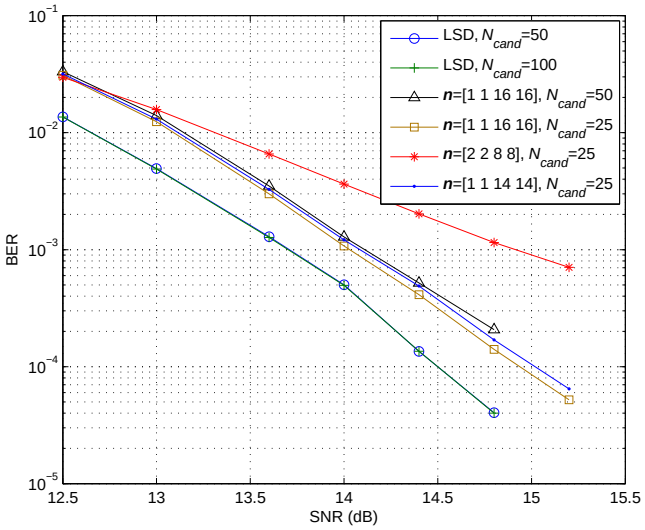

Figure 5.6: BER performance comparison between LSD and LFSD detection of Golden codes in the 2×2 DVB-T2 system with 16-QAM modulation over a TU6 channel.

the LSD algorithm to the LFSD with $\boldsymbol{n} = [1\ 1\ 16\ 16]$, we observe that for $N_{cand} = 100$, 75% of the LSD solutions are obtained visiting a lower number of nodes than with the LFSD. If N_{cand} is reduced up to 50, this value rises to 95%. By using the tree configuration of the LFSD $\boldsymbol{n} = [1\ 1\ 14\ 14]$, the complexity difference between both decoders increases. In this case, 50% and 90% of LSD tree searchs for $N_{cand} = 100$ and 50, respectively, will have a higher complexity than the LFSD algorithm.

In Figure 5.7, we have been able to distinguish the sequential nature of the LSD tree search and its variable complexity, and how the design of the LFSD maintains fixed the search complexity allowing a practical hardware implementation. If we now calculate the CDF per tree level, we can actually appreciate the complexity differences in terms of the number of operations per level, being higher when such level is closer to the bottom. One can observe in Figure 5.8(a) that for the lowest level $i = 1$, the LFSD decoder visits less nodes than the LSD with $N_{cand} = 100$ for most of the channel realisations. When the number of candidates of the LSD is reduced to 50, the 50% of the solutions for $\boldsymbol{n} = [1\ 1\ 14\ 14]$ and 10% for $\boldsymbol{n} = [1\ 1\ 16\ 16]$ are reached with a lower number of visited nodes. As the level is closer to the top of the tree, the difference becomes smaller, visiting almost the same number of nodes at $i = 4$ with the LSD.

Regarding the number of operations in the LFSD search, let us denote m_d as the number of multiplications required to calculate $u_{ii}^2 |s_i - z_i|^2$, considering that u_{ii}^2 no longer needs to be computed. The computed Euclidean distance has been ℓ^2 distance whereas many other approximations can be found in the literature. Therefore, $m_d = 3$. In addition, let us define m_c as the number of multiplications required for each complex product. A direct implementation of the complex product has $m_c = 4$. However, it can be reduced up to

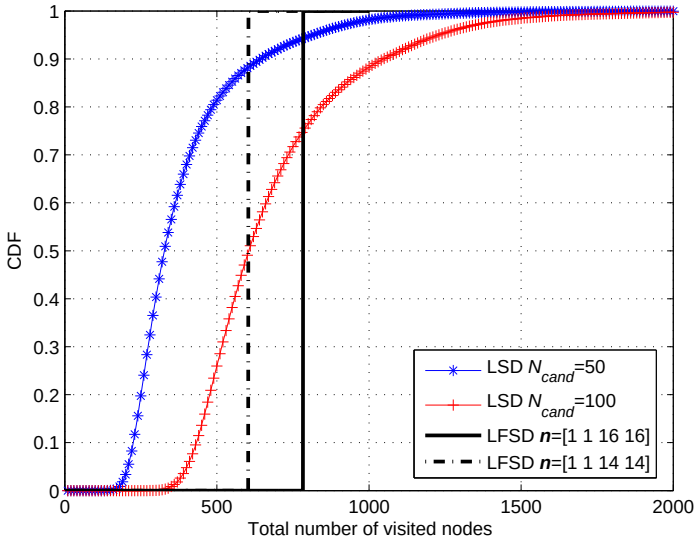

Figure 5.7: CDFs of the overall visited nodes in the LFSD and LSD detections of Golden codes with 16-QAM modulation in the 2×2 DVB-T2 system over a TU6 channel with SNR=14.8 dB.

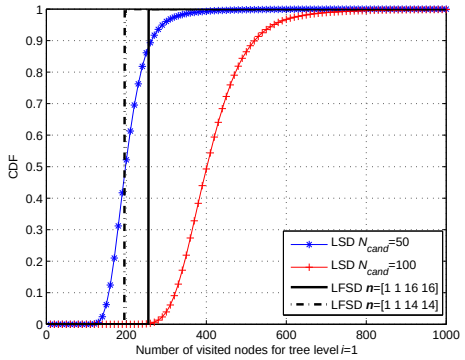

(a) Tree level $i = 1$

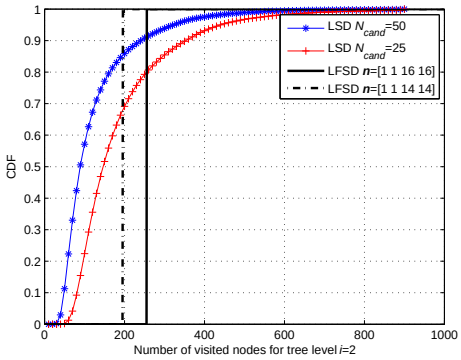

(b) Tree level $i = 2$

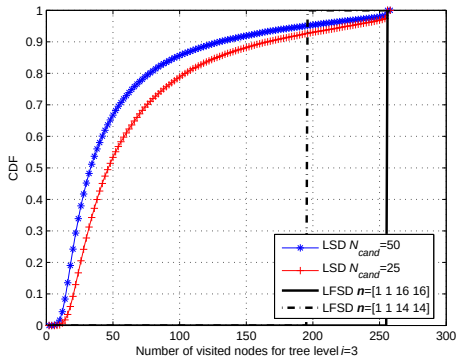

(c) Tree level $i = 3$

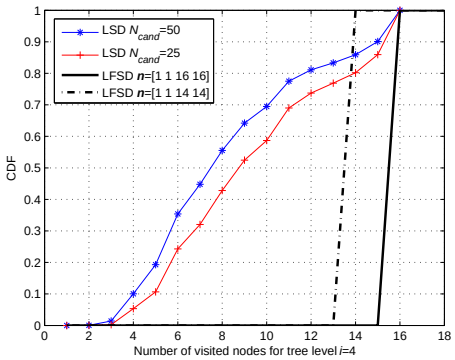

(d) Tree level $i = 4$

Figure 5.8: CDFs as a function of the number of visited nodes at levels $i = 1, 2, 3$ and 4 for the LFSD and the LSD detections of Golden codes with 16-QAM modulation in the 2×2 DVB-T2 system over a TU6 channel with SNR=14.8 dB.

$m_c = 3$ with a expense of extra additions. Therefore, if we consider that the necessary number of multiplications to compute one node at level i is

$$N_{mult\_node\_i} = m_d + (Q - i)\, m_c, \tag{5.12}$$

the number of multiplications required in the complete search stage can be then expressed as

$$N_{mult} = \sum_{i=1}^{Q} \left(m_d \prod_{j=i}^{Q} n_j + (Q - i)\, m_c \prod_{k=i+1}^{Q} n_k \right), \tag{5.13}$$

where the first term inside the sum represents the number of multiplications in the metric calculation and the second term is related to the successive calculation of z_i in (5.5). The proposed algorithm has the same complexity in the tree search stage as in [Barbero06a, Barbero08]. Nevertheless, unlike the Barbero's LFSD, where the ordering preprocessing requires $Q - 1$ matrix inversion operations, the proposed algorithm only performs Q vector norm calculation.

5.4 Chapter Summary

This chapter has presented a novel LFSD algorithm design for the detection of FRFD codes with low complexity in future SFBC-enabled TDT systems. Due to the FRFD code design, the ordering stage of the algorithm proposed by [Barbero06a] for spatial multiplexing MIMO systems does not adjust to the SFBC channel structure. Through the study of the equivalent channel matrices, a new channel ordering procedure has been developed improving the previously introduced LFSD performance and achieving a close-to-optimal result with a fixed-complexity, overcoming the sequential nature of the LSD tree search and its variable complexity, which result in a problem for real hardware implementations. Hence, the design of the proposed LFSD makes it possible to implement a parallel architecture of the algorithm that can be fully pipelined and maintains fixed the search complexity.

The algorithm has been analyzed in a DVB-T2 framework through MATLAB simulations. First of all, a trade-off between complexity and performance has been found. Due to its fixed complexity, LFSD provides a list of candidates which does not correspond to the list ML given by the LSD. The reliability of the list will vary in accordance to the size of the tree search (n_T) and the number of candidates (N_{cand}). Hence, a battery of simulations have been carried out in order to observe the behavior of the algorithm for the Golden and the low-complexity SS codes as a function of these two parameters with and without ordering stage. As a result, we have proved that the ordering preprocessing stage results advantageous for Golden codes due to their inherent symbol power distribution and that SS codes offer a

good performance without any ordering. In addition, we can conclude that reduced N_{cand} values offer better performance when we decrease the size of the search, i.e. n_T.

Once a N_{cand} value of 50 has been chosen, BER performance simulations have been presented as a function of SNR. We have observed that the computation of $n_T = 4P^2$ Euclidean distances offers almost the same performance as LSD. When it is reduced downto $n_T = P^2$, the performance is maintained close to the LSD with a loss of 0.4 dB. In these simulations, we have also provided the comparison with respect to the LFSD in [Barbero06a], where a gain of 0.75 dB is achieved. On the other hand, several tree search configurations have been proposed to reduce the search complexity, being the most promising $\boldsymbol{n} = [1\ 1\ 14\ 14]$ with $N_{cand} = 25$ since it maintains a similar performance as the previously stated configurations.

Last part of the chapter presents some complexity considerations of the proposed LFSD. By paying attention to the CDFs of the visited nodes through the tree structure, we have noticed the variable nature of the LSD algorithm. Even though the average figures of the LSD could be lower than LFSD for some configurations, CDF curves depict how the number of visited nodes can become much greater for certain channel realisations, specially at last levels of the tree where the required number of operations is higher. The proposed LFSD allows us to overcome this problem with a feasible fixed complexity and close-to-optimal results. Indeed, a lower overall complexity is required compared to the LFSD in [Barbero08] due to the reduction of the number of operations at the proposed ordering stage.

Chapter 6

Summary and Conclusions

In this PhD dissertation, we have analyzed the behavior of multi-antenna diversity techniques, specifically SFBCs, in DTV scenarios and proposed novel detection and decoding designs in order to reduce the complexity at the receiver. As a starting point, the DVB-T and DVB-T2 standards have been implemented in MATLAB as well as several MIMO techniques. First of all, BER performance comparison of the state-of-the-art diversity techniques have been carried out in Chapter 2 for both DVB-T and DVB-T2 systems over common TDT propagation scenarios. As has been shown, Alamouti code-based OSFBC presents better results in comparison to CDD since it obtains a performance gain similar to MRC using transmit diversity, which results less expensive than a second antenna at the receivers. This scheme obtains good performance in both fixed and mobile receptions when signal are synchronized. However, the study of the distributed OSFBC behavior in SFN networks shows a loss of the overall performance, reaching a critical limit, i.e. error floor over the QEF, if the delay is close to the GI length.

Chapters 3 and 4 are focused on the study of 2×2 FRFD SFBCs in last-generation DTV systems through error-performance and detection complexity analyses. The use of channel coding based on LDPCs involves a soft-output MAP detector which results in an increase of the detection complexity. The reduction of that computational cost can be achieved through the use of FRFD SFBCs, which have an inherent low detection complexity at the cost of sacrificing performance gain. Two FRFD SFBC codes have been chosen in order to assess the mentioned statements. On one hand, the Golden code, which achieves the maximal coding gain, and on the other hand, the low-complexity SS code with lower performance. These codes have been implemented in a DVB-T2 framework since it includes the last-generation technologies. Simulation results show a better performance than the 2×2 DVB-T2 OSFBC for the same raw bit rate in Rayleigh channels. However, we obtain an opposite behavior when propagation conditions are based on Ricean channels. FRFD SFBCs can allow us to increase the data bit rate if low-complexity detection algorithms are developed since the detection complexity grows exponentially as a function of the modulation order and the number of coded symbols. For that purpose, LSD-based detection techniques have been proposed in the literature. The complexity analysis of LSD algorithm showed

that the detection stage can be performed with an average smaller number of operations. Nevertheless, its variable complexity depending on the noise level and the channel conditions and its sequential nature result in a problem from a practical point of view. As a result, a fixed-complexity detector has been proposed in such a way that it can be fully pipelined in a hardware implementation.

Starting from the concept of the LFSD for spatial multiplexing MIMO systems, a redesign of the previously proposed algorithm has been carried out for FRFD SFBCs with close-to-LSD performance. Due to the two-dimensional transmission of SFBCs, the ordering procedure proposed for one-dimensional transmission in spatial multiplexing modes does not take into account the correlation between subchannels. Therefore, the tree configuration and the subchannel ordering processes can be modified reducing the necessary number of operations at that stage and optimizing the performance of the algorithm. Simulation results proved the behavior of the algorithm compared to the LSD and the LFSD for spatial multiplexing. On one hand, results have showed better performance than the LFSD for spatial multiplexing. On the other hand, we have observed a performance close to the LSD algorithm maintaining a reasonable fixed complexity which would make a realistic hardware implementation feasible.

6.1 Thesis Contributions

The main contributions of this research work are the following:

- Performance comparison of the multi-antenna diversity techniques CDD, Alamouti SFBC and MRC in fixed and mobile DVB-T reception environments.
- Analysis of diversity techniques included in the DVB-T2 standard over Rayleigh and Ricean channels.
- Simulation-based analysis of the DVB-T and DVB-T2 self-interfered SISO reception in SFN networks. This work was published in [Sobron09a, Sobrón09b].
- Performance study of the distributed DVB-T2 MISO scheme reception in SFN networks depending on attenuations and delays of the transmitted signals. The work was published in [Sobrón10d].
- Development of a soft MAP detection approach for FRFD SFBCs in DVB-T2-based systems according to candidate lists. Optimization of the soft method finding the trade-off between number of candidates and performance.
- Performance comparison of Golden code, low-complexity SS code and DVB-T2 SFBC in a DVB-T2 framework over TDT scenarios. Published in [Sobron10c].

- Novel design of an ordering algorithm for the LFSD detection of FRFD codes, specially Golden codes. Optimization analysis of the LFSD algorithm as a function of the tree configuration and the number of candidates. Comparitive analysis of the performance and complexity of the proposed LFSD and the LSD in TDT environments. This work has been submitted for its possible publication in [Sobron10a, Sobron10b].

6.2 Suggestions for Further Research

Many issues described in this PhD dissertation can be addressed in the future as an improvement and extension of the current work. These are some of the suggestions for further research:

- As we have seen for the DVB-T2 MISO scheme, a loss of performance appears when transmitted signals are delayed between them. Other works have stated this problem with FRFD codes giving solutions such as 3D schemes [Nasser08a]. Therefore, an extension of those works can be carried out focusing on a detection point of view.

- From our best knowledge, FRFD STBC/SFBC designs have been usually optimized assuming Rayleigh channel conditions. Therefore, the design of FRFD SFBC for Ricean channels could be stated.

- Real-valued implementation of the proposed LFSD algorithm. In this work, a complex-valued version has been implemented. However, using a real-valued implementation, the tree search has more degrees of freedom and as a consequence, an improvement of performance might be possible. For that purpose, a review of the ordering procedure should be necessary.

- There exist multiple designs of FRFD SFBC codes apart from those which this research work has been addressed to. Therefore, the application of the proposed ordering and LFSD algorithm to other existing FRFD codes could allow us to obtain a more general framework for SFBC comparison.

Appendix A
Publications

The following papers have been published or are under preparation for publication in refereed journal and conference proceedings. Those marked by † are directly related to the research work of this thesis.

Book Chapter:

- M. Mendicute, I. Sobrón, L. Martínez and P. Ochandiano, "Digital Video" chap. DVB-T2: New Signal Processing Algorithms for a Challenging Digital Video Broadcasting Standard, pp. 185-206, InTech, Feb. 2010. †

Journal paper:

- I. Sobrón, M. Barrenechea, P. Ochandiano, L. Martínez, M. Mendicute and J. Altuna, "Low-Complexity Detection of Space-Frequency Block Codes in LDPC-Based OFDM Systems", submitted to *IEEE Transactions on Communications* (under review). †

International conference papers:

- M. Mendicute, I. Sobrón, J. Del Ser, P. Prieto and R. Isasi, "Design, simulation and implementation of a channel equalizer for DVB-T on-channel repeaters", in *3rd IARIA International Conference on Systems and Networks Communications (ICSNC '08)*, Silema, Malta, Oct. 2008.

- I. Sobrón, M. Mendicute, L. Martínez and P. Ochandiano, "Impact of self interference in DVB-T2 broadcasting single frequency networks", in *Proc. 9th International Workshop on Electronics, Control, Modelling, Measurement and Signals (ECMS '09)*, pp. 97-103, Mondragon, Spain, Jul. 2009. †

- L. Martínez, J. Robert, H. Meuel, I. Sobrón and M. Mendicute, "Improved Robustness for Channel Estimation without Pilots for DVB-T2", in *Proc. IEEE International Symposium on Broadband Multimedia Systems and Broadcsting (BMSB '10)*, pp. 1-5, Shangai, China, Mar. 2010.

- I. Sobrón, M. Mendicute and J. Altuna, "Full-Rate Full-Diversity Space-Frequency Block Coding for Digital TV Broadcasting", in *Proc. 18th EURASIP European Signal Processing Conference (EUSIPCO '10)*, pp. 1514-1518, Aalborg, Denmark, Aug. 2010. †

- P. Ochandiano, I. Sobrón, L. Martínez, M. Mendicute and J. Altuna, "Analysis of ICI compensation for DVB-T2", in *Proc. 7th International Symposium on Wireless Communication Systems (ISWCS '10)*, pp. 427-430, York, United Kingdom, Sep. 2010.

- I. Sobrón, M. Barrenechea, P. Ochandiano, L. Martínez, M. Mendicute and J. Altuna, "Low-Complexity Detection of Golden Codes in LDPC-Coded OFDM Systems", submitted to *IEEE International Conference on Acoustics, Speech and Signal Processing (ICASSP '11)*, Prague, Czech Republic, May 2011 (under review). †

National conference papers:

- V. Atxa, I. Sobrón, J.M. Zabalegui, J. Altuna, M. Mendicute and I. Marcos, "Análisis sobre la ecualización de canal en la cabecera de un gap-filler doméstico para DVB-T", in *Proc. XX Simposium Nacional de la Unión Científica Internacional de Radio (URSI '07)*, La Laguna, Spain, Sep. 2007.

- M. Mendicute, P. Prieto, I. Sobrón, J. M. Zabalegui and R. Isasi, "Diseño, simulación e implementación de un ecualizador de canal para gap-fillers de DVB-T", in *Proc. XXI Simposium Nacional de la Unión Científica Internacional de Radio (URSI '08)*, Madrid, Spain, Set. 2008.

- I. Sobrón, J. Del Ser and M. Mendicute, "Estudio y simulación de repetidores regenerativos y no regenerativos en redes de difusión DVB-T", in *Proc. XXI Simposium Nacional de la Unión Científica Internacional de Radio (URSI '08)*, Madrid, Spain, Set. 2008.

- I. Sobrón, P. Ochandiano, L. Martínez, M. Mendicute and J. Altuna, "Análisis de robustez de DVB-T2 en redes SFN", in *Proc. XXII Simposium Nacional de la Unión Científica Internacional de Radio (URSI '09)*, Cantabria, Spain, Sep. 2009. †

- L. Martínez, I. Sobrón, P. Ochandiano, M. Mendicute and J. Altuna, "Estimación de canal para transmisión multiantena y recepción móvil en DVB-T2", in *Proc. XXIII Simposium Nacional de la Unión Científica Internacional de Radio (URSI '10)*, Bilbao, Spain, Sep. 2010.

- P. Ochandiano, I. Sobrón, L. Martínez, M. Mendicute and J. Altuna, "Detección iterativa en receptores DVB-T2", in *Proc. XXIII Simposium Nacional de la Unión Científica Internacional de Radio (URSI '10)*, Bilbao, Spain, Sep. 2010.

- I. Sobrón, P. Ochandiano, L. Martínez, M. Mendicute and J. Altuna, "Transmisión SFBC distribuida en redes SFN de DVB-T2", in *Proc. XXIII Simposium Nacional de la Unión Científica Internacional de Radio (URSI '10)*, Bilbao, Spain, Sep. 2010. †

References

[Al-Semari97] S. Al-Semari and T. Fuja, "I-Q TCM: reliable communication over the Rayleigh fading channel close to the cut-off rate", *IEEE Transactions on Information Theory*, vol. 43, no. 1, 250–262, January 1997.

[Alamouti98] S. Alamouti, "A simple transmit diversity technique for wireless communications", *IEEE Journal on Selected Areas in Communications*, vol. 16, no. 8, 1451 – 1458, October 1998.

[ARIB01] ARIB, "Transmission System for Digital Terrestrial Television Broadcasting STD-B31 v1.0", 2001.

[ATSC05] ATSC, "ATSC Digital Television Standard (A/53) Revision E, with Amendments No. 1 and 2", December 2005.

[Barbero06a] L. Barbero, *Rapid prototyping of a fixed-complexity sphere decoder and its application to iterative decoding of turbo-MIMO systems*, Ph.D. thesis, University of Edinburgh, 2006.

[Barbero06b] L. Barbero and J. Thompson, "Performance analysis of a fixed-complexity sphere decoder in high-dimensional MIMO systems", in *Proceedings IEEE International Conference on Acoustics, Speech and Signal Processing (ICASSP'06)*, 2006.

[Barbero08] L. Barbero and J. Thompson, "Extending a fixed-complexity sphere decoder to obtain likelihood information for turbo-MIMO systems", *IEEE Transactions on Vehicular Technology*, vol. 57, no. 5, 2804 – 14, September 2008.

[Belfiore04] J. Belfiore, G. Rekaya, and E. Viterbo, "The golden code: A 2 x 2 full-rate space-time code with non-vanishing determinants", in *2004 IEEE International Symposium on Information Theory, Proceedings*, p. 308, IEEE, 2004.

[Bello63] P. A. Bello, "Characterization of randomly time-invariant linear channels", *IEEE Transactions on Communications Systems*, vol. CS-11, 360–393, December 1963.

[Bolcskei00] H. Bolcskei and A. J. Paulraj, "Space-Frequency Coded Broadband OFDM Systems", in *IEEE WCNC*, vol. 1, September 2000.

[Boutros03] J. Boutros, N. Gresset, L. Brunel, and M. Fossorier, "Soft-Input Soft-Output Lattice Sphere Decoder for Linear Channels", in *Proc. IEEE Global Telecommunications Conference (GLOBECOM '03)*, vol. 3, pp. 1583–1587, San Francisco, CA, Dec. 2003.

[Burg05] A. Burg, M. Borgmann, M. Wenk, M. Zellweger, W. Fichtner, and H. Bolcskei, "VLSI Implementation of MIMO detection using the sphere decoding algorithm", *IEEE Journal of Solid-State Circuits*, vol. 40, no. 7, 1566 – 1576, 2005.

[Clarke89] R. H. Clarke, "A statistical theory of mobile radio reception", *Bell System Technical Journal*, vol. 47, 957–1000, 1989.

[Conway88] J. H. Conway and N. J. A. Sloane, *Sphere Packings, Lattices and Groups*, Springer-Verlag, New York, 1988.

[Corre05] Y. Corre, A. Fluerasu, E. Hamman, L. Houel, Y. Lostanlen, and A. Sibile, "Result of a measurement campaign of DVB-T signals with an indoor two antennas diversity receiver", Document td(05) 099, COST 207, Lisbon (Portugal), November 2005.

[COST20789] COST207, "Digital land mobile radio communications (final report)", Tech. rep., Commision of the European Communities, Directorate General Telecommunications, Information Industries and Innovation, 1989.

[Cox73] D. C. Cox, "910 MHz Urban Mobile Radio Propagation: Multipath Characteristics in New York City", *IEEE Transactions in Vehicular Technology*, vol. 22, no. 4, 104–110, November 1973.

[Dai05] Y. Dai, S. Sun, and Z. Lei, "A comparative study of QRD-M detection and sphere decoding for MIMO-OFDM systems", in *16th IEEE International Symposium on Personal Indoor and Mobile Radio Communications (PIMRC 2005)*, pp. 186–190, September 2005.

[Damen03] M. O. Damen, H. El Gamal, and G. Caire, "On maximum-likelihood detection and the search for the closest lattice point", *IEEE Transactions on Information Theory*, vol. 49, no. 10, 2389 – 2402, 2003.

[Dammann01] A. Dammann and S. Kaiser, "Standard conformable antenna diversity techniques for OFDM and its application to the DVB-T system", in *Proceedings IEEE Global Telecommunications Conference*, vol. 5, pp. 3100 – 3105, San Antonio, TX, 2001.

[Dammann07] A. Dammann, R. Raulefs, and S. Plass, "Soft cyclic delay diversity and its performance for DVB-T in ricean channels", in *GLOBECOM*, pp. 4210 – 4214, Washington, DC, United States, 2007.

[Dammann09] A. Dammann and R. Raulefs, "Evaluation of diversity gains for the next generation of terrestrial DVB", in *Proceedings 14th International OFDM-Workshop (InOWo 2009)*, Hamburg, Germany, 2009.

[deJong05] Y. L. C. de Jong and T. J. Willink, "Iterative tree search detection for MIMO wireless systems", *IEEE Transactions on Communications*, vol. 53, no. 6, 930–935, June 2005.

[Di Bari08] R. Di Bari, M. Bard, Y. Zhang, K. M. Nasr, J. Cosmas, K. K. Loo, R. Nilavalan, H. Shirazi, and K. Krishnapillai, "Laboratory Measurament Campaign of DVB-T Signal With Transmit Delay Diversity", *IEEE Transactions on Broadcasting*, vol. 54, no. 3, 532–541, September 2008.

[Di Bari09] R. Di Bari, M. Bard, A. Arrinda, P. Ditto, J. Cosmas, K. Loo, and R. Nilavalan, "Rooftop and Indoor reception with transmit diversity applied to DVB-T Networks: a long term measurement campaign", in *IEEE International Symposium on Broadband Multimedia Systems and Broadcasting*, Bilbao, May 2009.

[DVB09] DVB, "Implementation guidelines for a second generation digital terrestrial television broadcasting system (DVB-T2)", Document A133, February 2009.

[ETSI97] ETSI, "Digital video Broadcasting (DVB); Framing structure, channel coding and modulation for digital terrestrial television (DVB-T) ETS EN 300 744", March 1997.

[ETSI04] ETSI, "Digital Video Broadcasting (DVB); Transmission System for Handheld Terminals (DVB-H). EN 302.304 V1.1.1", November 2004.

[ETSI06] ETSI, "Digital Video Broadcasting (DVB); Second generation framing structure, channel coding and modulation systems for Broadcasting, Interactive Services, News Gathering and other broadband satellite applications EN 302 307 V1.1.2", June 2006.

[ETSI09] ETSI, "Digital Video Broadcasting (DVB); Frame structure channel coding and modulation for a second generation digital terrestrial television broadcasting system (DVB-T2). ETSI EN 302 755 V1.1.1", September 2009.

[EVS06] EVS, "Mobile and Portable DVB-T/H Radio Access. Part 1: Interface Specifications.", EVS-EN 62002-1:2006, 2006.

[Fincke85] U. Fincke and M. Pohst, "Improved methods for calculating vectors of short length in a lattice, including a complexity analysis", *Mathematics of Computation*, vol. 44, no. 170, 463 – 71, April 1985.

[Fluerasu05] A. Fluerasu, A. Sibile, Y. Corre, Y. Lostanlen, L. Houel, and E. Hamman, "A measurement campaign of spatial, angular, and polarization diversity reception of DVB-T", Document TD (05) 019, COST 273, Bologna (Italy), January 2005.

[Foschini96] G. J. Foschini, "Layered Space-Time Architecture for Wireless Communication in a Fading Environment When Using Multi-Element Antennas", *Bell Labs Technical Journal*, vol. 1, no. 2, 41–59, Oct. 1996.

[Foschini98] G. Foschini and M. Gans, "On limits of wireless communications in a fading environment when using multiple antennas", *Wireless Personal Communications Magazine - Kluwer Academic*, vol. 6, no. 3, 311 – 335, 1998.

[Gallager63] R. G. Gallager, "Low Density Parity Check Codes", in *Research Monograph Series*, 21, MIT Press, Cambridge, Mass., July 1963.

[García-Lozano10] M. García-Lozano, S. Ruiz-Boqué, and F. Minerva, "Static Delays Optimization to Reduce Self-Interference in DVB-T Networks", in *IEEE International Symposium on Broadband Multimedia Systems and Broadcasting (BMSM)*, 2010.

[Gesbert03] D. Gesbert, M. Shaffi, D.-s. Shiu, P. J. Smith, and A. Naguib, "From Theory to Practice: An Overview of MIMO Space Time Coded Wireless Systems", *IEEE Journal on Selected Areas in Communications*, vol. 21, no. 3, 281–302, April 2003.

[Gomez-Calero09] C. Gomez-Calero, L. Cuellar, L. de Haro, and R. Martinez, "A 2 x 2 novel MIMO testbed for DVB-T2 systems", in *IEEE International Symposium on Broadband Multimedia Systems and Broadcasting. BMSB '09.*, June 2009.

[Guena04] A. Guena, D. Zapparata, A. Sibille, and G. Pousset, "Mobile diversity reception of DVB-T signals using roof or window antennas", Document TD (04) 014, COST 273, Athens (Greece), January 2004.

[Guey96] J. Guey, M. Fitz, M. Bell, and W. Kuo, "Signal design for transmitter diversity wireless communication systems over Rayleigh fading channels", in *1996 IEEE 46th Vehicular Technology Conference, Proceedings - Mobile Technology for the Human Race (VTC 96)* , vol. 1-3, pp. 136–140, IEEE, Vehicular Technol Soc; IEEE, Atlanta Sect, I E E E, 1996.

[Guo06] Z. Guo and P. Nilsson, "Algorithm and implementation of the K-best sphere decoding for MIMO detection", *IEEE Journal on Selected Areas of Communications*, vol. 24, no. 3, 491–503, March 2006.

[Hagenauer96] J. Hagenauer, E. Offer, and L. Papke, "Iterative decoding of binary block and convolutional codes", *IEEE Transactions on Information Theory*, vol. 42, no. 2, 429 – 45, 1996.

[Hakala07] P. Hakala and H. Himmanen, "Evaluation of DVB-H Broadcast Systems Using New Radio Channel Models", Tech. Rep. 817, TUCS Turku Centre for Computer Science, March 2007.

[Hassibi02] B. Hassibi and B. Hochwald, "High-rate codes that are linear in space and time", *IEEE Transactions on Information Theory*, vol. 48, no. 7, 1804 – 24, 2002.

[Hassibi05] B. Hassibi and H. Vikalo, "On the Sphere-Decoding Algorithm I. Expected Complexity", *IEEE Trans. Signal Processing*, vol. 53, no. 8, 2806–2818, Aug. 2005.

[Hochwald03] B. Hochwald and S. ten Brink, "Achieving near-capacity on a multiple-antenna channel", *IEEE Transactions on Communications*, vol. 51, no. 3, 389 – 99, 2003.

[Hoeher92] P. Hoeher, "A Statistical Discrete Time Model for the WSSUS Multipath Channel", *IEEE Transactions on Vehicular Technology*, vol. 41, no. 4, 461–468, November 1992.

[Horseman03] T. Horseman, J. Webber, M. Abdul-Aziz, R. Piechocki, M. Beach, A. Nix, and P. Fletcher, "A software and hardware evaluation of revolutionary Turbo MIMO OFDM schemes for 5GHz WLANs", in *Proc. 57th IEEE Vehicular Technology Conference (VTC '03-Spring)*, vol. 4, pp. 2788–2792, Seoul, Korea, Apr. 2003.

[ISO00] ISO, "ISO/IEC 13818: Standard MPEG-2", 2000.

[ist07] "Telematic link: http://dea.brunel.ac.uk/pluto/publications.php", 2007.

[ITU06] R. S. G. ITU, "Preliminary Report on the Channel Model Development for Hand Held Reception", Document 6E/335-E, March 2006.

[Jakes94] W. C. Jakes, *Microwave Mobile Communications*, Wiley-IEEE Press, May 1994.

[Jaldén07] J. Jaldén, L. G. Barbero, B. Ottersten, and J. S. Thompson, "Full Diversity Detection in MIMO Systems with a Fixed-Complexity Sphere Decoder", in *IEEE International Conference on Acoustics, Speech, and Signal Processing (ICASSP Š07)*, Honolulu, Hawaii, USA, April 2007.

[JTC93] JTC, "Final Report on RF Channel Characterization", JTC(AIR)/93.09.23-238R2, September 1993.

[Kaiser00] S. Kaiser, "Spatial transmit diversity techniques for broadband OFDM systems", in *Proceedings IEEE Global Telecommunication Conference*, pp. 1824–1828, November 2000.

[Kyro07] M. Kyro, *Multi-Element Antenna for DVB-H Terminal*, Master's thesis, Helsinki University of Technology, October 2007.

[Lee06] J. Lee and S.-C. Park, "Novel techniques of a list sphere decoder for high throughput", in *Proc. International Conference on Advanced Communication Technology (ICACT 06)*, pp. 1785–1787, Phoenix Park, Korea, February 2006.

[Lu00] B. Lu and X. Wang, "Space-time code design in OFDM systems", in *IEEE Global Telecommunications Conference (GLOBECOM '00)*, vol. 2, pp. 1000–1004, 2000.

[Ma03] X. Ma and G. B. Giannakis, "Full-diversity full-rate complex-field space-time coding", *IEEE Transactions on Signal Processing*, vol. 51, no. 11, 2917–2930, 2003.

[Mannino08] C. Mannino, F. Rossi, A. Sassano, and S. Smriglio, "Time Offset Optimization in Digital Broadcasting", *Discrete Applied Mathematics (Elsevier)*, vol. 3, no. 156, 339–351, 2008.

[MBRAI07] E. MBRAI, "Mobile and portable DVB-T/H radio access - Part 1: Interface specification", EICTA MBRAI 2.0, June 2007.

[Mendicute10] M. Mendicute, I. Sobrón, L. Martínez, and P. Ochandiano, *Digital Video*, chap. DVB-T2: New Signal Processing Algorithms for a Challenging Digital Video Broadcasting Standard, pp. 185–206, InTech, February 2010.

[Mitchell06] J. D. Mitchell, P. N. Moss, and M. J. Thorp, "A dual polarisation MIMO broadcast TV system", British Broadcasting Corporation (BBC), December 2006.

[Morgade09] J. Morgade, J. Pérez, J. Basterrechea, A. Arrinda, and P. Angueira, "Optimization of the Coverage Area for DVBT- Single Frequency Networks Using a Particle Swarm Based Method", in *IEEE Vehicular Technology Conference Spring (VTC 2009 Spring)*, Barcelona (Spain), April 2009.

[Moss08] P. N. Moss, "2-by-2 MIMO portable reception channel model for dual-polar terrestrial transmission", British Broadcasting Corporation (BBC), July 2008.

[Motivate00] Motivate, "Deliverable 06: Reference Receivers Conditions for Mobile Reception", AC 318 Motivate., January 2000.

[Nasser08a] Y. Nasser, J.-F. Helard, and M. Crussiere, "3D MIMO scheme for broadcasting future digital TV in single-frequency networks", *Electronics Letters*, vol. 11, no. 13, 829–830, June 2008.

[Nasser08b] Y. Nasser, J. Hélard, and M. Crussière, "System Level Evaluation of Innovative Coded MIMO-OFDM Systems for Broadcasting Digital TV", *International Journal of Digital Multimedia Broadcasting*, vol. 2008, 12, 2008.

[Nasser08c] Y. Nasser, J.-F. Hélard, M. Crussiere, and O. Pasquero, "Efficient MIMO-OFDM schemes for future terrestrial digital TV with unequal received powers", in *IEEE International Conference on Communications (ICC'08)*, pp. 2021–2027, Beijing, China, May 2008.

[Nour08] C. A. Nour and C. Douillard, "Rotated QAM Constellations to Improve BICM Performance for DVB-T2", in *Spread Spectrum Techniques and Applications, 2008. ISSSTA apos;08. IEEE 10th International Symposium on*, 25-28, pp. 354–359, August 2008.

[Paredes07] J. Paredes, A. B. Gershman, and M. Gharavi-Alkhansari, "A 2 x 2 space-time code with non-vanishing determinants and fast maximum likelihood

decoding", in *IEEE International Conference on Acoustics, Speech, and Signal Processing, Pts 1-3*, vol. 2, pp. 877–880, IEEE Signal Proc Soc, IEEE, 2007.

[Paredes08] J. M. Paredes, A. B. Gershman, and M. Gharavi-Alkhansari, "A New Full-Rate Full-Diversity Space-Time Block Code With Nonvanishing Determinants and Simplified Maximum-Likelihood Decoding", *IEEE Transactions on Signal Processing*, vol. 56, no. 6, 2461–2469, June 2008.

[Park05] S. Y. Park, S. K. Choi, and C. G. Kang, "Complexity-reduced iterative MAP receiver for spatial multiplexing systems", *IEE Proc. on Communications*, vol. 152, no. 4, 432–438, August 2005.

[Patzold02] M. Patzold, *Mobile Fading Channels*, John Wiley and Sons, 2002.

[Paulraj03] A. Paulraj, R. Nabar, and D. Gore, *Introduction to Space-Time Wireless Communications*, Cambridge University Press, Cambridge, UK, 2003.

[Penttinen08] J. T. J. Penttinen, "The SFN gain in non-interfered and interfered DVB-H networks", in *The Fourth International Conference on Wireless and Mobile Communications*, pp. 294–299, Athens, Greece, July 2008.

[Proakis95] J. G. Proakis, *Digital Communications*, McGraw-Hill, 3rd edn., 1995.

[Radosavljevic09] P. Radosavljevic, Y. Guo, and J. Cavallaro, "Probabilistically bounded soft sphere detection for MIMO-OFDM receivers: algorithm and system architecture", *IEEE Journal on Selected Areas in Communications*, vol. 27, no. 8, 1318 – 30, 2009.

[Rinne00] J. Rinne, "Some elementary suboptimal diversity reception schemes for DVB-T in mobile conditions", *IEEE Transactions on Consumer Electronics*, vol. 46, no. 3, 847 – 850, 2000.

[Robertson95] P. Robertson, E. Villebrun, and P. Hoeher, "A Comparison of Optimal and Sub-Optimal MAP Decoding Algorithms Operating in the Log Domain", in *Proc. IEEE International Conference on Communications (ICC '95)*, vol. 2, pp. 1009–1013, Seattle, WA, Jun. 1995.

[SAC06] SAC, "GB20600-2006 Framing structure, Channel coding and modulation for digital television terrestrial broadcasting system", 2006.

[Samuel07] M. Samuel and M. P. Fitz, "Reducing The Detection Complexity By Using 2x2 Multi-Strata Space-Time Codes", in *IEEE International Symposium on Information Theory. ISIT 2007.*, pp. 1946–1950, Nice, June 2007.

[Sanchez-Varela00] M. Sanchez-Varela and M. Garcia-Sanchez, "Analysis of polarization diversity at digital TV indoor receivers", *IEEE Transactions on Broadcasting*, vol. 46, no. 4, 233 – 239, 2000.

[Sanchez-Varela01] M. Sanchez-Varela, M. García-Sánchez, L. Lukama, and D. J. Edwards, "Spatial Diversity Analysis for Digital TV Systems", *IEEE Transactions on Broadcasting*, vol. 47, no. 3, 198–206, September 2001.

[Santella04] G. Santella, R. De Martino, and M. Ricchiuti, "Single Frequency Network (SFN) planning for digital terrestrial television and radio broadcast services: the Italian frequency plan for T-DAB", in *Vehicular Technology Conference. VTC 2004-Spring. 2004 IEEE 59th*, vol. 4, pp. 2307–2311, May 2004.

[Schnorr91] C.-P. Schnorr and M. Euchner, "Lattice basis reduction: improved practical algorithms and solving subset sum problems", in *Proceedings Fundamentals of Computation Theory (FCT'91)*, pp. 68–85, 1991.

[Sezginer07] S. Sezginer and H. Sari, "Full-rate full-diversity 2x2 space-time codes of reduced decoder complexity", *IEEE Communications Letters*, vol. 11, no. 12, 973–975, DEC 2007.

[Sezginer09] S. Sezginer, H. Sari, and E. Biglieri, "On High-Rate Full-Diversity 2 x 2 Space-Time Codes with Low-Complexity Optimum Detection", *IEEE Transactions on Communications*, vol. 57, no. 5, 1532–1541, MAY 2009.

[Shannon48] C. Shannon, "A mathematical theory of communications", *Bell Labs Technical Journal*, vol. 27, 379–423, 1948.

[Sobron09a] I. Sobron, M. Mendicute, L. Martinez, and P. Ochandiano, "Impact of self interference in DVB-T2 broadcasting single frequency", in *9th International Workshop on Electronics, Control, Modelling, Measurement and Signals, ECMS 2009.*, Mondragon, Spain, July 2009.

[Sobrón09b] I. Sobrón, P. Ochandiano, L. Martínez, M. Mendicute, and J. Altuna, "Análisis de robustez de DVB-T2 en redes SFN", in *Proc. XXII Simposium Nacional de la Unión Científica Internacional de Radio (URSI '09)*, Cantabria (Spain), September 2009.

[Sobron10a] I. Sobron, M. Barrenechea, P. Ochandiano, L. Maritinez, M. Mendicute, and J. Altuna, "Low-Complexity Detection of Space-Frequency Block Codes in LDPC-Based OFDM Systems", August 2010.

[Sobron10b] I. Sobron, M. Barrenechea, P. Ochandiano, L. Martínez, M. Mendicute, and J. Altuna, "Low-Complexity Detection of Golden Codes in LDPC-Coded OFDM Systems", October 2010.

[Sobron10c] I. Sobron, M. Mendicute, and J. Altuna, "Full-Rate Full-Diversity Space-Frequency Block Coding for Digital TV Broadcasting", in *The 18th European Signal Processing Conference (EUSIPCO-2010)*, Aalborg, Denmark, August 2010.

[Sobrón10d] I. Sobrón, P. Ochandiano, L. Martínez, M. Mendicute, and J. Altuna, "Transmisión SFBC distribuida en redes SFN de DVB-T2", in *Proc. XXIII Simposium Nacional de la Unión Científica Internacional de Radio (URSI '10)*, Bilbao, Spain, September 2010.

[Sumii05] K. Sumii, T. Nishimura, T. Ohgane, and Y. Ogawa, "A simplified iterative processing of soft MIMO detector and turbo decoder in a spatially multiplexed system", in *Proc. 61st IEEE Vehicular Technology Conference (VTC 05-Spring)*, vol. 2, pp. 882–886, Stockholm, Sweeden, May 2005.

[Surendra Raju04] M. Surendra Raju, A. Ramesh, and A. Chockalingam, "LLR based BER Analysis of Orthogonal STBCs using QAM on Rayleigh Fading Channels", in *Proc. IEEE PIMRC'2004*, Barcelona, September 2004.

[Tarokh98] V. Tarokh, N. Seshadri, and A. R. Calderbank, "Space-time codes for high data rate wireless communication: Performance criterion and code construction", *IEEE Transactions on Information Theory*, vol. 44, 744–765, March 1998.

[Tarokh99] V. Tarokh, H. Jafarkhani, and A. Calderbank, "Space-time block codes from orthogonal designs", *IEEE Transactions on Information Theory*, vol. 45, no. 5, 1456 – 1467, 1999.

[Telatar99] I. E. Telatar, "Capacity of multi-antenna gaussian channels", *European Transactions on Telecommunications*, vol. 10, no. 6, 585–595, Nov. 1999.

[Tirkkonen00] O. Tirkkonen, A. Boariu, and A. Hottinen, "Minimal nonorthogonality rate 1 space-time block code for 3+ tx antennas", in *IEEE International Symposium of Spread Spectrum Technology*, pp. 429–432, 2000.

[Tirkkonen02] A. Tirkkonen and R. Kashaev, "Combined information and performance optimization of linear MIMO modulations", in *Proceedings 2002 IEEE International Symposium on Information Theory*, pp. 76 –, Piscataway, NJ, USA, 2002.

[Vikalo04] H. Vikalo, B. Hassibi, and T. Kailath, "Iterative Decoding for MIMO Channels Via Modified Sphere Decoding", *IEEE Trans. Wireless Commun.*, vol. 3, no. 6, 2299–2311, Nov. 2004.

[Viterbo93] E. Viterbo and E. Biglieri, "A Universal Decoding Algorithm for Lattice Codes", in *Proc. Quatorzieme Colloque GRETSI (GRETSI '93)*, vol. 1, pp. 611–614, Juan Les Pins, France, Sep. 1993.

[Wittneben93] A. Wittneben, "A new bandwidth efficient transmit antenna modulation diversity scheme for linear digital modulation", in *Proceedings IEEE International Conference on Communications (ICC 1993)*, pp. 1630–1634, Geneve, Switzerland, May 1993.

[Wolniansky98] P. Wolniansky, G. J. Foschini, G. Golden, and R. Valenzuela, "V-BLAST: An architecture for realizing very high data rates over the rich-scattering wirelss channel", in *Proceedings URSI International Symposium on Signals, Systems and Electronics (ISSSE'98)*, pp. 295–300, September 1998.

[Yao03] H. Yao and G. W. Wornell, "Achieving the the full MIMO diversity-multiplexing frontier with rotation based space-time codes", in *Allerton Conference of Communication, Control and Computing*, Monticelo, October 2003.

[Zhang07] Y. Zhang, J. Cosmas, K.-K. Loo, M. Bard, and R. Bari, "Analysis of cyclic delay diversity on DVB-H systems over spatially correlated channel", *IEEE Transactions on Broadcasting*, vol. 53, no. 1, 247 – 254, 2007.

[Zhang08] Y. Zhang, C. H. Zhang, J. Cosmas, K. K. Loo, T. Owens, R. D. Bari, Y. Lostenlan, and M. Bard, "Analysis of DVB-H Network Coverage with the Application of Transmit Diversity", *IEEE Transactions on Broadcasting*, vol. 54, 568–577, 2008.

[Zheng03] L. Zheng and D. N. C. Tse, "Diversity and multiplexing: a fundamental tradeoff in multiple antenna channels", *IEEE Transactions on Information Theory*, vol. 49, no. 5, 1073–1096, May 2003.